MECHANICAL AND MICROSTRUCTURAL CHARACTERIZATION OF COLD METAL TRANSFER WELDED ALUMINIUM METAL MATRIX COMPOSITE JOINTS

**A Thesis Submitted
In Partial Fulfilment of the Requirements for the
Degree of**

DOCTOR OF PHILOSOPHY

**in
Mechanical Engineering**

by

HARI SHANKER

(2K17/PhD/ME/28)

Under the Supervision of

DR. REETA WATTAL

(Professor, Department of Mechanical Engineering)

DEPARTMENT OF MECHANICAL ENGINEERING

DELHI TECHNOLOGICAL UNIVERSITY
DELHI-110042 (INDIA)

JULY, 2024

DELHI TECHNOLOGICAL UNIVERSITY
BAWANA ROAD
DELHI-110042 (INDIA)

CANDIDATE'S DECLARATION

I, Hari Shanker, (2K17/PhD/ME/28) hereby declare that the work done in this thesis titled **"MECHANICAL AND MICROSTRUCTURAL CHARACTERIZATION OF COLD METAL TRANSFER WELDED ALUMINIUM METAL MATRIX COMPOSITE JOINTS"** is an original and own work carried out by me under the supervision of Dr. Reeta Wattal, Professor, Department of Mechanical Engineering, Delhi Technological University, Delhi. The thesis has been prepared under the guidelines and regulations of Delhi Technological University, Delhi. The research work reported and the findings concluded and presented in the thesis have not been submitted and reported for any award of the degree or diploma either part or full time in any university or institute. As per my knowledge and understanding, this research work is free from all plagiarized content.

HARI SHANKER
(2K17/PhD/ME/28)
Department of Mechanical Engineering
Delhi Technological University

Place: Delhi

Date:

DELHI TECHNOLOGICAL UNIVERSITY
BAWANA ROAD
DELHI-110042 (INDIA)

CERTIFICATE BY THE SUPERVISOR

Certified that **Hari Shanker** (2K17/Ph.D./ME/28) has carried out his research work presented in this thesis entitled **"MECHANICAL AND MICROSTRUCTURAL CHARACTERIZATION OF COLD METAL TRANSFER WELDED ALUMINIUM METAL MATRIX COMPOSITE JOINTS"** being submitted for the award of the degree of **Doctor of Philosophy** in Mechanical Engineering, to Delhi Technological University, Delhi, India, is a bonafide record of the original research work carried out by him under my supervision and guidance. The research work reported in this thesis has not been submitted to any university or institute for the award of any degree.

Signature
(Dr. Reeta Wattal)
Professor
Department of Mechanical Engineering
Delhi Technological University

Date:

ACKNOWLEDGEMENTS

ABSTRACT

Technologists are being encouraged to develop useful and efficient methods and procedures for the production and joining of Al-alloys and their metal matrix composite by the growing application of aluminum in numerous industries. It has been noticed that AA7475 plates and sheets are currently used in high-performance aviation applications. However, due to the challenging-to-weld nature of the Al-alloy, the primary obstacle to these applications is the appropriate joining technique.

This investigation primarily aims to evaluate and assess the ripeness of the Cold Metal Transfer welding process for hybrid aluminum metal matrix composites (AMMC). The CMT or cold metal transfer, refers to a modified MIG welding process. Researchers are getting more interested in CMT as an advanced welding technique. The latest developments in this field, include the improved mechanical properties of Al alloys and their metal matrix composite, and the development of efficient welding procedures. To evaluate the weld efficiency, measurements were made of its mechanical characteristics and microstructure, including its tensile strength, yield strength, elongation, microhardness, interface structure, microstructure, and fracture process. To produce welded connections with the best mechanical qualities, an attempt is made to determine the welding technique that is free from all welding imperfections, such as gas porosity, spattering, and intermetallic production.

The objective of the present investigation is to characterize the mechanical and microstructural behaviours of aluminium metal matrix composite (AMMC) of AA7475 alloy in T7351 temper conditions by using a bottom pouring stir casting machine. The hybrid composite was formed using SiC, B_4C, MoS_2, and Gr as reinforcements in different sets of combinations. The mechanical properties were studied of all three sets of fabricated composites. The composite sample showing the best mechanical properties is re-casted using a stir-casting machine with a squeeze-casting arrangement operated by the human-machine interface (HMI). The mechanical properties were

tested and reported for the chosen composite of Al7475 alloy. To check the weldability of the composite a sample was prepared and welding was performed using a robotic CMT welding setup. To join the samples, the Taguchi orthogonal array of L9 was used to optimize the welding parameters. The mechanical characteristics, fracture behaviour, and morphology of the welded joints were examined. As compared to the base metal (BM) and heat-affected zone (HAZ) the weld metal (WM), has a lower value of tensile strength and hardness. All the welded joints fail at the weld metal. The weld metal is the weakest link of the welded sample. The weld metal (WM) has the lowest hardness, which is 64.69 % of the base metal (BM). The microstructure of the weld area was analysed for the welded joint. The final welding parameters were used to perform the confirmatory test. The mechanical and microstructural properties of the confirmatory test sample validate the final welding process parameters.

The final welding parameters were also used to weld the samples of AA7475 alloy in T7351 temper conditions as a confirmatory test. The samples were prepared and welding was performed. The mechanical properties were tested and the microstructure was analysed and reported. After analysing the tensile strength (TS), yield strength (YS), and percentage elongation, it was found that the weld metal (WM) had an elongation of 6.2%, which is considerably less than 13.2% of the base metal (BM) and a bit lower than 8.4% of the heat affected zone (HAZ). Hardness tests were conducted, and the results showed that the weld metal had reduced hardness values. The WM has the lowest hardness, just 58.24 % of the BM. Typical metallographic images of CMT welded samples were analysed for the AA7475-T7351 joint. At base metal, HAZ, and weld metal, the micrograph and associated Energy Dispersive X-ray (EDX) examination were performed. The dispersion of precipitates throughout the weld was assessed using EDX. Analysis and discussion were carried out regarding the EDX data obtained from the top, middle, and root portions of the weld.

The fractography of WM from the fractured tensile sample was also studied and reported. Weld metal (WM), base metal (BM), as well as the generation of the secondary phase in the heat-affected zone (HAZ), were all evaluated using EDX and SEM micrographs.

TABLE OF CONTENTS

LIST OF FIGURES

LIST OF TABLES

LIST OF ABBREVIATIONS

Abbreviations		Full Form
SCC	:	Stress Corrosion Cracking
MMC	:	Metal Matrix Composite
AMMC	:	Aluminium Metal Matrix Composite
AMC	:	Aluminium Matrix Composite
FSW	:	Friction Stir Welding
LBW	:	Laser Beam Welding
CMT	:	Cold Metal Transfer
CMT+P	:	Cold Metal Transfer Plus Pulse
CMT-ADV	:	Cold Metal Transfer Advance
CMT-PADV	:	Cold Metal Transfer Advance Pulse
PW	:	Plug Welding
MAG	:	Metal Active Gas
DWB	:	Chill-Block Direct Welding
GMAW	:	Gas Metal Arc Welding
KB	:	Kissing Bond
HAZ	:	Heat Affected Zone
FZ	:	Fusion Zone
PMZ	:	Partially Melted Zone
PWHT	:	Post Welded Heat Treatment
CTWD	:	Contact tip to Workpiece Distance
XRD	:	X-ray Diffraction
WM	:	Weld Metal
BM	:	Base Metal
EQZ	:	Equiaxed Fine Zone
U-CMT	:	Ultrasonic Assisted Cold Metal Transfer
GTAW	:	Gas Tungsten Arc Welding
OSZ	:	Averaging Softened Zone
OCP	:	Open Circuit Potential
DW-CMTP	:	Double Wire Pulsed Cold Metal Transfer
TEM	:	Transmission Electron Microscopy

Abbreviations		Full Form
EPMA	:	Electron Probe X-ray Microanalysis
CAB	:	Controlled Atmosphere Brazing
AIN	:	Aluminium Nitride
UTS	:	Ultimate Tensile Strength
AMNC	:	Aluminium Matrix Nano Composite
MWCNT	:	Multi-walled Carbon Nanotubes
TS	:	Tensile Strength
YS	:	Yield Strength
GL	:	Gauge Length
ANOVA	:	Analysis of Variance
ASTM	:	American Society of Testing and Materials
FESEM	:	Field Emission Scanning Electron Microscopy
EDAX	:	Energy Dispersive Analysis X-ray
FZ	:	Fusion Zone
VH	:	Vickers Hardness

LIST OF SYMBOLS

Symbol		Meaning
T	:	Temper
AA	:	Aluminium alloy
S^2	:	Variance
n	:	Number of observed values
V	:	Voltage
I	:	Current
W_{fr}	:	Wire Feed Rate
HV	:	Hardness Value
Pt	:	Point

+

CHAPTER 1
INTRODUCTION

1.1 INTRODUCTION

The increasing demand for lightweight structures in different industrial and aerospace applications where the strength-to-weight ratio is the main focus to create a preferential atmosphere and ultimately energy saving. Although modern aluminum composites have high corrosion resistance, fatigue life, less weight, as well as high specific strength impart a way to replace the existing with reasonable properties. However, the high initial cost as well tedious maintenance process limits it in large-level industrial applications. As compared to other high-performance materials, aluminum, and its alloys are low-cost alternatives, reproducible in nature, and can bear a relatively high level of stress. In the current scenario, it is needed to develop highly tailored aluminum alloys that can not only fulfill the demand of large industrial and aerospace applications but also dominate over the other existing composite materials. The automobile, marine, and aerospace part and component manufacturing industries also have a focus on the recycling capability of materials, so that cost reduction can be achieved in many applications [1-5]. Also, it is felt that if steel can be replaced successfully by some lightweight material, the issue of weight and energy savings can be resolved. Aluminum alloy is an attractive engineering material for the construction and aviation industries because of its excellent corrosion-resistant properties, moderate specific strength, as well as formability. The critical properties of these alloys that need to be strengthened are Young's modulus, fatigue tolerance, and fracture durability [6-9]. The development of materials with improved structural stability and life cycle costs is a current problem.

1

In the current scenario, Al-alloys seem to be very attractive materials in terms of their strength-to-weight ratio, large electrical and thermal conductivity, good recycling capability, high corrosion resistance as well as good damping capacity. The drawbacks of the Al alloy are its inability to be processed at elevated temperatures, its poor modulus of elasticity, and some high-strength Al alloys that are susceptible to corrosion. Aluminum alloys, thermal, mechanical, and fatigue properties are influenced by the above-mentioned problems [10-11].

Keeping in focus on improving the mechanical characteristics of aluminium alloys like their specific strength, and fracture toughness. It is needed to control the level of impurity elements like silicon (Si) and iron is an important step in the fabrication of Al-alloys. The 7000 series of Al-alloys are known for their high fracture toughness as well as strength. Also, the corrosion resistance behaviour of an Al alloy is affected by the environmental conditions in which they were used and the alloying elements that exist with the alloy. The physical and chemical variables that exist in the environment are capable of corroding the alloy. The simultaneous effect of continued tensile stress and a corrosive environment force some of the Al-alloy for stress corrosion cracking (SCC). The 2000, 7000, and their tempered conditions are an important category of Al-alloys that are most susceptible to stress corrosion cracking. The 7xxx series, the highest strength commercially available Al-alloy is made by the addition of copper with an Al-zinc-magnesium system in addition to a small amount of manganese and chromium. In comparison to the 2000 series of Al-alloy, the 7000 series alloy carries high strength and fracture toughness. The high strength and fatigue behaviour of a material is always important data for the design and development of the aerospace structure. Under constant loading conditions the fatigue crack growth of non-lithium 2000 series Al-

alloy is better than 7000 series Al-alloy. Due to their better physical and mechanical properties, like high specific strength, high corrosion resistance, better fracture toughness, and better recycling capability, Al-alloys are the most preferred material for transportation and structural industries in the current situation. The demand for Al-alloy in industries especially in the transportation and aerospace industries is increasing because of the above-mentioned mechanical and physical properties. Al-alloy 2xxx, 6xxx, and 7xxx series fall under the most important category for applications in transportation and aircraft industries [1].

The 7000 series of Al-alloy is an Al-Mg-Zn-Cu-based Al-alloy in which the AA7475 lies and is made by a small modification in AA7075. The Al-alloy 7475 can work in an environment of a corrosive nature due to its high strength, high fracture toughness, and large resistance to fatigue crack propagation. These properties in AA7475 are achieved by changing the quenching and aging condition and also by reducing the iron and silicon content of AA7075.

The total content of silicon and iron in AA7475 is 0.22%, whereas it was 0.90% in AA7075. These changes in AA7075 alloy resulted in a new material having a high strength level among all the Al alloys available and having good and favourable mechanical properties for applications in automobiles and aircraft. The AA7475 alloy also shows excellent corrosion resistance as well as fatigue properties. The mechanical properties that are associated with the AA7475 alloys can fulfil the needs of the aerospace and automobile industries in many applications. By using suitable reinforcement material, the mechanical and microstructural properties can be enhanced for AA7475 alloy. So, it is observed that as the aerospace and automobile industries

require lighter and stronger materials, the need for the fabrication of newer materials leads the way for aluminium metal matrix composite (AMMC).

The outstanding attributes of AA2000 and AA7000 alloys, such as their high strength, stiffness, resistance to corrosion, and fracture toughness, make them the preferred materials for structural parts in the aerospace industry [2-3]. By incorporating some reinforcements in the Al-alloys, a metal matrix composite is formed with enhanced properties. These AMMC replaced the Al-alloys with improved mechanical characteristics like good wear properties, outstanding strength-to-weight ratio, as well as fatigue behaviour. The enhanced mechanical and wear properties of the formed composite of Al-alloy make them favourable for the parts and components in aircraft industries, and automobiles. With suitable reinforcement like ceramic particles, they are capable of working at elevated temperatures [3]. The hard ceramic reinforcements also improve the tribological properties of fabricated composite [12]. Many qualities like high modulus of elasticity, good wear resistance, and high strength make the AMMC suitable for many engineering applications [4]. However, the incorporation of ceramic reinforcements in the Al-alloy, which carries hard and brittle behaviour makes the composite suffer and sacrifices its toughness and ductility, and limits its applications [5-6]. Hybrid MMC which is fabricated by utilizing two or more reinforcements, shows better mechanical properties than only a single reinforcement or monolithic composite [4]. The hybrid composites are made to get the combined effect of reinforcing particles that are used to form the composite [13]. It was found that there are many series of Al alloys in which AMMC was fabricated using different fabrication techniques by the researchers to improve its properties. The reinforcements that are currently used to form the single as well as hybrid composite are Al_2O_3, SiC, B_4C, TiB_2, TiC, TiO_2, Gr, MoS_2,

etc. have been reported in the literature to enhance the properties of Al-based metal matrix composite. MoS_2 and SiC are the reinforcements that are used to form the composite and processed by friction stir process to gain the combined advantages of both and can able to meet all expectations of Al-based composites [14].

The wear resistance of metal matrix composite reinforced by B_4C shows tremendous improvements due to excellent interfacial bonding with aluminium matrix. The addition of some reinforcements like (MoS_2) molybdenum disulfide and (Gr) graphite as solid particle reinforcement provides lubricating behaviour along with hard ceramic particles and is capable of increasing the frictional and wear characteristics of the hybrid composite. The use of hard ceramic particles improves the mechanical characteristics of the material while solid lubricant particles like Gr and MoS_2 participate to reduce the friction coefficient [15-20]. Solid lubricant particles decrease mechanical characteristics like hardness but concurrently enhance tribological behaviour in the composite matrix [21]. The hybrid combinations of nano-reinforcements of $B_4C+Al_2O_3+Gr$ are delivering excellent wear properties in the composite material.

The data found was scanty on 7xxx series advanced Al alloys like AA7475 and especially for a hybrid composite of AA7475 alloy. A hybrid composite is formed when two or more reinforcements are added to the base material to gain the properties of all reinforcements in combinations. Synergy in the composite is obtained by gaining the combined effect of the reinforcements. Simultaneously it provides an improvement in many mechanical properties like wear, lubricating, hardness, etc.

The limitation that is associated with the metal matrix composite is its cost of processing. Many methods are available to fabricate metal matrix composite out of which the vortex or melt stir casting provides a large volume of processing, is simple

5

in operation, flexible, has a wide range of material applications, and is for the production of large size part and component. So, the vertex or stir-casting technique is the most used method at the commercial level for the fabrication of MMC. The objective of the fabrication of MMC is to produce a material that is homogeneous, isotropic, and environmentally benign by utilizing various types of reinforcements in different sets of combinations. Particle-reinforced metal matrix composites are most useful due to their simple and similar processing technique that is used for monolithic materials.

As the need for complicated structures grows, so does the need for better connecting methods. Techniques for welding aluminum and steel are very similar. Welding is the most frequent connecting method for Al alloys. Welding is a joining method that has several advantages, including high joint efficiency, ease of setup, flexibility, and cheap fabrication costs. Welding, despite its numerous advantages, entails melting the parent material, which changes the microstructural and mechanical characteristics of a substance [22-23]. Unlike carbon steels, which harden when heated by an arc, the basic Al alloy softens when heated by an arc. The recent advancements with improved properties of aluminum alloys [24], as well as high-performance welding techniques [25], are being explored. Pulsed DE-GMAW [26], Laser welding [27-29], FSW, ultrasonic welding, adhesive bonding, soldering, and brazing have all revolutionized the welding of thin as well as thick-section materials and dissimilar metals by providing strong weld bead aesthetics and a controlled metal transfer rate [24]. The need to join dissimilar materials is increasing day by day to create new structures and parts with smart properties. A part may be sensitive to wear at a high temperature in one area but requires good corrosion resistance in another usage. Development in the welding of

dissimilar materials with arranged properties has permitted new ways for lightweight structures, next-generation medical products, consumer devices, and many more industrial and manufacturing applications [30-31]. Many studies reveal that the joint efficiency of the weld created by FSW welding is higher than the other conventional welding processes. However, under all operating environments, the FSW welded joint has a shorter fatigue life than the parent metal. It is also felt that surface roughness seriously affects the fatigue life of a material [32-33]. Also, a very common and serious defect that takes place in aluminum alloys during weld solidification is porosity and this is due to the evolution of hydrogen gas. When it comes to aluminum welding, porosity has a big impact on the weld bead consistency, the form, the structure of the weld, and the weld's properties. So, for suitable weld quality, the welding parameter is taken and the method adopted is working as a deciding factor.

Because aluminum is a strong and lightweight material tends to be easily recyclable so it can be used in different automobile applications. The application of aluminum in the form of thick and thin sections is common in different industrial sectors, but making a thin sheet weld structure that is less than 3mm is tedious with conventional methods. The main problems that were realized during welding are burn-through and distortion, lack of control on penetration was also observed which limits its usage [34-35]. So, with the low heat input mechanism, CMT is found suitable to weld thin sheets of Al alloys [36]. Now, the CMT is felt to be a viable route to weld the structure made up of thin sheets of aluminum. It is also established to weld the structure of dissimilar materials together, such as welding of Al and Mg together to form a combined structure that reduces the structure's weight while also lowering the cost of the parts and components [37-39]. To ensure the Al/Mg joints have higher strength in the current situation, friction-stir connects as well as a diffusion bonding process [40], are used.

However, FSW is observed as less flexible [33], while diffusion bonding provides lower welding efficiency and requires the use of a vacuum chamber [41]. Solid-state welding uses are somewhat limited as a result of these issues. Meanwhile, tungsten inert gas (TIG) welding [42], metal inert gas (MIG) welding [43], laser welding process [44-45], as well as many other conventional welding processes, forms an intermetallic compound film that adversely affects the joint strength [46]. Then creation of intermetallic compound layers is prevented by coupling it with the CMT process, which has a lower heat intake. Another uncommon structure that has been achieved by using the CMT process is the better linking of Al and Steel metals. Meanwhile, it was hypothesized that low-heat-input CMT welding will reduce the distortion of thin sheets of pure aluminum while also improving gap-bridging capability [47]. The CMT method will generate a spatter-free weld joint with outstanding gap-bridging abilities and low heat input. CMT welding is mostly investigated by joining Mg alloy and Al alloy [37, 46, 48-49].

As a result, the CMT is characterized as a new technique that is largely applied to repeatedly and consistently weld materials that are similar and diverse [50]. The electrode is heated and a small quantity of liquid droplets is formed during the CMT welding process in maximal current mode. To stop the globular transfer, the current is quickly decreased to a background current, where it remains until the short-circuiting. The voltage reaches its zero value during the short-circuiting phase which makes the electrode, strike to the workpiece. A feedback signal is sent to the wire feeding system and then the liquid droplet formed at the tip filler wire electrode will make contact with the weld pool. Because of the retraction force, the liquid bridge can be broken and the molten metal droplet formed at the tip of the electrode is transferred to the weld pool. After that, the

cycle is restarted and the arc is reignited [51–54]. In this, the primary development is the incorporation of wire motion in the welding as well as for integrated process monitoring. The wire retraction motion allows the molten metal to enter into the welding pool despite any electromagnetic force during the short circuit period. So, the heat input as well as the spatter can be reduced significantly [55]. While in the traditional MIG short-circuiting process of metal transfer a substantial rise in the current, is the cause to encourages the fluid bridge to rupture with comparatively greater electromagnetic force. Researchers have been exploring CMT welding since 2004 when Fronius Company introduced this new kind of reduced heat input welding method. Despite the efforts of the researchers, the mechanical and interfacial properties of aluminum and its alloys will change after joining because of the melting of base metal while welding. Because of the less energy input of the CMT, the deformation in base metal was decreased as compared to other conventional welding methods. CMT welding has numerous advantages that make it an attractive process including extremely low thermal input (90 % less thermal input), tremendous gap bridging capability of 2.5 mm, dissimilar welding joint from steel and aluminum with higher welding speeds (5 times faster as compared to conventional welding processes), extremely low welding time (as low as a fraction of a second only), permits the welding of thin to thick section, environment friendliness (no smoke or fumes), low dilution during cladding 75 % less dilution (2 times faster), weld-seam with 99 % less spatter and ultra-high- precision MIG/MAG welding techniques.

Investigation shows good mechanical strength and low corrosion characteristics as the GMAW welding process was used to join SS 304 and SS 400 low-carbon steel in dissimilar welding [56]. As the GMAW is used to join iron and steel, it is also a generally used method for connecting parts and components of Al-alloy like cars, ships, bridges, as

well as pressure vessels. To join Al alloys, studies have been done to determine the effect of implementing alternating shielding gases for AA6082 T6 welding and it was found that it reduced the porosity, provided moderate strength, and increased travel speed which resulted in reduced heat input and distortion and increased productivity [57]. Also, the investigation was done to determine the impact of filler wire on the microstructural and mechanical characteristics of dissimilar aluminium alloy of AA 5083 as well as AA 6061 T6 welded by MIG welding and it is concluded that the filler wire ER5356 is more appropriate for better mechanical properties, tensile strength, % elongation, hardness as well as reduced porosity [58]. Despite improved mechanical and microstructural properties, the above traditional welding methods are unable to join some hard-to-weld aluminium alloys. Because of its low heat input and higher welding speed, laser beam welding (LBW) provides both technical and economic benefits over traditional methods. The effect of filler wire on porosity formation, microstructure, and tensile strength in the welding of AC-170PX Al-alloy of 1.1 mm thickness by a high-power disc laser welding was investigated and it has been observed that the filler wire such as AA5083 and AA3004, has improved tensile strength, microstructure characteristics and drastically reduced the porosity due to high content of Mg and manganese [59]. Al alloys, on the other hand, are difficult to connect with LBW due to rapid heat transmission in the welding piece and the low viscosity of the weld pool before solidification [60]. Now, the FSW is a solid-state welding method capable of producing high-quality defect-free joints in 7075 Al alloys. Due to its high welding efficiency, eco-friendly nature, as well as adaptability, it is considered a green technology. FSW has become more popular for the fabrication of a high-quality weld of Al alloys such as 2000, 5000, 6000, and 7000 series, as well as Al matrix composites. FSW can connect Al alloys that were previously thought to be difficult

or impossible to fusion weld like AA 7050, and AA 7075 [61]. In dissimilar combinations, AA6061 and Mg-AZ-31B were successfully welded in different welding conditions and offsetting by using Friction Stir Welding, compared the outcome with other methods, and concluded that the Friction Stir Welded joint had higher strength [62]. Similarly, AA6061 and 1Cr18Ni9Ti were Friction Stir Spot Welded for a 2 mm thick plate, and it is concluded that the microstructure and shear strength for the dissimilar joint depends on the rotational speed of the tool, depth of penetration, welding time, as well as on the axial force. With an increase in the value of the depending parameters the shear strength first increases and then decreases [63].

FSW was used to weld the different grades of Al-alloy in similar and dissimilar combinations and it is observed that the maximum strength that is achieved is not more than 75-85% of the base material strength [64]. Also, the defects can affect the performance of FSW joints, like other joining methods. When welding parameters like tool pressure, rotation, speed of welding, along with the design of the pin and shoulder, are not optimized, the material flow due to weld temperature might be affected, and resulting in defect development. In FSW, the tunnel and lack of penetration/ kissing bond (KB), residual at the joint line, granule breakdown, and flash on the surface are all common issues [62]. Due to inadequate tool alignment, a smaller pin length, insufficient depth of plunge, kissing bond, and a lack of penetration may be the source of failure initiation. The FSW technology has enabled the connection of 7xxx alloys without the introduction of faults that can occur during fusion welding. However, because AA7475 is an age-hard-enable alloy, joining it using FSW/fusion welding techniques is exceedingly challenging. Today Al alloys, along with their different tempers, make up a diverse and adaptable set of production materials. Understanding the distinctions between the different

series of Al alloys and their welding characteristics as well as various performances and weldability characteristics, makes it critical to develop an effective welding technique for optimal product design. When compared to other welding techniques, CMT welding has less heat input, good gap bridging abilities, less dilution, quick functioning, and less spatter making it a very attractive and promising method for joining such difficult-to-join Al alloys. To explore the capability of CMT, AA5083 and AA6082 alloys were joined by using the CMT, and MIG welding processes, the tensile and fatigue test results were compared, and observed that the CMT welding showed superior value as compared to MIG welding [65]. Due to its distinct benefits over traditional MIG and other welding, CMT, welding is a potential method for improving the mechanical properties of difficult-to-weld 7xxx series Al-alloy.

The hard-to-weld 7xxx series Al alloy can potentially have its mechanical properties improved through the use of a cold metal transfer (CMT) welding process. As compared to other welding techniques, CMT welding is a suitable welding process for hard-to-weld high-grade aluminium alloy and its metal matrix composite. The major advantages of using CMT welding are its low cost and versatility. Despite the enormous potential to circumvent most of the drawbacks of welding these alloys, a few studies have been conducted on CMT welding of Al alloys from the 7000 series that are heat-treatable.

1.2   INTRODUCTION TO THE CMT WELDING PROCESS

To clearly understand the CMT system and process, the line diagram of a CMT welding process and equipment that are commonly used are illustrated in Figure 1.1. It has a CMT power source to supply the controlled heat input, a high-speed camera to capture the droplet transfer image, a wire feed unit with a welding torch to supply the feeler wire, and a sensing probe to control the arc voltage and the welding current. An oscilloscope as an imaging system is used to take the image of metal transfer. The welding set-up in Figure 1.2 is a CMT welding machine, a KUKA welding robot, and a wire feeder used to manufacture the robotic CMT joints [66].
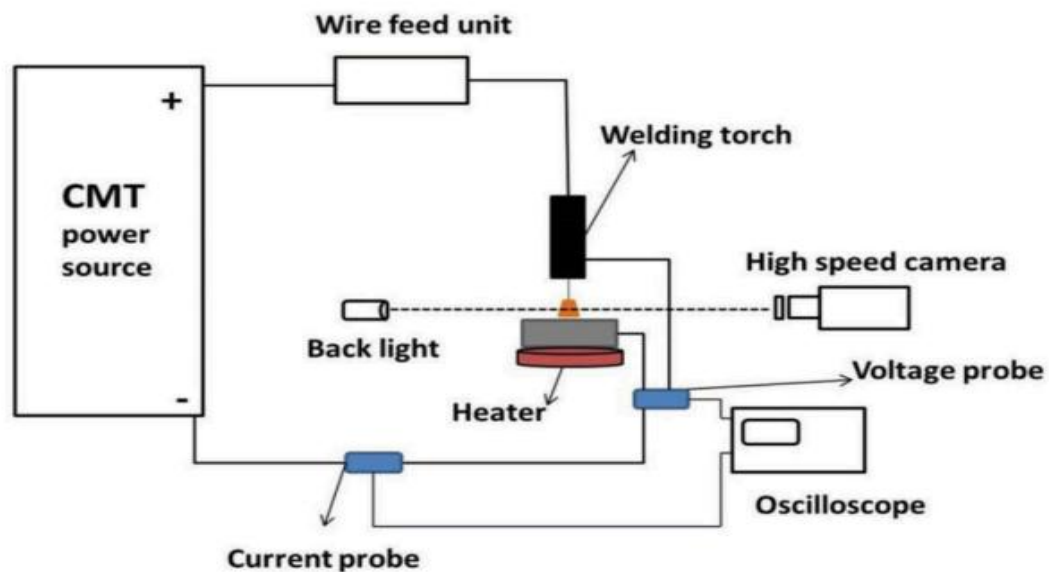
Figure 1.1: The experiment processing equipment and process of CMT welding [66].
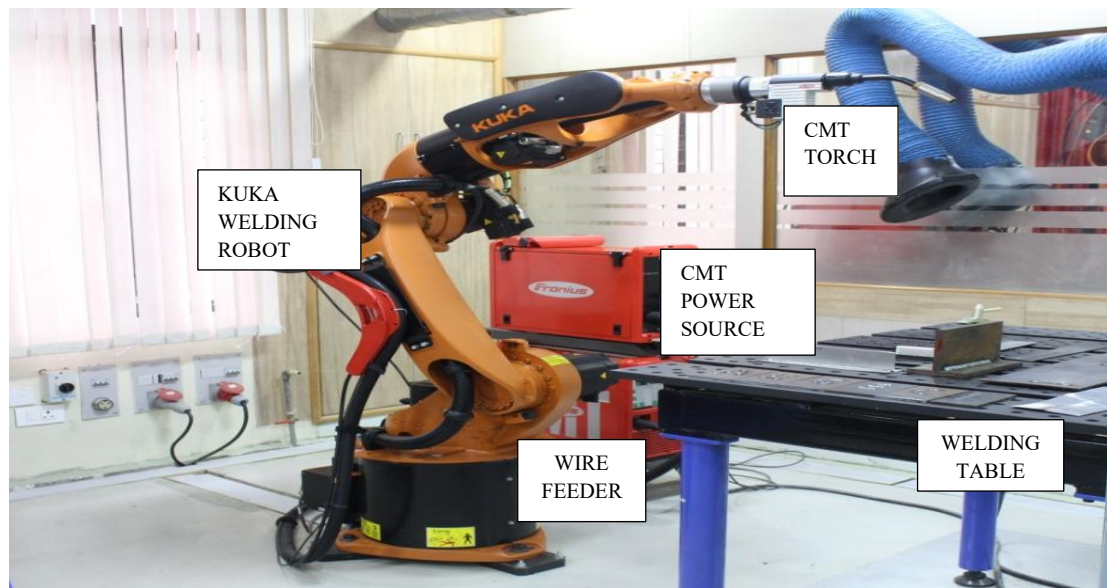
Figure 1.2: The Robotic CMT welding setup.

To perform the CMT weld it is necessary to know the welding power source and its current-voltage waveform for a complete weld cycle. The three phases of the CMT system with current and voltage waveform are shown in Figure 3, [67]. In the first phase, the heating of the wire electrode takes place to produce the droplet and it is done by the peak current phase. The next phase, known as the background current phase, is when the low-value current is maintained until the short-circuiting process occurs.
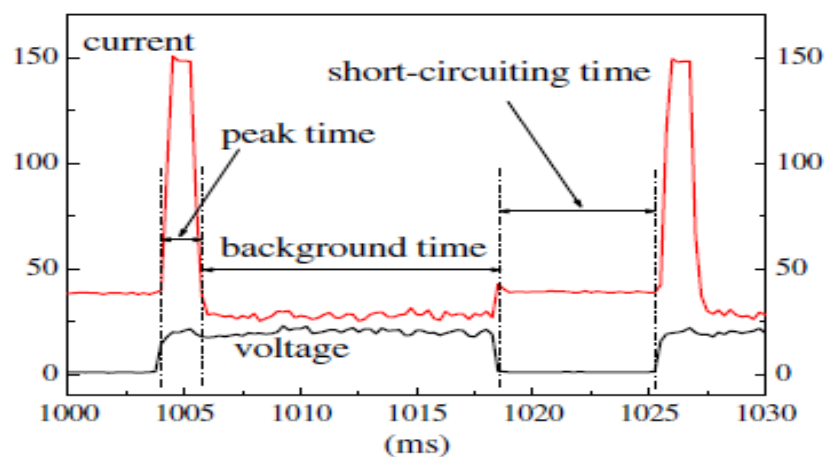
Figure 1.3: A Voltage and Current Waveform of CMT Welding Process [67].

14

In the third phase, the wire will make close contact with the welding pool, and at the same point in time, the voltage of the arc reaches zero value and then a return signal is transmitted by the wire feeder. The cable tributary then provides the wire with the back-drawing power. The movement of molten metal into the weld reservoir is aided by this critical back-drawing force. This phase is known as the short-circuiting phase. After the short-circuiting phase, the CMT weld cycle is completed.

Higher welding speed, shorter welding time, and more accurate control are the outcomes of the CMT welding process and are needed to solve the challenges associated with the use of traditional welding methods. CMT Welding is the alternative method that overcomes all the above-mentioned difficulties. Therefore, it seems that the CMT welding process may have the potential to provide a solution for future welding applications.

1.2.1 Components of CMT Setup

Wire feeder – A wire feed unit to feed the filler wire smoothly and precisely from the wire spool to the workpiece. A four-roller drive system is used to feed the wire.

Wire Buffer – It is used to make the travel of wire smooth and also decouples the front and rear wire drives.

MIG/MAG Welding Power Source – An inverter power source equipped with a fully digitized microprocessor-controller that ensures high precision, and excellent weld quality for the welding process.

Robacta Drive CMT Welding torch- An embedded robotic gearless welding torch with a completely dynamic AC servo-motor control system that can move the wire

forward and backward up to 90 times per second while maintaining precise wire feed and continuous contact pressure.

Cooling Unit – To ensure the sufficient water cooling of a welding torch, a reliable, modular, and fully designed cooling system is applied.

Contec Contacting System- To keep the contact forces that exist between welding wire and contact surfaces under the specified target span, the two movable half shells are used and the contec used is suitable for all diameters and materials. The contec tip is so designed that, it will minimize uneven wear in the process.

1.3   APPLICABILITY OF THE CMT PROCESS AND ITS VARIANTS

Considerable thought must be put into joining aluminium and its alloys. When using aluminium alloys in fusion welding, solidification/centre-line cracking is a common occurrence. These types of failure conditions are due to the large difference in the liquid and solid interface temperature at the time of cooling of metals. A large number of stresses are induced due to the contraction of metal which leads to failure /defects. A heat-affected zone due to variation in heating and cooling patterns generally decreases the joint strength of the heat-treatable alloy. In addition, to the above-mentioned troubles, some more problems occurred with the welding of aluminium alloys, including improper mixing of base and filler materials, the generation of intermetallic, in a fusion zone, the presence of a large size porosity, and a reaction in molten metals and its constituents. Steel and aluminium alloys are difficult to weld together due to large variations in their properties like melting points, thermal conductive properties, electrical resistivity, and high thermal correlation coefficient. Corrosion is a significant concern in dissimilar material welding due to differences in electrochemical potential.

Galvanized steel was used in the majority of instances with steel substrate materials because the Zn-coating film protects the steel plate from oxidizing before welding. To ensure the proper filler metal wetting on the steel board, it is needed to restrict the formation of an oxide film.

The need for CMT is felt when:

1. Effects of heat affected zone (HAZ) due to welding heat are undesirable. HAZ is the reason for the change in the microstructure of the base metals and hence causes a change in properties.

2. Traditional fusion welding unavoidably creates a fusion zone and brings about a thick intermetallic consolidation layer, which sternly affects the joint strength and creates a crack in the weld. Even for Al/Steel diverse metal joints with excellent efficiency, the forming of intermetallic consolidation can be reduced using low heat input CMT welding methods [34].

3. Differences between the solubility and melting points of dissimilar metals cause problems in making a sound joint. CMT provides a better solution to tackle it.

4. Several conditions like surface finish, stress aggregation, microstructural blend, cold mass fragments, and enduring stresses in welding are all factors that have been found to influence the fatigue strength as well as fatigue crack extensions of AMC FSW joints [21]. This is considered to be overcome by CMT and pulsed cold metal transfer (CMT+P) welding.

5. Other features of CMT welding are to creation of a spatter-free weld joint, excellent gap-bridging ability, and low heat intake. These features led to enhanced tensile properties when compared to conventional welds.

17

6. Using CMT welding will ensure cost-effectiveness in long uses, for the equipment, tooling, application, low energy needs, and high joint quality, which gives a relative cost comparison among the various joining methods.

Therefore, on account of tremendous joint efficiencies, substantial mechanical characteristics, greater fatigue/wear resistance, and excellent microstructural stoutness; this process is found suitable for welding parts and components of very high strength. The applications of CMT, include welding of cryogenic engines, aircraft fuselages, new-generation automobiles, marine parts, and spacecraft bodies. Aluminium and its alloys, which are used in many structural components such as aerospace, high-speed railways, and vehicle parts production, can be both thin and thick. Furthermore, it was determined that the traditional CMT joining process was insufficient to weld aluminium structures having thicknesses of more than 3 mm due to its lower heat intake. As a result, it was thought that traditional CMT welding was limited to thin-sheet engineering applications. As a result: the three new processes are introduced by the Fronius company that provide the perfect solution for joining thin as well as thick sheets in any application and that ensure magnificent results. They are:

Pulsed Cold metal transfer (CMT+P): Thin sheets and thick plates of aluminium and its alloys are commonly used in aircraft, railroad transports as well as in automobiles. However, the CMT welding process is restricted to thin sheets only in many engineering applications. To fulfil the needs, a new welding process is required that can weld the thin sheets as well as thick plates and the new CMT process called CMT plus pulse (CMT+P) is introduced by the Fronius company. To transmit one droplet per pulse during the cold metal transfer period, the CMT+P combines a projected transfer mode with a short circuit transfer mode.

During the pulse period of welding, it provides a high welding current as well as increased heat input to weld the thick plate. So, this arrangement adds more heat input in the welding process with combinations of pulsed cycle and CMT cycle. The introduction of a pulse in this process is in a delicately controlled and adjustable manner which results in an extensive performance and pliability.

Cold metal transfer advanced (CMT-ADV): This mechanism was found even cooler than the traditional CMT process. The process control is integrated into the welding current's polarity. To ensure CMT welding stability during the short-circuit process, polarity reversal was used. As a result, the thermal input was tightly regulated, the gap-bridging potential was extremely high, and the deposition rate was increased by up to 60%.

Cold metal transfer advanced pulse (CMT-PADV): In this process the integration of negatively poled cold metal transfer cycles with anodically poled pulse cycle takes place. The method can attain significant proficiency in the arc as well as high precision. Figure 1.4 (a, b, c, d) depicts voltage and current waveforms for traditional cold metal switches to, CMT-pulse, CMT-advance, and CMT-advance pulse.
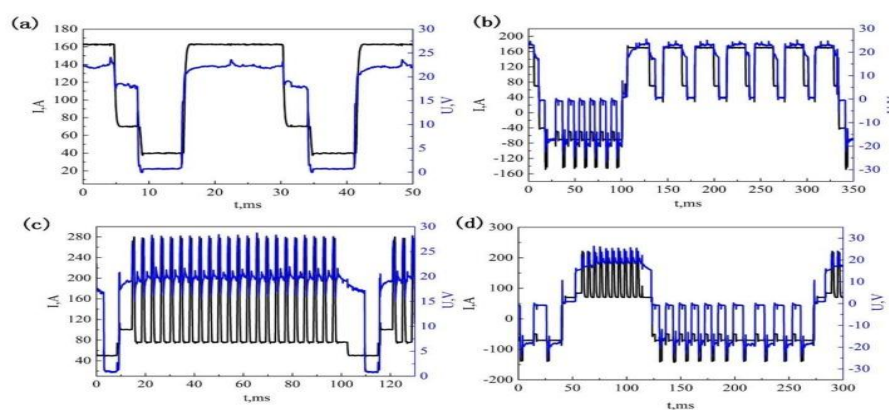
Figure 1.4: Shows (a) CMT (b) CMT+P (c) CMT-ADV (d) CMT-PADV Waveforms [48].

Alloy 7475 sheet and plate are now being used in high-performance aviation applications for fracture important components. Given these facts, it is predicted that the use of suitably treated AA7475 alloys and fabricated AMMC with suitable reinforcement in hybrid mode will safely lower the total weight of aeronautical structures, which is an essential- criterion for such purposes. The present analysis aims to learn more about the mechanical and microstructural characteristics of CMT welded AA7475 alloy in T7351 temper and its fabricated composite, the mechanical characteristics of welded CMT joints will be assessed. As a result, the research explores the potential benefits of the CMT technique to join the difficult-to-weld Al alloys and their AMMC.

1.4 CMT MODES OF METAL TRANSFER

CMT welding operates through several modes of metal transfer, offering versatility and control in the welding process:

Spray Arc Mode: In this mode, a continuous welding wire feed is used along with the high current, causing the wire tip to melt and spray tiny droplets into the weld pool. This mode is suitable for thicker materials and higher deposition rates.

Pulsed Arc Mode: Pulsed arc mode is often utilized during the peak current phase of CMT welding. It involves pulsing the welding current at specific frequencies and amplitudes, ensuring stable arcs, controlled heat input, and consistent bead appearance.

Short Arc Mode: This mode operates with lower welding currents and shorter arc lengths, making it suitable for thinner materials. It is commonly employed during the short current phase of CMT welding, providing precise arc and weld pool control.

These modes of metal transfer offer adaptability to various material thicknesses, joint configurations, and welding requirements while ensuring high-quality welds with minimal distortion and spatter. The flexibility to switch between these modes enhances the versatility and control of CMT welding.

1.4.1   Salient Features of CMT

1.   CMT welding of Al, creates an ultra-light gauge joint, with double welding speed.

2.   Extremely low thermal input, 90 % less thermal input.

3.   Outstanding capacity to bridge gaps, with a 2.5 mm (0.1 in) gap.

4.   Steel/Al hybrid joint higher welding speeds (5 x faster) TIG cold-wire.

5.   Extremely low welding time (as low as a fraction of a second only).

6.   Permits welding of thin to thick sections.

7.   Environment-friendly (no smoke or fumes).

8.   Extremely low dilution during cladding 75 % less dilution (2 x faster).

9.   Less spatter welding with CO_2 as gas shield/steel, measured over 1m of welding

    length and weld seam with 99% less spatter.

10.   Ultra-high-precision MIG/MAG welding process.

So, it can be inferred that the CMT welding process is an ideal welding process for both automated and manual processes every time.

1.4.2 Advantages of CMT Welding:

1. **Low Heat Input**: CMT welding minimizes the heat input for welding, reducing the risk of distortion and maintaining material properties.

2. **Precise Control**: This technique offers precise control over welding parameters, ensuring consistent and high-quality welds.

3. **Minimal Spatter**: CMT welding produces minimal spatter, resulting in cleaner welds and reducing the need for post-weld cleanup.

4. **Versatility**: It can be used with various materials, including aluminum, stainless steel, and others, making it suitable for a wide range of applications.

5. **Thin Material Welding**: CMT welding is well-suited for welding thin materials, providing strong and reliable welds without distortion or burn-through.

6. **Reduced Distortion**: With controlled heat input and precise control, CMT welding minimizes distortion, maintaining the integrity of welded components.

7. **High Efficiency**: Its efficiency and productivity are enhanced due to consistent weld quality, reducing overall production costs, and improving throughout.

8. **Increased Weld Strength**: CMT welding produces welds with high strength and integrity, ensuring the reliability and durability of welded structures.

9. **Enhanced Operator Comfort**: The low spatter and reduced heat input make CMT welding more comfortable for operators, leading to better working conditions.

10. **Adaptability to Automation**: CMT welding can be easily integrated into automated welding systems, further improving efficiency and consistency in production processes.

1.4.3 Limitation of CMT Welding:

1. **Equipment Cost**: The initial investment for CMT welding equipment can be relatively high compared to traditional welding methods, which may pose a barrier to adoption for some users.

2. **Complexity**: CMT welding requires specialized equipment and training for proper implementation, leading to increased complexity compared to simpler welding techniques.

3. **Limited Penetration**: Due to its low heat input nature, CMT welding may struggle with achieving deep penetration in thicker materials, potentially limiting its applicability in certain scenarios.

4. **Sensitive to Material Condition**: CMT welding can be sensitive to variations in material thickness, surface condition, and fit-up accuracy, requiring careful preparation to achieve optimal results.

5. **Process Sensitivity**: The effectiveness of CMT welding can be influenced by factors such as wire feed speed, voltage, and arc length, requiring precise parameter control for successful welds.

6. **Skill Requirement**: Mastering CMT welding techniques requires training and experience, and operators may need time to become proficient in optimizing settings and parameters for different applications.

7. **Limited to Certain Materials**: While versatile, CMT welding may not be suitable for all materials or welding positions, potentially limiting its utility in specific fabrication scenarios or industries.

The effectiveness of this process control is demonstrated in the deposition rate analysis of the CMT Process on a workpiece made up of mild steel with 3 mm, revealing minimal variation in welding frequency with different welding parameters [68]. Cold metal transfer welding finds frequent use in welding thin sheets of low carbon, dissimilar junctions, and aluminium [69-71].

1.5   MOTIVATIONS

Despite extensive work done by the researchers, it was observed that the mechanical and microstructural properties of base material will change due to melting, during the welding process of Al-alloy and its metal matrix composite. The melting of base material during welding will reduce the strength. In the current scenario, the FSW as green technology and diffusion bonding is used to form a weld in high-strength Al-alloy. However, the FSW showed poor flexibility, and the diffusion bonding was observed as a less efficient welding process and needed a vacuum chamber to perform the weld. So, these solid-phase welding processes have limitations in their application. On the other side TIG welding, MIG welding, laser, and many more conventional fusion welding processes, create a fusion zone that generates thick intermetallic compound layers, that are prone to crack and tremendously affect the joint strength. CMT is a short-circuiting metal transfer technique based MIG welding process that requires little heat input and produces no spatter. CMT welding as a low heat input welding process is capable of reducing the formation of intermetallic compound layers and also capable of welding dissimilar metals like Al and steel with excellent welding performances. CMT Welding is the alternative method that overcomes all the above-mentioned difficulties. Therefore, there is a need for CMT welding.

1.6 OUTLINE OF THE THESIS

To evaluate the performance of the CMT welding process for welding metal matrix composite of hard-to-weld AA7475 in T7351 alloy in tempered condition and its MMC, which has applications in aerospace, automobiles, and marine sectors was performed. The mechanical and microstructural properties were analysed and reported for the welded samples. The current study is divided into six chapters. A detailed description of the chapters is given below:

CHAPTER 1 INTRODUCTION

The detailed introduction and applications of AA7475 alloy in the different modern sectors where low-weight and high-strength materials are required are discussed in this chapter. The CMT welding process as a low heat input advanced welding method with its waveform and variants, applicable for low melting point material were discussed in detail. Also, the fabrication process of aluminium metal matrix composite (AMMC) by using a stir-casting setup and process in a hybrid form where two or more reinforcements were used was discussed in detail. The robotic CMT welding as a new and advanced welding method was used to weld a fabricated metal matrix composite of Al7475 alloy.

CHAPTER 2 LITERATURE REVIEW

A thorough assessment of the literature was done about the creation of metal matrix composite, its welding, and also the welding of Al-alloy. The literature that deals with the applicability of CMT welding for different series of Al alloys with age hard enables AA7xxx alloy and fabrication process of metal matrix composites by using reinforcement

in hybrid forms were studied and discussed. Based on the literature review, and from the conclusion of the reviewed literature, the motivation, the research gaps, and the problem statement were finalized. The conclusions of the literature review and problem statement will help to decide the research objectives and be presented at the end of the chapter.

CHAPTER 3 METHODOLOGY FOR FABRICATION OF AMMC

The experimentation process to fabricate a hybrid aluminium metal matrix composite is discussed in this chapter. The experimental setup and process, selection of material, reinforcement selection, and plan of experimentation are discussed in detail. The chapter also contains the details of the base material, reinforcement compositions, and composite material properties. The experimental setup and procedure were discussed to form a composite with suitable reinforcements. Different combinations of reinforcement were tried to form a composite and described in detail. Finally, the mechanical properties were tested for different sets of fabricated composites, and the final composite was selected and re-casted, based on the best mechanical properties, and analysed.

CHAPTER 4 METHODOLOGY FOR CMT WELDING OF FABRICATED AMMC

This chapter carries the details about the investigation of welding parameters, methods, and process parameters to form an AMMC weld. The robotic CMT welding setup, filler material used, and welding process are described in detail. The welding process variables are optimized by using an experimental design. The optimized parameters are used to weld the fabricated hybrid composite. Finally, the hybrid AMMC was welded by using a robotic CMT setup, and the welded plate and samples were prepared for mechanical and microstructural examination.

CHAPTER 5 RESULT AND DISCUSSION

The results were discussed in detail by analysing the microstructural and mechanical properties of the fabricated metal matrix composite and its weld. To verify the process parameters, various mechanical attributes were examined such as microhardness, % elongation, yield strength, tensile strength, and microhardness. The TS, YS, percentage elongation, microhardness, as well as microstructure, were used to discuss the findings of casted composite and its weld. The chosen welding parameter is used to validate the experimental results through the confirmatory test. The final welding parameters are also applied to weld the Al-alloy 7475 in T7351 tempered conditions. The microstructure and mechanical properties with SEM and its corresponding EDX were used to analyse the weld sample. The fractography of tensile-tested samples was used to describe the findings in detail.

CHAPTER 6 CONCLUSIONS AND FUTURE SCOPE

The conclusions and findings are reported in this chapter for the research work performed to fabricate an aluminium metal matrix composite by using more than two reinforcements of micro size in a hybrid form and to weld the fabricated metal matrix composite of AA7xxx series alloy by using the robotic CMT welding process. The findings from the formed composites were also concluded and reported. The measure findings are supported by the confirmatory test performed on fabricated composite as well as on Al7475 in T7351 tempered base alloy. This section ends by listing the conclusion of welded Al7475 in T7351 tempered base alloy. Finally, the future direction of the conducted research work is discussed at the end.

CHAPTER 2

LITERATURE REVIEW

2.1   INTRODUCTION

Nowadays, the aerospace, automotive, and other transportation industries employ aluminum alloy and its composite extensively because of its exceptional mechanical qualities, which include outstanding strength, high corrosion resistance, lightweight, high toughness, and good recycling capabilities. Al-alloys show improved mechanical, microstructural, tribological, corrosion, and wear properties by 30-40% when they are reinforced by some reinforcement particles like carbon, B_4C, SiC, Al_2O_3, Gr, CNT, graphene, MoS_2, etc [72-75]. If the particle size of reinforcements is less than 100 nanometres, the formed composite is known as an aluminum matrix nanocomposite (AMNC) [76]. AMNC is currently used to improve the properties of engineering materials [77]. It has been observed that the nano-particle-reinforced composite shows superior properties as compared to the micro-sized particle-reinforced composite material [78-81]. However, it was found that as the concentration of hard ceramic particles increases in the metal matrix composite, the metal matrix composite starts losing its tensile strength and ductility with improvement in hardness [82-84]. Whereas, in the case of nano-particle-reinforcement the ductility is maintained with the increase in yield and tensile strength [85]. Nano-particle reinforcements additionally impart better creep and fatigue resistance [86], but the cost of using nano-reinforcements is comparatively high. The AMMC overall provides better mechanical, wear, corrosion, fatigue, and creep resistance by maintaining high strength and lower weight with low density [87-88]. The limitation that is associated with the AMMC is its high cost of

fabrication [89]. The stir-casting process is considered to fabricate the AMMC because it is less costly as compared to other fabrication processes [90]. The fabrication of AMMC high-cost consuming process and the cost reduction can be done by using cheaper reinforcement, a large volume of production, and a simple fabrication process. Because of the aforementioned characteristics, stir-casting is thought to be the most cost-effective method for the fabrication of AMMC.

The existing literature can be classified into the following groups that deal with:

i.   CMT welding as an effective route of welding Al alloy and AMMC

ii.   Previous Studies on MMC and its processing.

iii.   Studies for selection of suitable reinforcement for Al-based metal matrix composite (AMMC).

2.2 CMT WELDING OF ALUMINIUM ALLOYS

2.2.1 2XXX Series

The Al-alloys of the 2000 series is a set of hard alloys carrying a chemical composition, in terms of wt.%: Cu- 2.5, Zn <1.3, Fe <0.25, Mg- 0.52, Mn-1, and Si >0.10-0.35, the rest being aluminium, and some foreign elements and contaminations. The copper in the composition is increasing its substantial strength and incubating precipitation hardening and decreasing the ductility as well as corrosion resistance. The 2000 series aluminium alloy layer is used in forged, heavy, and extruded materials, first-stage fuel tanks, multistage rockets, vehicle frames, and suspension systems (AA2014) [91-92]. AA2017 series of alloy sheets have applications mainly for rivets, common mechanical parts, propellers, and their accessories. The AA2024 alloy plate is mostly used in aircraft systems, rocket parts, vehicle hubs, propellers, and other similar applications.

Aluminium alloy plate AA2036 is often found in car body parts. Aluminium alloy layers AA2048 and AA2124 were mostly used in ordinance structural components and aerospace. AA2218 series of aluminum alloy plates are used in the pistons of heavy-duty diesel engines, aircraft engines, cylinder heads, compressor rings, and impellers of jet engines.

CMT is a corrected model of the MIG welding technique made of short-circuiting exchange and distinguished by less heat intake and no-spatter joining operation, according to Fang et al. [93]. The basic objective of this analysis is to look at the waveform of the CMT mechanism in terms of current, voltage, and metal transfer mode. A signal is sent to the blow torch as the puddle reaches contact with the weld repository, which switches the path of the flowing wire, allowing the span made of liquid to blow out as well as material flowing into the welding tank. As soon as the droplet comes into close contact with the weld reservoir, a signal is sent to the wire feeder, which turns the direction of the advancing wire, splitting the flow of liquid and feeding the metal into the weld pool. As a result, the metal transfer mechanism can be concluded to be very stable by using regulated auxiliary back-drawing ability and unique wave capabilities. Placing beads on a plate of thin and clean Al sheets reveals a strong appearance due to the spatter-free welding process [93]. In the CMT method, the weld bead assembly is very consistent and smooth. During the arc-ignition time, the duration of the liquid droplet affixing at the electrode tip is almost equal to the diameter of the wire, and the prone breakup of liquid duration is very steady. Due to this, the heat input is diminished promptly. CMT's low heat intake promotes gap bridging, thus eliminating the deformation of thin sheets welding of Al and its alloys [93].

Baoqiang et al. [94], have investigated the use of CMT and its derivatives on the geometry of the welded joint, heat inputs, and porosity for a high-strength Al alloy joint (AA2219-T851) with ER2319 filler wire. Gas pores were found in great numbers in the upper and bottom regions of welds, as per the research. In contrast to the standard CMT techniques, the CMT+P process effectively increases the weld melting region. Porosity can be reduced by applying the right amount of heat. A finger-shaped geometry can be accomplished using the CMT-advance technique with a substantial reduction in melting depth. Additionally, this looked at the energy inputs and metal transfer processes for different droplet transfer modes. The geometry of the weld bead was represented by a welded strengthening (dH), melting depth (D), melted height (H), and width of melting (B). The diameter and reinforcement for the weld are found to be lower as the welding speed increases, which corresponds to a reduced heat input for all CMT methods. As a result, for all modes of the CMT operation, the energy input has a notable impact on the weld bead configuration [94].

The various processes and their heat input have a noticeable effect on the porosity. As a result, it can be inferred that using the necessary HI (heat input) to minimize porosity is beneficial. With reduced HI, the CMT-advance procedure decreases the number of pores and their size, making it more difficult to locate pores. Using the CMT-advance pulse phase [94-95], the gas porosity is almost eliminated. Porosity has been seen to have a direct relationship with grain size in previous studies [96-97]. It is advantageous to effectively remove porosity by providing the requisite heat input, by using the CMT-advance pulse (CMT-PADV) method. The CMT-PADV method almost eliminates porosity. In the traditional CMT system, a small finger-shaped molten pool is formed, preventing gas holes from escaping; at the same time, the coarse columnar grain

structure promotes porosity creation. As a result, the samples created via the traditional CMT procedure have a huge number of pores. Even though the HI of the CMT+P method is higher than that of the standard CMT method with the same WFS (wire feed system) and WS (welding speed), the porosity will still be greatly reduced. It is noted that the weld pool volume is larger, implying that the chances of gas escapement are greater than in the traditional CMT method with similar melting widths. The CMT-ADV method reveals a finger-shaped geometry having lower HI as well as a blend of finer columnar as well as equiaxed grain patterns. The CMT-ADV method generates much shallower penetrations, reducing its impact on gas escapement dramatically. Since the CMT-ADV process has a lower heat input (HI) than the CMT+P process, the structure of the grains is found to be more polished. The CMT-PADV technique allows for the lowest dilution and finest grain structure which is equiaxed. This technique combines the benefits of the CMT-P as well as CMT-ADV, making it the most efficient and effective for removing porosity entirely [94].

2.2.2 5XXX Series

The 5000 series of aluminium/magnesium alloys are a set of hard alloys. These have Mg - 0.2 to 6.2% and carry the maximum strength out of all available non-heat-treatable Al alloys. The other constituents with this series of Al alloys are manganese, chromium, and titanium. They provide very good corrosion resistance for marine applications. This category of Al alloys has wide applications in sheets, plates, wire, tubes, welding rods, electrodes, conductors, forging stocks, and foils. These alloys are preferably used for automotive structural parts [98-99]. Low to moderate strength and high weldability are both properties of the 5000 series Al alloys. They are not very

suitable for cold working operations at elevated temperatures and can lead to stress corrosion.

Zapico et al. [100], worked on an AA5754 Al-Mg alloy plate having a width and length in the direction of welding which is 180 mm and 300 mm respectively. A welding power source, a robotic arm, an oscilloscope, and a thermocouple data acquisition device were all used in the experiment. A time-dependent volumetric heat flux diffusion model for automatic CMT welding is proposed in this work. The simulation tests for fugitive and steady-state diffusion of temperature within the weld and HAZ were conducted. The developed simulation gives us a chance for process optimization and sensitivity investigation in future applications [101]. The material properties were assumed to be temperature-dependent in this study. For both calculations, the thermal conductivity and basic heat capacity values for Al/Mg alloy were used. While using liquid-phase material characteristics, the latent heat of melting was not taken into account to make the model useable. Fourier's rule for heat conduction was used to design a heat transfer pattern in the workpiece. The average temperature of 1300^0C is considered after the steady-state conditions have been reached in approximately 5s. The elimination of the oxide phase is aided by the high-temperature gradient across maximum and ordinary temperatures, which limits welding energy and thus extends the HAZ. The simulation showed the fundamental phenomena that explain the experimentally measured advances in weld quality of thin Al-alloy plates when compared to traditional joining techniques. The thermocouple temperature readings and a microscopic examination of the fusion zone were studied, proving the model validity [100].

2.2.3   6XXX Series

The main constituents of 6000 series Al alloys are the Al-Mg-silicon with Mg 1% and Si 1% are found useful in the fabrication industry and used primarily in the form of structural components. Al alloys in the 6XXX series are known for their low cost and reasonable strength and their uses depend on the maturity of their joining methods. They can be joined with both 4xxx series and 5xxx series filler wire, depending upon the applications. Al 6061 is widely used in the automobile industry [2], as well as in marine structures, pipelines, aircraft parts, and components.

Pickin et al. [102], have studied the CMT as an automatic dip transfer joining procedure that features monitored material discharge during the wire electrode's short circuit to the workpiece. CMT welding has a higher electrode melting coefficient than MIG welding, according to tests. A marginal change in electrode deposition may be used to measure penetration by changing the frequency of the short circuit. The electrical oscillations of the welding process have been recorded, as well as the weld penetration patterns are analysed during the tests, which are carried out on an AA 6111 plate. As compared to the pulsed MIG operation, CMT has a lower thermal input while still having a higher wire melting coefficient. The following relationships for CMT are obtained from SPMIG welding: (i) SPMIG; $W_f = 0.0480$ Im (ii) CMT; $W_f = 0.0583$ Im. Weld bead penetration is reduced as the short circuit period increases, but the weld material deposition is slightly reduced. The penetration depth can be monitored by keeping a constant frequency of triggers and adjusting the quantity of CMT power surges. It is observed that by increasing the short circuits, shallower penetration takes place due to reduced thermal input. Control over-penetration was done by varying both that are each pulse of peak current and the number of applied pulses. When pulsed MIG

welding is combined with CMT-P welding, a thicker material plate can be welded while maintaining reasonable weld bead aesthetics and control over penetration. As a result, with the above-mentioned features, CMT emerges as an extremely competitive welding process for welding Al and its alloys [102].

Cornacchia et al. [103] assessed the surface morphology of the welds and mechanical characteristics of the weldments, and the weld performance was compared with modern welding methods such as CMT as well as fiber laser-MIG combination joining on a 6005AT6 corrugated piece. To measure the effect of these diverse welding techniques on the characteristics of Al-alloy, an ER 4043 cable was used as filler material for all welding forms. A welding system with argon as protecting gas was used to create the seam welds. Manual CMT welding was done using a Fronius Trans-Plus Synergic 5000 CMT welding unit. The mechanical and metallurgical effects of fiber laser-MIG combination, MIG, and CMT welds of aluminium and its alloys were compared. The macrostructures reveal that the fiber laser joint has higher quality in the form of welding defects. The amount of porosity in MIG welds is higher than in CMT welds, but it is not as large as in fiber laser-MIG hybrids. The microstructures of all three joining methods are identical, with dendrites, defining the weld seam. The heat-impacted region of a MIG weld is greater than that of a CMT or fiber laser weld. In comparison to MIG and CMT, the mechanical properties of the fiber laser MIG hybrid welds are excellent. So, it was stated that fiber lasers are suitable for the majority of applications due to their high precision power, decent beam efficiency, low maintenance costs, comparatively lower heat supply, lower electrical energy consumption, and small size [46-47]. The macrostructures reveal that fiber laser welds have superior efficiency in terms of welding defects. However, the disadvantages of laser welding include intense melting of reflecting

or thermally conductive materials, high laser tool costs, and the risk of welding flaws like porosity in acutely penetrating weld fusion regions, which limits its applications. Also, intermetallic was perceived at the interface of HAZ/FZ for all the processes. Similar microstructures were observed for all three joining methods and the weld seam was characterized by dendrites. As a result, it is anticipated that a reduction in localized energy intake would minimize the PMZ, there is a softening, and as a result, hot cracking will be minimized in the case of CMT which dominates its uses over the other [103].

Ahmad, et al. [104], have investigated the effect of post-welded heat treatment (PWHT), quenching as well as aging produced artificially, on the properties of AA6061 Al alloy weld, produced by applying the GMAW CMT technique. Heat therapies in solution, accompanied by aging and water quenching at a specified temperature probe, are used for Al alloys in the 6xxx series. For the welding process, an ER 4043 filler was used. The welding samples were isolated from the non-heat-treated and PWHT samples. It was also noted that the elongation or distortion is not localized in the heat-affected region for an extended period. As a result of the tensile specimen's limited elongation capacity for an as-welded joint, the specimen's fracturing during processing was localized in the HAZ, which is considered the most fragile portion of the sample. According to the findings of the experiment, the larger value of resilience, shear stress, and flexural strength can be due to PWHT's ability to provide precise and consistent distribution of particles at the weldment. As compared to an as-welded joint, these characteristics resulted in superior tensile properties. Since the weld has increased strength level as a consequence of the PWHT update, the welded structure had a comparatively strong deformation capability. In comparison to other welds, PWHT weld has highly precise and regular positioning of particulates, which evolves as the

primary donation for the PWHT weld's excellent tensile and toughness effects [104].
The effect of heat application at immediate/post-T6 laser-welded A356 Al metal
indicates that post-T6 surface treatment results in high structural stiffness and strength
as compared to a weld without T6 thermal treatment. The heat treatment mechanism
was found to cause the coarse particle framework to shift from an irregular to a virtually
globular form. The precipitates in an externally aged joint are extraordinary and appear
uniformly dispersed in the matrix [105-106]. PWHT improved the hardness, tensile
properties, and strength of GMAW CMT-welded AA6061 joints [107-108].

The aim of Pascoal et al. [109], was to test and optimize the bead distance, penetration,
and reinforcement of robotized MIG welding using Al 5754 wire over a 6082-T6 Al-
alloy sheet. The experimental arrangement used Taguchi L27 orthogonal array to study
and took into account 12 welding criteria with three stages for each. Spray and pulsed
cold metal transfer were the two methods of metal transfer that were subjected to the
battery of checks. The width of the weld bead, the depth of penetration, and the
reinforcement were all used to control the quality of the weld. The weld width seems
to increase with the number of pulses. Since the number of pulses determines the heat
and intensity of the molten pool, it has a big influence on the weld bead size. Heat input
rises in proportion to the number of pulses. The penetration depth and weld span both
decline as the number of CMT power spikes is on the rise. The angle of interaction
increases from 30 to 126 degrees by raising the pulse/weld cycle from zero to twelve.
The wettability of the molten pool is significantly enhanced by the added pulse. The
contact angle decreases as the increase in the frequency of the short circuit of the CMT,
resulting in a lower heat supply. The contact angle falls from 100 to 24 as the quantity
of CMT electric shock per weld time increases from one to eight. The CMT + P method

was used to calculate all of the weldment in this analysis and was found to be a reliable joining technique with no spattering. CMT pulses provide a higher arc current than CMT alone. In CMT + P welding, expanding the number of pulses results in a much greater penetration depth and weld bead touch angle [109].

The CMT + P transfer mode, according to Pang et al. [110], is a combination of a single droplet of every pulse expected transfer mode and a cold metal transfer short circuit mode. Both experiments were carried out with AA6061-T6 as base metal and with a filler thread of ER4043. A weld interval is made up of pulse duration as well as the period of CMT short-circuit. The wire electrode melts and is forced into the weld zone after the spark activates. The wire electrode is then withdrawn, and the liquid metal bridge is ruptured with the aid of the back-drawing power. The weld pool wettability is greatly improved by the applied pulse. If the quantity of CMT power surges continues to grow, the heat input decreases, lowering the touch angle. The CMT pulses have significantly more arc current than CMT alone. The arc energy distribution has been modified, which increases the magnitude of the heating rate. As the amount of CMT power surges grows, so does the weld penetration. To improve the penetration depth as well as the weld bead contact angle, the frequency of surges throughout the CMT + P phase might be increased [110].

Caruso et al. [111], studied the characteristics of weld formed for AA 6005-T6 alloy using combined laser-MIG and CMT welding. On welded sections, the tensile, bending, shear, as well as fatigue tests were conducted to assess the comparative performance of the hybrid laser-MIG, FSW, and CMT welding process with the MIG welding. The data was closely examined, and a comparison of all the above welding techniques was presented. MIG welding was found to be more ductile in a tensile test than the other

three approaches, although both hybrid laser-MIG and FSW procedures outperformed over conventional MIG welding in a load resistance test. When comparing all three weldings in the bending test, no major differences were found. When it comes to shear resistance, MIG welding is more ductile than both hybrid laser-MIG and FSW procedures, while both hybrid laser-MIG and FSW procedures have improved load resistance activity than conventional MIG welding. Finally, the fatigue life test showed that, when hybrid laser-MIG and FSW welding were compared to MIG welding, the cycles to failure increased, while the cycles to failure decreased in CMT welding in comparison to MIG welding [111].

Yang Lei et al. [112], compared three welding arc modes based on the CMT welding method, namely traditional, pulsed, and CMT to determine the best welding arc modes. The AA6061-T6 was used in this analysis, with the ER 4043 as filler metal. Four different types of CMT spot welding techniques for joining Al alloys were advocated to address the problems with SPR: direct welding (DW), plug welding (PW), and DW on the chill block (DWB). Weld strength, microhardness, surface morphology, ductility, and fracture mechanics were used to assess the relative efficiency of the four modes. The best process model was chosen based on these evaluations. Among all the welding arc mechanisms and material piles investigated, the CMT arc phase created the least possible welding flaws, like gas pores or partial ripping, resulting in welded joints with the highest mechanical properties. Welding the bottom sheet with a chill block inhibits weld metal from pouring out, speeds up heat loss at the welded bottom, and reduces the HAZ inside the bottom sheet. Since the CMT arc mode causes no partial tearing, this weld has the strongest load-bearing portion and as a result, the highest lap shear pressure. Welding deficiencies including partial splitting made it difficult to

achieve optimum welds while using the plug welding (PW) mode. The weld's fracture propagation stage was significantly higher in DW mode [112].

For AA6061 alloy joints, the effect of gap width on weld properties was analysed by Guojina et al. [113]. The effect of several factors on the development of welds, as well as the methodologies that activate the C + A patterns, on gap-bridging performance, was investigated. Both tests used, an Al-6061 as base metal with a filler material of ER4043. CMT Advanced 4000R welding technology was used in conjunction with a robot from ABB in this research. The lap joint style was chosen to keep the distance width even and consistent. The volume of molten metal and the wire feeding speed are both the same, but the distance diameter varies. When there is enough molten metal to cover a small hole, a huge welding seam results. To fill a larger hole, a substantial amount of filler metals is needed. The size of the fusion zone varies depending on the wire feeding speed. By the higher pace of wire fed, the wetting angle decreases and the weld formation improves with the larger penetration. The strength of the joint is linked to this aspect. The fusion zone's hardness was higher compared to the base metals. The HAZ was the site of fracturing [113]. The researchers looked at bead shape, microhardness, shear resistance, fracturing characteristics, and forming mechanism. The bead shape was influenced by the wireless power transfer pace and cord offset. The wire offset was significantly changed to improve the visibility of the welding beads. The required standards for different gap spacing were established after a series of experiments. The tension concentration in the weld root can increase as the gap diameter widens. Because of the various wire offsets, the arc's heat contribution to the lower plate is different. This will be the primary cause of the varying joint strengths. Porosity is minimal in broken surfaces, independent of the void depth. The presence of

pores allows tension to concentrate and the joint strength to deteriorate. The consequences of these porosities are not very important, based on the findings of the shear strength examination data. Since the CMT configuration has a higher thermal input than that of the C + A mode, the C + A feature has a larger wetting angle. Besides that, the C + A mode's aggregation area is larger than that of CMT configurations. When the gap diameter widened, so did the penetration, and as the gap widened, so did the shear pressure. The fusion zone hardness was higher compared to the base material. Increased gap depth has little effect on hardness. The joint's fracturing mode was a ductile fracture. Regardless of gap depth, the broken surfaces had low porosities. Near the pole, there was no visible microcracking. The HAZ was the site of the crack. The C + A mode had a higher deposition efficiency than the universal CMT mode due to the larger negative polarity droplets. The heating rate of the CMT phase was roughly 1.37 times as much as the C + A mode [113].

Koli et al. [114], have worked to utilize bead-on-plate measures to assess the effectiveness of CMT joining. For this, the weld metal configurations of three different CMT, MIG-P fusion welding synergic, and MIG Skilled were investigated. The experiments were carried out on the AA6061-T6 plate and the bead-on-plate was investigated with ER4043 (AlSi5%) filler wire. As control factors, welding speed, flow rate of shielding gas, and contact tip-to-work-piece distance (CTWD) were held constant. Monitoring the weld metal arrangement contrasts and the weld beads were processed by all three procedures. The microstructure is described using optical microscopy as well as Field Emission Scanning Electron Microscopy (FESEM). As a result, CMT has lower residual stresses than MIG Pulse and MIG Manual. CMT has a

finer grain structure than MIG P as well as MIG M because of its better hardness attributes [114].

2.2.4   7xxx Series:

In the 7XXX Series of Al-Zn alloys, the Zn content is from 0.8 to 12 %, and they are among the strongest Al-alloys. Critical applications, like aero-planes, transportation, and professional sports goods also use these alloys. The 7xxx series of Al alloy is mostly welded by using 5xxx series filler wires. The CMT process has become a sound approach for improving the mechanical properties of a hard-to-weld 7xxx series Al alloy. Even though heat-treatable 7xxx series Al alloys can be welded with CMT welding to address the majority of the welding constraints, a few works have been undertaken in this area. The CMT welded joints mechanical properties are compared to those of other welding methods to examine the process potential advantages for joining 7000 series Al alloys that seem to be hard to weld [115].

Elrefaey et al. [115], have investigated the interaction between the micro-structure and its material performance of 7075-aluminum alloy and their comparable characteristics after welding. In this experiment, a 2 mm thick T6 (solution treated + artificially aged) layer of Al-alloy 7075 was used. Coupons are sliced and then arranged in a butt weld so that there is no space between the sheets. Argon shielding gas was turned on before 3 seconds the arc reached, with a gas flow rate of 15 liters per minute. The robotic CMT was used to do the welding, with the torch set at a 10^0 angle from the perpendicular axis. The joints have fine cross-section weld profiles and tidy bead profiles. Ripples that are consistent, tight, and uniform suggest a good weld that is free of contamination or cracks. The joints have almost no spatter, demonstrating the CMT process ability to

manufacture joints with almost no weld spatter. Pores were detected in the joint pass, with the majority of them in the middle and lower levels. In addition, hardly any spatter, cracks, or quite low porosity is found in the CMT 7075-T6 joint [116]. The weldment microstructure reveals equiaxed grains. The grains have a dendritic form, and the outside of the weld has even more columnar dendritic cells than dendrites in the center due to the temperature gradient, from a WM SEM micrograph. The region between both the WM as well as the BM can be divided into two main sections: the partly melted zone (PMZ) and also the HAZ. The EDS study of permeated particulates confirmed the equimolar stoichiometry spread of HAZ grains. The microhardness distribution along with the joint increases steadily from WM to HAZ. Hardness values are found to be the lowest in the WM. The WM had the lowest microhardness in contrast to the BM, and the HAZ had a marginal hardness decline [117]. In the WM, the reinforcement elements Zn and Mg are much smaller than in the BM. The weldment microstructure reveals equiaxed grains. The absence of alloying elements, precipitates, and particle sizes pervasiveness within WM leads to lower microhardness [95]. The mechanical property coefficients of the joint were 77 percent, 60 percent, and 69 percent, respectively, for yield strength, total tensile strength, and elongation [115].

Selvamani et al. [118], used a sophisticated TPS 400i Cold Metal Transfer welding system to join AA7075 alloys, to better appreciate the weldment homogeneity in terms of micro-hardness as well as the interaction between fracture toughness and joint morphology. The microstructure of the weld revealed no flaws in the weldment, as well as uniform grain distribution and only minute pores. The durability of the weld zone was discovered to be weaker than the base metal including HAZ when the microhardness gap between the weldments was tested [119]. Because of the regulated

heating rate during the welding and the rapid solidification of the melted liquid, the HAZ was observed to be quite narrow [118-120]. The weld zone produced fine grains with no phase transformation flaws, as well as the HAZ was realized to be very short. As a consequence of the tests, the hardness of various regions and their respective particle shape of the joints are compared. To match the experimental data sets, a linear equation has been used, that was governed by the given regression model: -1.1017 (particle size) + 169.97 Hv. The slope (1.1017) of the above regression equation is negative, meaning that the hardness of the completely deformed area decreases with the increase in grain size. The adverse correlation between the grain size and the hardness of the CMT-welded AA7075 Al alloy joints is observed. There were no solidification defects in the weld, and the grains were homogeneous as well as very fine.

The WM hardness was found to be lower than the HAZ and base metals, and the joint has no defects and small grains within WZ, according to the metallurgical description. The regression study slope is negative, meaning that the hardness of the fully deformed area decreases as grain size increases. The hardness of CMT welding of AA7075 Al alloy welds was in inverse proportion to grain size [118].

2.2.5 CMT Welding for Dissimilar Metal Joining

The CMT process is capable of efficiently producing a dissimilar metal joint. CMT welding has been the "hot direction" for solving the problem of dissimilar metal joining because of its high accuracy. As a result, a low-heat-input, high-performance fusion welding process [121], could provide a viable option for implementing aluminium in many applications.

In this regard, an aluminum alloy is joined with zinc-coated steel by Zhang et al. [122] and the arc characteristics, as well as a droplet transfer mechanism, were studied, using video monitoring at high speeds. The objective of the research is to look into the CMT modes of metal transfer and arc characteristics, as well as how it could be used to weld and braze the aluminium as well as Zn-coated steel in a lap configuration. To determine the welding process applicability in the joining of dissimilar metals, the tensile properties and microstructure of the weld were examined. The hot-dip galvanized steel plate having a thickness of about 0.6 mm and plain Al 1060 sheet with a thickness of around 1 mm were used in the welding processes. The filler material was an Al-Si alloy wire. The sample surfaces were cleaned with acetone before welding. The findings demonstrate that CMT can produce no-spatter welding using less energy input during the welding process. The CMT technique enables dissimilar metals to be joined without cracking in a lap joint, such as aluminium and zinc-coated steel tube. Fe_2Al_5 and $FeAl_3$ phases make up the intersection of steel and weld metal. There is a complex layer of transparent intermetallic coating between both the steel as well as the work material formed during the welding process. Both of the fractures were found in the aluminium heat-affected territory. The CMT metal transfer system is highly durable, and the arc heating action can be altered by back-drawing power and special wave control features. Using the CMT technique, it is possible to join dissimilar materials like aluminium to zinc-coated steel sheets without cracks. To maintain joint strength, the width of the intermetallic coating could be controlled [122].

In a study performed by Shang et al. [123], the 6061 Al alloy was bonded with the AZ31B Mg alloy by CMT welding using copper wire (HS201) as the filler material. In this experiment, extruded AZ31B Mg alloy samples were welded together with 6061 Al alloy

samples. SEM, optical microscopy, and energy-dispersive X-ray diffraction (EDX) were all utilized to examine the characteristics of Mg/Al CMT weldment. It was discovered that the microhardness on both faces of a fused zone improved sharply, on both the Mg and Al sides. In the sides of fusion zones for both the Mg and Al, micro-hardness increased significantly. The fusion region intermetallic compound coating on the Mg side of the joint was brittlely broken, with a lot of Cu_2Mg intermetallic compounds spread around. In terms of dissimilar metals under the right operating conditions, CMT may successfully join Mg/Al metals [123].

It has been reported by Gungora et al. [124], that the pulsed robotic CMT and CMT-MIG methods have been used to weld the excellent corrosion resistance and medium strength AA5083-H111 as well as 6082-T651 Al alloy. The aim of the investigation is just to assess the mechanical behaviour of similar and dissimilar weldments of aluminum alloys 5083-H111 and 6082-T651. Joints were fabricated using 6 mm thick sheets as both similar and dissimilar metal combinations. According to the findings, CMT-MIG provides high welding speed, good joint efficiency with excellent tensile as well as fatigue tolerance. M55 denotes weld of 5083 to 5083 and M66 denotes 6082 to 6082 alloys, as well as dissimilar alloys M56 refers to welding 5083 to 6082 alloys. In comparison to the M55 joint, tensile test specimens from the M56 and M66 joints were broken at the HAZ of the 6082 as base material. The best fatigue result is achieved by 5083 identical weld joints M55, trailed by 6082 identical weld connections M66, and 5083 to 6082 dissimilar weld junctions M56. These findings were paralleled in the porosity as well as yield stress of the associated joints [124].

The development of the microstructure at the fusion boundary and its influence over the TS value of the CMT weld formed for Al 5754 and Al 5083 alloys have been studied by Rajeshkumar et al. [125]. The study shows that a non-dendritic equiaxed fine zone (EQZ) has recently developed between the PMZ and the WM zone. In addition to having a broader EQZ at the Al 5083 interface, the Al 5754 interface also features coarser-grained EQZ. WMZ dendrites at the AA5754 interface are coarser than those at the A5083 interface, apart from all these variations. The aforementioned characteristics have significantly reduced the AA5754 interface strength. Strength ratings are less favourable in the interface regions than in the WMZ. It was concluded that the primary cause of the decline in the strength value at the interfaces is the existence of EQZ rather than WMZ. Additionally, Si segregation is higher at the EQZ grain boundaries over both interfaces. Non-dendritic EQZ had developed at the dissimilar weldment surfaces [125].

Koli et al. [126] have made an effort to produce the joints, for which ultrasonic-assisted CMT (U-CMT) welding is used to investigate the enhancement in mechanical characteristics as well as microstructural alterations. Numerous improvements in the quality of the joint could be observed with the use of CMT welding assisted by ultrasonic vibration. Using ultrasonic vibrations, the molten weld region solidifies more quickly, enabling an additional base metal to come into contact with the filler material. The U-CMT welded connections, result in an increased weld width and penetration depth, while lowering the contact angle. Furthermore, when ultrasonic vibrations are used during welding, the welded material has a finer grain structure. It generates cavitation, which aids in the refining of grains. With ultrasonic vibrations during CMT, the mechanical characteristics of the welded connection improved.

Due to grain refinement, ultrasonic-assisted CMT welding produces fine equiaxed dimples as well as micro-voids on the worn surfaces of the tensile samples. A honeycomb-like arrangement is also visible, indicating that maximal strength is expected. The radiography test shows that ultrasonic vibrations minimize porosity in the welded specimen. The study revealed that, by using ultrasonic vibrations, the weld bead dimensions are increased for the same welding settings. Tensile strength and microhardness have both been improved. Grain refining occurs in ultrasonic vibration samples; however, grain refining does not occur in non-vibration samples. As compared to CMT, U-CMT has a higher percentage of Al-Si in globular form, which minimizes porosity [126].

Çömez et al. [127], have investigated the corrosion characteristics of dissimilar Al-joints that must be evaluated to forecast the effect of the welding methods on possible corrosive agent-caused failures in their structures. The impact of heat on the mechanical characteristics as well as on the corrosion rate of AA5754 and AA7075 joints welded by CMT by employing ER5356 filler wire is investigated in this work. Because of the vaporization of zinc, pore development was detected in the HAZ of the AA7075 alloy. In contrast, the pore-free microstructure of the AA5754 side of the weld was seen. Hardness testing was used to determine over-aging in AA7075 base metal, and increased heat input exacerbated the detrimental effects of over-aging on mechanical properties. A ductile fracture was revealed by a fracture area with fine dimples. The corrosion rate decreased as heat input increased, owing to the protective effect of AA7075 base metal over-aging. The corrosion rate gradually decreased as heat input increased [127].

In this study, AA5754 and AA6061 were welded by using the CMT process, which is the best method for combining thin sheets and incompatible materials, as studied by Comez et al. [128]. Grain coarsening and excessive aging both decreased the tensile strength. The specimen with the less heat input displayed the slowest rate of corrosion. Small pits of dissolution were seen over the AA6061-WM interface for the weld specimen carrying lower heat input. It was found that the WM and BM of the specimen under high heat input were significantly pitted and corroded. It was reported that, as the heat input increases the TS of AA5754 and AA6061 weld declines. The corrosion test report reveals that, in addition to causing pitting corrosion, the increased value of heat will also reduce resistance to corrosion and induce intergranular corrosion [128].

Cao et al. [129], studied the types of filler wire on the efficiency of CMT-plug welding of thick Mg-AZ31 galvanized steel samples. The MgAZ31 with galvanized steel connections was subjected to mechanical and micro-hardness examinations. In particular, the static strength, as well as the fracture mechanism of junctions with different wires, are analysed based on weld quality. Furthermore, for a 1mm galvanized steel CMT plug attachment with 3mm in thickness MgAZ31 metal, a suitable wire is proposed. The MgAZ31 alloy and galvanized steel with MgAZ61 wire were joined using a CMT-plug weld. MgAZ31 galvanized sheet metal was plug welded using Mg-Zn eutectic by CMT with thin Fe-Al interlayer contributed to higher joint static strength and precision. An excellent Mg-AZ31 and galvanized steel couplings with MgAZ61 wire were produced across all wires assessed in this study. The results revealed that the MgAZ31 weld metal fracturing pattern pulled out, due to the formation of a thin fusion zone between WM and the base metal. Whereas galvanized steel with Mg AZ31

couplings constructed by using NRNiCu-7 wire achieved high pseudo-tensile strengths, localized flaws were frequently induced in the weld metals, possibly causing concern about the joint fatigue strength. Based on these findings, joining, using a CMT plug with MgAZ61 wire to connect steel that has been galvanized and MgAZ31 is recommended [130]. In high-tech industries such as automobiles, electronics, and aerospace, magnesium alloys are the best and lightest metal for parts and components [131-133]. On the other hand, welding technology for Mg alloys and other low melting points and high-strength metals is a hot subject of research right now. The intersection of new manufacturing materials necessitates the development of Al and Mg alloys in welding technology [134]. To achieve higher strength Al/Mg joints, FSW [135-136], as well as diffusion bonding [137-138] are currently in use. As a consequence, solid-phase links have a limited range of uses. In the meanwhile, TIG welding [139], MIG joining [140], laser welding [141-142], and other forms of traditional welding process continue to produce a thick intermetallic compound in the fusion region, resulting in cracks that compromise joint strength severely [143]. With a lower thermal supply, CMT welding has been shown to minimize the generation of intermetallic compounds [144] and has been used to produce Al/Steel dissimilar metal joints with good efficiency [144-145]. The intermetallic compounds eventually resulted in joint embrittlement and tension accumulation, lowering joint strength [143]. The fracturing was caused by brittle intermetallic materials that were constantly spread in the fusion field [146]. Fracture took place on the Mg side in the fusion region, where the micro-hardness value was highest [143-146], and brittle fracture mode was present. Before destructive trials, non-destructive studies like sensory and radiological analyses were carried out [147].

In an investigation done by Kang et al. [148], less energy-input CMT arc welding was used to join the hot-dip aluminized steel tubes with Al 5052 alloy. The dissimilar metal joint was explored with Al 4043, Al 4047, Al5356, and Al 5183, four distinct kinds of filler wires. Al 5052/aluminized steel CMT arc joining with different filler metals was investigated in this analysis and observed that the joining characteristics were similar to those of galvanized steel/Al 5052.

This welding research aims to join dissimilar materials together. Steel and Al alloys are difficult to weld together due to large variations in properties like melting points, thermal conductive properties, electrical resistivity, and high thermal correlation coefficient. The wettability of galvanized steel was strengthened by the filler metal's high Si content, which increased the molten pool fluidity; yet, the aluminized steel wetting was unaffected by the filler metal. The tensile shear strength of all material combinations increased as the tensile shear test speed was increased as an outcome of the strain rate impact. The IMC sheet thickness was lower when aluminized steel was used instead of galvanized steel. To study the impact of thick IMC films, an experiment was conducted with just an aluminized steel plate that had been pre-heated before braze welding. Aluminized steel was heated at 600°C in the operation for 16 hours and produced the IMC coating which was twice as thick as that of the aluminized steel plate originally supplied [148]. Microcracks with porosities develop resulting in a thinner IMC layer with a lower tensile strength. As opposed to aluminized steel samples, galvanized steel samples had greater wettability. The joint strength deteriorated when the salt spray period was extended in a salt spray corrosion investigation [148].

Xiea et al. [149], Studied the localized microstructure, mechanical characteristics, as well as fracture pattern of the Al5.5Zn2.5Mg2.2Cu Al-alloy was successfully fused by utilizing CMT welding. The robotic CMT technology was used to butt weld the Al5.5Zn2.5Mg2.2Cu Al-alloys. Closely comparable Al5.5Zn2.5Mg2.2Cu Al-alloy plates have just been welded with each other in a butt joint configuration. Over 360 hours of natural aging, its microstructure, mechanical characteristics, as well as tearing behaviour of the weld junction were examined. According to the microstructure study of the joint created by using a CMT process, the HAZ has fibrous tissue grade over the localized areas in SSZ > OSZ > BM, as well as the fibrous tissue coarsening in SSZ > OSZ > BM. The WZ fracture surfaces include tiny intermetallic dimples with a smoother rim, indicating strong plasticity, from the SEM fractography review. The fracture surfaces of the BM, which are made up of broken precipitates and tiny dimples, prevent dislocation movement and increase the BM strength. The precipitated layer coarsening, as well as the HAZ precipitate-free zone extension, are both effects of the HAZ, which are the key reasons that contribute to a decrease in mechanical characteristics in comparison to the BM, resulting in a considerable decrease in stiffness, but a bigger elongation. According to SEM fractography analysis, the HAZ precipitates are coarser at the grain boundaries than the BM. Within a matrix, a large quantity of secondary phase granules was precipitated, reducing the HAZ strength [149].

Aluminum alloy to steel CMT arc spot welding was reported by Lei et al. [150]. The welding torch movement was regulated by an ABB IRB 1410 industry robot, which used a Fronius Trans-Pulse Synergic 3200 CMT welding system to perform CMT arc spot-welds of aluminium to galvanized steel sheet. The welding wire used was $AlSi_5$ ER-4043 with pure argon as shielding gas. The welds were examined and compared

after exposure concerning macro and microstructure, mechanical characteristics joint geometry, and other factors. The open circuit potential (OCP) of zinc coating on the steel plate was found to be the lowest, corresponding to the weld bottom surface. The Fe-Al IMC layer in the interface that was combined with zinc equally had a very low open circuit potential (OCP). Because of the mixed build-up of zinc vapor during welding, the OCP of the aluminum weld metal was significantly greater and reduced from the weld surface to the failing interface. The steel substrate has the strongest corrosion resistance, as shown by its highest positive OCP. For periods of 20 and 63 cycles, salt spray penetration testing was done on the welds regardless of e-coating. The electrolyte solution moved toward the weld notch root throughout the salt spray tests by penetrating along the gap between the welded Al and steel sheets. The average strength decreased by 12% after 20 cycles of exposure to salt spray and by 41% after 63 cycles, along with a shift in the fracture mode. Because zinc has the highest potential for negative electrochemical reactions, the zinc coating on the steel surface would corrode first. The zinc-rich zone at the weld notch root is then attacked by the electrolyte as it penetrates. Thus, even in the absence of full joint penetration into the Al-steel overlapped area, e-coating provided noteworthy corrosion protection for coupon-level testing [150].

Yang et al. [151] studied the relationship between the spark noise signal time-frequency spectra for the AA6061 alloy sheet weld quality and the mechanism behind the production of CMT arc sound. Based on the experimental work, it has been found that for the aluminum, the CMT butt welding defect recognition, particularly of the burn-through and lack of fusion defects of thin plates, the multi-channel time-frequency has higher recognition accuracy than the single-channel time-frequency.

The timing signal known as the CMT arc noise originates from a strongly associated with the change in CMT arc energy. The arc energy changes three times throughout the three cold and hot processes that alternate in a CMT cycle. A peak arc sound pulse is produced as a result of an arc energy change.

Zhao et al. [152] have conducted experiments for welding the Al-2A14-T6 alloy by using a Fronius TPS 2700 digital pulse CMT welding machine by varying the current. Mechanical properties were tested microstructure was analysed and drawn the conclusion from surface morphology. It was reported that the weld bead width gradually widens, the weld formation coefficient exhibits a tendency of first falling and then increasing, the porosity increases, the grain size increases, and the mechanical characteristics gradually degrade as the welding heat input increases.

Chinnasamy et al. [153] have conducted research to weld a high-strength AA-2014 Al-alloy in T6 condition by using CMT+P Welding to check the weld performance. After evaluating the mechanical and microstructural characteristics, it was determined that the arcing as well as short-circuiting periods, in addition to the pulsing mechanism, aid in the weld dendritic grain refinement, additionally increasing the weld metal region hardness. Joint efficiency is increased to 67% of the weld metal. Grain development and the production of lower eutectic components in the HAZ caused the failure at the P-CMT AA2014 joint.

Zhang et al. [154] have tried to solve the problems associated with the welding of Al-alloy like low welding efficiency as well as joint strength. For this, the AA7075-T6 was welded by using a double-wire pulsed cold metal transfer (DW-CMTP) process. The welding was performed using ER5356 welding wire of 1.2 mm diameter. The mechanical properties were tested and the microstructure was analysed for the weld

sample and observed that the highest tensile is 63% of the base material and the fracture of location is weld metal. Tensile strength decreases with increasing heat input.

2.3   PREVIOUS STUDIES ON MMC AND ITS PROCESSING

2.3.1   Metal Matrix Composites

The metal-matrix composite (MMC) is a material mixture, one of which is a metal, in which certain qualities are obtained through the meticulous mixing of various ingredients. The addition of a high modulus, high-strength refractory particle strengthens the ductile metal matrix and results in mechanical properties that are somewhere between those of the matrix alloy and the ceramic reinforcement. Composite materials consist of two phases: the continuous matrix and the reinforcement, which is a non-continuous, scattered phase. Based on matrix constituents, the composites have three categories: organic, metal, and ceramic matrix composites. When compared to other materials, MMC offers substantial benefits when it comes to damping capacity, strength, specific modulus, stiffness, resistance to wear, and lower weight.

By using various processing techniques, the main goal is to fabricate MMC that can provide homogenous, high manufacturing capability, isotropic, and environmentally beneficial products. Particulates and whiskers were the two different forms of reinforcement available for MMCs. Particle types include alumina, silica, boron, magnesia, boron nitride, alumina-silica, zirconia, TiB_2, SiC, and B_4C. The primary drawback of MMC is the comparatively expensive, cost of reinforcing materials and production. Particles are the most often used and least expensive type of reinforcement. To get a suitable reinforcement the following reviews were done:

Aluminum oxide particles are a cheap substitute that is most frequently used for casting applications, as reported by Mavhungu et al. [1]. However, silicon carbide (SiC) and boron carbide (B$_4$C) particles are currently the most widely utilized MMC materials systems in aircraft, and automobiles, as well as in other industrial applications. The maker of contemporary MMC material systems frequently uses a variety of ceramic reinforcements; their mechanical and physical characteristics are compared. In regards to compressive strength, heat conductivity, a small coefficient of thermal expansion, large specific thermal conductivity, moderate hardness, modulus of elasticity, as well as density, the SiC particle-reinforced MMC material has been demonstrated to be the most suitable. This also compares the industrial fabrication processes for aluminium matrix composites and finds that stir casting, a liquid state process, is the most effective method in terms of cost (least expensive method), damage to reinforcement, and range of size and volume. Stir casting is hence one of the low-cost AMS manufacturing processes that are available. Several well-established uses for SiC-reinforced aluminum metal matrix composites include propeller shafts, brake rotors, calipers, sprocket pulleys, pistons, connecting rods, sprockets, liners, drive shafts, engine cradles, bicycle fork brace, multichip electronic modules, PCB Heat sink, etc. by various companies like Duralcan, Martin Marietta, Lanxide, Nissan, Dow chemicals, Lotus Elisse, Volkswagon, MC-21, Dia-Compe, etc. So, stir casting techniques are being considered for future research work due to the low-cost process, large volume production capability, and simplicity in the process. The material that may be selected is aluminium base MMC reinforced with SiC particles due to its high industrial applications.

According to Baisane et al. [2], the low density, precipitation-strengthened nature, high resistance to corrosion, good thermal and electrical conductivity, and large damping

characteristics of Al alloys, make them highly desirable. Melt stir casting is a popular processing technique because it is very easy to use, adaptable to high production volumes, and provides a great range of materials and processing parameters. It is the most cost-effective approach and can be used to produce very large components. It is also recommended that careful consideration be given to several significant variables to use the stir casting process and to create superior particulate-reinforced MMCs with desired mechanical characteristics. These variables include (1) the kind, size, and weight percentage of reinforcement (2) the temperature at which the system operates and remains stable (3) the stirrer design, location, and speed (4) the temperature at which the reinforcement particles, crucible, and stirrer are preheated (5) solidification behavior during casting (6) the composition of the crucible, stirrer, and mold (7) the technique of adding particles, etc. As per the literature, it is concluded that the slurry viscosity, temperature, wetting of particles, rate of solidification, and retaining of gases, all have a significant impact on the particle distribution in the matrix material. The volume fraction should also be less than 10%. Consequently, the matrix grain size or spacing will be finer or more consistent with a better particle distribution. Often oxides, carbides, or borides (Al_2O_3, SiC, or TiB_2) with a volume component of less than 30% are used as ceramic reinforcements for structural and wear-resistant applications. In electronic packaging applications, the reinforcement volume fraction might potentially reach 70%.

The findings indicate that the lower-cost reinforcements, easier fabrication techniques, and larger production volumes can all help to save costs. Particulate reinforcements are readily available and reasonably priced. Stir casting is also the most cost-effective processing technique. In most cases, surface tension can be reduced by applying a

mechanical force, which increases wettability. Reinforcement wettability with the molten alloys can be increased by applying different metallic coatings on the reinforcement. The formation of porosity will be influenced by the different process parameters like the time of retention, speed of stirring, the size of the impeller, as well as impeller location. As the temperature rises, the chemical reaction rate between reinforcement and molten metal increases. Before adding the SiC particle to the molten solution, it can be pre-treated by baking it for a few hours at a temperature between 700 ^{0}C and 1,200 ^{0}C to prevent the creation of Al$_4$C$_3$.

The AA7075 alloy finds application in the aircraft and automotive industries because of its exceptional strength and hardness, as per the study of Saravanan et al. [3]. Owing to their exceptional strength, wear resistance, fracture toughness, and stiffness, composites made of aluminum alloys are highly desired. Furthermore, when ceramic particles are used as reinforcement, these composites perform better at higher temperatures. When preparing the MMC by stir casting, the process parameters that need to be taken into account are, rotational speed: it makes sense to rotate at the fastest possible speed to prevent ripping. Stirring speed: a crucial process variable that encourages wettability or the connection of the reinforcement and matrix. The pace at which the metal is stirred directly affects how the metal flows. According to a study by Rajesh Kumar et al. [125], the ideal stirring speed range is between 300-600 rpm. The % wettability will rise as the solidification rate quickens. Stirring temperature: the matrix particle dispersion is influenced by variations in viscosity. The viscosity of the liquid decreases as the processing temperature is raised in conjunction with an increase in the stirring holding time. The chemical reaction between the reinforcement and matrix is also accelerating. Once more, the study conducted by Rajesh Kumar et al.

[185], analysed that maintaining the AA6061 at 630°C retains it in a semisolid form. Reinforcement pre-heat temperature: it was reported by Pradeep Sharma et al. [187], that the reinforcement was preheated for 30 minutes at a specific temperature of 500 ^{0}C to eliminate any moisture or other gases that may have been present. Preheating increases the wettability of the reinforcement with the matrix. Stirring period: stirring enables the uniform dispersion of the reinforcement particles with the molten metal and creates an ideal interfacial bond between the matrix and reinforcement. The stirring time is thought to be a crucial component between the matrix and reinforcement particles in the manufacturing of composites. Pouring temperature: in many alloys, a greater temperature encourages columnar growth, whereas a lower temperature is linked to maximal grain refinement and an equiaxed structure. To prevent coarse constructions and guarantee to enough metal flow and collapse resistance, a high enough pouring temperature is required. Mold temperature: for non-ferrous casting, the mould temperature should not be either too high or too low. The minimum thickness of the mould should be 25 mm, and this thickness should increase as the casting gets bigger and heavier.

Research on the wear behaviour of structural components has become more popular as a result of the use of hybrid composites in the aerospace and automotive industries for parts including drive shafts, cylinders, pistons, and brake rotors. Al-.5%Cu/10%TiC, a Metal Matrix Composite (MMC) material, offers greater yield strength, and hardness than Al-4.5%Cu alloy. Vickers hardness rose by around 35%, and ultimate tensile strength and yield strength increased by about 24% and 15%, respectively. The high hardness readings of the TiC were partly responsible for the increase in the hardness of the matrix. According to the current assessment of the literature, a lot of effort has been

made to make composites that are reinforced with diverse materials, such SiC, TiC, Al_2O_3, TiB_2, TiO_2, and B_4C, among others, to enhance the characteristics of various AMMC. The study concluded that stir casting is among the least expensive ways to make MMC. It has been noted that when strong ceramic reinforcement is added to the matrix material, the density of the composite rises. Meaningful study on the behaviour of hybrid composites under solid particle erosion is also lacking. Thirty percent more hardness and nearly twice as much tensile strength have been recorded compared to the base aluminum alloy.

Kumar et al. [155], experimented to create composite materials by using graphite, SiC, and Al_2O_3 particles to reinforce in Al-alloy 6061. It becomes necessary to create new materials to meet the demands of the contemporary engine. By employing the stir casting method to create an aluminium matrix composite material and characterizing its mechanical, metallurgical, and tribological properties, it was concluded that, with the current stir casting apparatus, it is possible to process the reinforcement up to 18% by weight. Since there is less graphite in the PAMC samples than in the parent matrix material Al6061, more porosity is created during the casting process. When graphite is used as a dry surface lubricant, the coefficient of friction between a steel disc and a PAMC pin can be lowered by up to 11%. The reinforcement with Al 6061+ (2.5% Al_2O_3 + 5% SiC + 6% Graphite) has the lowest coefficient of friction value.   The wear rate decreases with the inclusion of SiC, because of their cast state, PAMC components exhibit a brittle fracture in the tension test. SiC and Al_2O_3 additions result in a notable increase in UTS. The maximal tensile strength for the combination of Al 6061+ (2.5% Al_2O_3 + 5% SiC + 4% Gr) is obtained. The tensile strength increases by 28%.   The ductility of the PAMC decreases as the percentage of reinforcing increases. The

percentage of SiC hardness in PMAC keeps rising as it increases. It results from SiC hard ceramic nature. Al 6061+ (4% Al_2O_3 + 7% SiC) improves the material by nearly 90%.

Rambabu et al. [4] reported the criteria and properties for the selection of aluminium alloys for aerospace applications. Aluminium is a lightweight, relatively inexpensive material that can be produced by a simple fabrication process that in turn converts it into reduced costs. Aluminium alloys have a low modulus of elasticity, and a relatively limited capacity to withstand excessive temperatures (130 °C), and high-strength alloys, have a vulnerability to corrosion.

Copper, Magnesium, and Additional Elements: The most significant and adaptable class of commercially available high-strength aluminium alloys is Al–Cu–Mg alloys including manganese. Broadly speaking, when magnesium and manganese levels rise independently or concurrently, tensile strength generally rises as well. Yield strength increases as well, while less dramatically. Magnesium and manganese additions impair the alloys ability to be fabricated. Manganese also reduces the ductility of the alloy. While magnesium alloys improve their tensile qualities when heated, none of them noticeably outperform manganese. Three classes can be distinguished among Al–Mg_2Si alloys. The combined magnesium and silicon content in the first group is less than 1.5 weight percent in AA 6063. The second group, which boosts strength in the T6 temper, is said to have 1.5 weight percent or more of magnesium + silicon and further additives such as 0.3 weight percent Cu in AA6061. An alloy with 0.8 weight percent Mg_2Si gains roughly 70 MPa of strength when 0.2 weight percent Si is added. Greater surplus silicon concentrations provide fewer advantages. Magnesium and silicon can be mixed

in wrought alloys up to 1.5 weight percent to produce Mg_2Si, a heat-treatable alloy in the 6XXX series. High-purity aluminum-silicon casting alloys exhibit hot shortening up to 3 wt%-Si; the critical region lies between 0.17 and 0.8 wt% Si. Cracks are less common in alloys composed of magnesium, copper, and aluminum when silicon additions (0.5–4.0 wt %) are added.

Zinc-Magnesium-Copper: The high-strength 7XXX series Al-alloys are produced by adding copper to the system of aluminium, zinc, and magnesium along with minor but significant contents of manganese and chromium. The studies concentrate on enhancing mechanical qualities, strength, and fracture toughness in this work. Reducing the concentrations of silicon and iron impurities has been a significant step toward creating Al-alloys with significantly enhanced fracture toughness. When compared to 2XXX alloys, the 7XXX series of alloys may often achieve a better blend of fracture toughness and strength. Fatigue life and strength characteristics are crucial in designing data for airplane construction. Under constant amplitude stress, conventional 2XXX series Al alloys are commonly better than 7XXX series alloys in terms of fatigue crack growth. Corrosion is influenced by both chemical and physical environmental factors. Stress corrosion cracking (SCC) can cause significant damage to aircraft Al alloys. Specifically, the 2XXX-T8XX, 7XXX-T6XX, and 7XXX-T7XX tempers exhibit this vulnerability. Conventional fusion welding is not appropriate for the 2XXX and 7XXX alloys. However, FSR, a solid-state joining procedure, can be used to join them.

Sijo et al. [156], reported that the stir casting procedure is a straightforward, cost-effective, and large-volume production method among the available techniques. The main shortcomings of stir-cast Al-SiC MMC are the insufficient dispersion of SiC reinforcement within the matrix and the decreased wettability of SiC reinforcement

particles with molten Al. In composite materials, the non-continuous, dispersed phase is known as the reinforcement, whereas the continuous phase is called the matrix. The material used in the reinforcing phase might take the shape of flakes, particles, or fibers. The primary drawback of MMC is typically the comparatively expensive cost of reinforcing materials and production. The reinforcement material can be categorized into four main groups based on its shape. Particles, whiskers, continuous fibers, and short fibers, chopped fibers that may or may not be the same length. Particles are the most often used and least expensive type of reinforcement. Studies on MMC fracture toughness reveal that the composites with fine particles have better fracture toughness than those reinforced with coarse-grain particles.

Scanning electron microscopy (SEM) is used for mechanical characterization. It is discovered that the distribution of reinforcement particles is uniform in the range of 750^0C to 800^0C. This is because processing temperatures up to 800^0C cause the viscosity of aluminum to drop. When making composites, magnesium (Mg) is added to ensure that the reinforcement in the matrix is properly wettable. This will decrease the creation of a SiO_2 layer on the SiC surface, also enhancing the wettability of Al and SiC particles. The amount of wettability can be increased by employing fine-sized reinforcement because particles with larger surface areas are more wettable. Additionally, wettability can be increased by heating the alloy to higher temperatures, which will reduce its surface tension.

Increasing the weight percentage of reinforcement from 5% to 20% results in an increase in composite hardness, elastic modulus, fatigue behaviour, tensile strength, density, impact strength, and wear resistance; however, it also results in a decrease in

cooling rate, ductility, and forging ability. The final strength of the composite is raised by raising the volume proportion of reinforcement. An increase in holding time (10, 20, or 30 minutes) is proven to diminish the ultimate strength of composites. Microstructural factors like as shape, size, orientation, and distribution of the reinforcement have a significant impact on the elastic characteristics of MMC. Studies on MMC fracture toughness reveal that composites incorporated with fine-grain particles have better toughness than those reinforced with coarse-grain particles.

The fracture behaviour of the Al-SiC composite is studied by modelling and simulation. Stir casting involves real-time flow characteristic measurement, which is costly, time-consuming, and hazardous. It was concluded that a variety of parameters, including the distribution and types, volume, size, and shape of reinforcing particles, and manufacturing procedures, affect the mechanical properties of stir-cast composites. A consistent distribution of reinforcement is required to increase fracture toughness.

Miller et al. [5] explored the present state of aluminium alloy development for the automobile sector. The highly formable 5000 alloys are mostly employed for internal panel applications, while the heat-treatable 6000 alloys are preferred for exterior panel applications. In general, a 5.5% boost in fuel efficiency comes with every 10% reduction in weight. Aluminum castings make for nearly all of the pistons in car power trains, as well as about 75% of cylinder heads, 85% of intake manifolds, and the transmission (together with other parts like the drive shafts, rear axle, differential housings, etc.). A little over 40% of the wheels used in chassis applications are composed of aluminium castings, brake components, suspension (control arms, supports), steering components (airbag supports, steering shafts, knuckles, housings, wheels), and instrument panels. For structural sheet materials, impact energy absorption

and appropriate deep drawing behaviour are usually more important than strength, however, it may be a limiting factor in some circumstances. To achieve these specifications, 5xxx series alloys are the main choice in North America. In Europe, 6xxx-T4 materials are still widely utilized. In addition to 6xxx alloys with an exceptional balance between formability and roping performance and T4P (pre-bake treated) 6xxx alloys that provide a notable increase in strength after the panels have passed the paint bake line, new surface textures are being developed to improve surface appearance and forming for outer panels.

For structural use, 5xxx alloys containing 3.0% Mg should be developed to completely remove the possibility of intergranular corrosion degradation. Creation of aluminum alloys for structural uses in response to consumer demand for the idea of using unalloyed materials to maximize recycling possibilities. As was previously noted, brazed aluminum components are widely utilized in modern cars for climate control, charging air coolers, cooling engines and transmissions, and cladding layers made of low melting point silicon-based Al-alloy. Vacuum brazing was created in 1970 as a solution to the issues with the outdated dip brazing methods. Even though it was an environmentally favourable strategy, a large cash expenditure is needed. The flux used is water-insoluble and non-corrosive. This implies that to achieve the highest level of corrosion resistance, the appropriate alloy must be chosen for each application. Steel is anticipated to be the primary material of choice for automobile bodies for the ensuing ten years, according to the automotive industries future trend of lightweight materials. Up until now, the following issues have hindered the penetration of aluminium: the cost of raw materials; the cost of manufacture; the industrial structure; recycling; and laws. With collaborative efforts to advance high-volume production manufacturing

technologies, aluminium has a legitimate opportunity to increase its market share in automobile body applications.

Kumar et al. [6] focused their study on the synthesis and characterization of nanocomposites based on magnesium alloy (AZ91E) reinforced with nano-sized Al_2O_3 reinforcements. To create the composite, a unique semi-solid stir-casting method was used. Magnesium has a low density and strong strength. Another reason to be drawn to magnesium is its lower CO_2 emissions and capacity for recycling. Al_2O_3, on the other hand, is less expensive, has a high specific stiffness, and is very resistant to oxidation. The most stable hexagonal alpha phase is produced by Al_2O_3 particles at high temperatures, and they can exist in a variety of crystalline phases. This research seeks to fabricate magnesium MMC using the semi-solid stir casting method with nano Al_2O_3 reinforcements and a high-purity grade AZ91E magnesium alloy that is extremely resistant to corrosion. Density and porosity, microscopy results, mechanical properties, yield strength, tensile strength, ductility, elastic modulus, and fractography of tensile specimens are measured and analysed. It was discovered that adding nanoparticles caused the hardness, yield, and tensile strength of the composites to drop due to cluster formation after the amount of nano Al_2O_3 was increased to 2%. With an increase of 22.5% in macro hardness and 26.54% in tensile strength, the 2-weight percent Al_2O_3 reinforced AZ91E composite exhibits superior mechanical properties compared to the other reinforcements stated. Fractography shows that the composites exhibit a mixed mode of shear and fracture that is brittle, but the unreinforced AZ91E alloy fractures with a ductile nature.

A hybrid AMMC reinforced with titanium diboride and silicon carbide was prepared by James et al. [157]. Using the Vickers hardness testing apparatus, the hardness value of the composite has been ascertained through the hardness test. According to the hardness test, the hardness value increases with the addition of SiC and TiB_2 reinforcement. However, if reinforcement is increased to a weight of 15%, the hardness value decreases. According to the findings of tensile tests, the addition of SiC particles to base metal increased the composite strength by 20%, whereas the addition of TiB_2 resulted in a 50–60% drop in strength. An analysis of wear tests has been conducted to investigate TiB_2 wear resistance behaviour. The wear resistance behaviour of the composite was enhanced by the inclusion of TiB_2, as demonstrated by wear test analysis. The microstructural analysis demonstrates the presence of SiC and TiB_2 reinforcements and their even dispersion throughout the metal matrix. TiB_2 weight percentage with matrix is restricted to 2.5% since higher weight percentages lead to cluster formation and porosity. The hardness test of Al 6061 reinforced with SiC and TiB_2 clearly shows that the hardness value increases when TiB_2 is added to the aluminum matrix. It has also been observed that there is an abrupt drop in the hardness rating when the percentage of TiB_2 rises to 5%. Based on the experimental findings, 2.5 is determined to be the ideal percentage of TiB_2 reinforcement [157].

In addition, fracture, wear test, S/N ratio, and tool wear analysis are performed. The results indicate that SiC and TiB_2 are present in the metal matrix and are distributed therein, as demonstrated by the microstructural analysis. Cluster formation is induced by increasing the wi% of reinforcement (SiC10% & TiB_2 5%). As a result, for 10% SiC, the maximum percentage of TiB_2 in the matrix is 2.5%. Hardness measurements have shown that adding reinforcements influences the hardness value; nevertheless, adding TiB_2 up to 5% causes porosity, which also influences the hardness value. The microstructure analysis and the

tensile specimen were examined, and it was shown that cluster formation causes porosity, which in turn causes the strength of base Al-alloy to decrease. Wear research has demonstrated that TiB_2 particles improve a hybrid aluminum metal matrix wear resistance characteristic. According to experimental data, SiC 10% - TiB_2 0% specimens have 20% greater wear than Sic 10% - TiB_2 2.5% specimens. The study shows that the percentage of TiB_2 reinforcement, which accounts for 38.86% of surface roughness, is the most important element. The surface roughness value is increased by the addition of TiB_2 reinforcement. As per the Taguchi analysis, the ideal machining settings for the best surface roughness are as follows: 120 m/min of cutting speed, 0.3 mm/rev of feed rate, 0.5 mm of cut depth, and 0% of TiB_2 reinforcement. Tool wear study has shown that both abrasive and adhesive processes contribute to increased tool wear. High tool wear is caused by low cutting speed, high depth of cut, and increasing weight percentage of TiB_2 reinforcement; built-up edge formation degrades surface quality.

As reported by Saravanakumar et al. [158], copper and its alloys are used to make a wide range of components in the nuclear, thermal, chemical, electrical, and transportation industries. For copper matrix composite (CMC) applications, aluminum nitride (AlN) is a great option for reinforcement, especially in the electronics sector. The excellent thermal and electrical conductivity of AlN is widely recognized. AlN is also chemically and thermally stable, with a high dielectric constant and a low coefficient of thermal expansion [24–25]. The wear resistance of copper will increase when reinforced with AlN, and thermal stress in electrical and electronic components will be reduced. The study aims to use FSP to create Cu/AlN surface CMCs and examine their microstructural characteristics and sliding wear behaviour.

The microstructure of Cu/AlN surface composites was analysed, and the mechanical and wear behaviour of Cu/AlN CMCs was determined that, regardless of the volume %, the AlN particles were distributed uniformly throughout the copper matrix. AlN particle segregation and clustering were absent. There were no visible pores or interfacial reaction products. AlN particles and the copper matrix had a good connection. There was not enough of a temperature rise during FSP to cause any interfacial interaction between copper and AlN particles. Almost all of the AlN particles were distributed evenly across the stir zone depth. The composite showed annealing twins, ultrafine grains, and high-density dislocations. As the volume fraction of AlN particles grew, the wear rate of Cu/AlN CMCs reduced. Low coefficient of friction, smaller contact area, and increased hardness were all associated with increased wear resistance. AlN particles were distributed uniformly and exhibited strong interfacial bonding. During friction stir processing, AlN particles retained their size and form, and they had an impact on the wear resistance and mode of wear.

Gangil et al. [159] have thoroughly examined several aluminum alloy series, their uses, appropriate reinforcing, and processing techniques to enhance their qualities through FSP. The 1xxx Series Al-alloys are commercially pure aluminum (99% or higher), strain-hardenable, non-heat-treatable, and have high electrical conductivity, corrosion resistance, and formability. Their typical ultimate tensile strength (UTS) is between 70 and 185 MPa. It is widely utilized in chemical and electrical applications, such as in chemical equipment, tanks, foil, and strips for packaging. Heat-treatable Al-Cu alloys of the 2xxx series have a high room temperature strength and an enhanced UTS range of 185–427 MPa; they are mostly employed in aircraft and transportation applications. The main applications for the higher-strength alloys are truck bodywork (AA2014) and

interior aircraft structures (AA2024). Alloys in the 5xxx series Al-Mg alloys, which have a typical UTS range of 124-352 MPa and are widely utilized in cryogenic, marine, automotive, storage tanks, pressure vessels, and construction applications, are strain hardenable and have high corrosion resistance, toughness, and weldability. The primary application of AA 5083 is in the form of machined plates for high-speed ship hulls, decks, and superstructures. In contrast to wrought alloys, cast aluminum alloy composites are reported and debated to have a considerable number of alloying elements [159]. Al + Si + Cu or Mg alloys in the 3xxx series are used mostly in automotive pistons, pumps, and electrical systems. They have outstanding fluidity, high strength, and a high UTS range.

As studied by Mousavian et al. [160], the stir-cast aluminum matrix–SiC composites were treated with the hot extrusion technique to enhance their microstructure and lower cast part flaws. To increase SiC incorporation, Cr, Cu, and Ti were used as three different types of carrier agents when grinding SiC particles. To lower the cost of composite manufacture, large brittle ceramic particles were broken up into nanoparticles during ball milling. It was reported that the nano-composite superstructures were created by ball-milling large micron-sized SiC particles with three different types of carrier agents (Ti, Cr, and Cu) before their integration into the molten A356 aluminum alloy. The production of AMNCs ensued with the use of semi-solid stir casting, hot extrusion, potential separation of agglomerated particles, all enhanced interfacial bonding between the particle and matrix, and matrix structure refinement to attain a lower porosity content.

The author [160] concluded that lengthening the milling time reduced the particle size of the coarse SiC powders. Even after 36 hours of milling, tiny micron SiC particles measuring 10–20 μm were found, suggesting that not all of the big particles were reduced to submicron and nanoparticle size with extended milling time. The existence of nanoparticles, submicron particles, and fine micron particles in the A356 alloy matrix demonstrated the production of multimodal-sized SiC particles, which ranged in size from 50 nm to 20 μm. It was discovered that the distribution of nanoparticles and submicron particles could not be changed by the extrusion process. Nevertheless, during extrusion, a notable disintegration of silicon platelets was noted, resulting in a total modification of the composite microstructures. Additionally, it was discovered that the Ti carrier agent outperformed the Cu and Cr agents in terms of forming a composite with a higher concentration of fine ceramic particles and a more optimal ceramic dispersion. The strength and hardness of a composite containing Ti carrier agent were found to rise by more than 45% and 100%, respectively, however, Cr and Cu were found to be unsuitable for boosting the mechanical parameters.

Nandyala et al. [161] have fabricated a hybrid composite of Al 6068 as well as Al 7075 by using reinforcements of TiO_2 and BN through the Stir casting process. The total weight % of TiO_2 and BN are maintained at 3% and different sets of combinations were used. As a stir-casting process parameter, the stirring temperature is 750 ^{0}C, the stirring speed is 650 rpm, the pre-heat temperature of reinforcement is 350 ^{0}C and the stirring time is 15 min. The microstructural analysis and mechanical characteristics were assessed, and in conclusion, the hybrid MMC showed an improvement in wear behaviour compared with base alloys (Al6068 & Al7075). The tensile strength and

hardness were improved as compared with base alloys. Also, the reinforcement Tio_2 + BN combination showed a better result than single reinforcements.

Ananth et al. [162], fabricated an aluminium metal matrix composite for Al7050 by using a reinforcement of B_4C. Different sets of stir-casting process parameters were used to cast the composite. The reinforcement is heated at 400 ^0C for 30 min to remove the moisture. The different sets of stir casting parameters are as wt% of reinforcement, stirring time (10,15 and 20 min), melting temperature as (700, 750, and 800 ^0C), and stirring speed as (300, 350, and 400 rpm) were used. To increase the wettability of B_4C, 1% Mg is added to the molten Al-7050 [163]. The study found that the microhardness value was improved by 20.3% corresponding to the optimum value of the process parameter. Also, the 9 wt% of boron carbide addition is an optimum value to increase the microhardness.

Umanath et al. [164] performed their work to fabricate a hybrid metal matrix composite of AA7075 by using Sic/MoS_2 in different sets of combinations. The MoS_2 amount was kept constant at 1% and varied the amount of Sic as (3%, 6%, and 9% wt%). It was revealed that as the wt% of SiC increases, the hardness value improves. The maximum hardness was found at Al-7075+9% SiC+1% MoS_2. The size of the abrasive particles and the reinforcing elements determine the abrasive wear resistance. Conversely, a higher wear rate is caused by smaller abrasive particles than by bigger ones. As the test temperature increased, the hybrid composites resistance to abrasion reduced.

Kareem et al. [165], fabricated a metal matrix composite of Al-2024 by using lanthanum (La_2O_3) as reinforcement material. The composite was fabricated through a friction stir process (FSP). Consistency in the dispersion of reinforcement particles

across the matrix was found. The mechanical and wear properties were tested and the result revealed that there is a measured improvement in the value of tensile strength, hardness, wear resistance, and fatigue properties.

2.4 STUDIES FOR SELECTION OF SUITABLE REINFORCEMENT FOR AL-BASED METAL MATRIX COMPOSITE (AMMC).

The investigators experimented with various reinforcing materials, and each had different findings.

1. Reinforcement particles have been made using refractory powders such as Al_2O_3, SiC, TiN, TiC, Si_3N_4, B_4C, TiB_2, ZrO_2, MoS_2, and graphite (Gr). The qualities of the material are affected by the particles in their way.

2. Because MoS_2 and Gr have lubricating qualities, they improve wear resistance and reduce noise.

3. Al_2O_3 also offers better wear qualities because of its decreased friction.

4. The hardness and brittleness of SiC increase its resistance to abrasion.

5. The use of a hybrid reinforcement material can frequently result in synergy. This leads to the simultaneous improvement of multiple qualities (e.g., hardness and lubrication, strengthening and wettability, etc.).

6. The use of whiskers and glass carbon fibers simultaneously increases ductility and strength significantly.

7. When multi-walled carbon nanotubes (MWCNT) are used, the matrix and MWCNTs exhibit good interfacial bonding and wetting, as well as a high dislocation density and ultra-fine grain size.

Mavhungu et al. [1] stated that silicon carbide (SiC) and boron carbide (B_4C) particles are the most often utilized MMC materials systems in the aerospace, automotive, and other

industries. Al oxide particles, on the other hand, are a low-cost alternative and are most frequently employed for casting applications. In terms of compressive strength, thermal conductivity, poor thermal expansion coefficient, large specific thermal conductivity, mild hardness, elastic modulus, and density, SiC particle-reinforced MMC material was shown to be the most suitable. One of the less expensive manufacturing technologies for AMC that is now accessible is stir casting [1].

A thorough analysis by Baisane et al. [2], reported that consideration is given to several important factors to produce high-quality particulate-reinforced MMCs with the desired mechanical properties using the stir casting technique. These factors include (1) the type, size, and weight fraction of reinforcement elements; (2) the design, position, and speed of the stirrer; (3) the operating and holding temperature; (4) the duration and temperature of the preheating process for the stirrer, mold, and reinforcement particles; (5) the material of the crucible, stirrer, and mould; (6) the method of particle addition; (7) solidification behavior during casting, respectively.

The literature suggests that the following factors significantly affect particle distribution in the matrix material: heating temperature, viscosity of the slurry, particle wetting, solidification rate, and minimizing gas entrapment. Stir casting is also the most cost-effective processing technique. By applying different metallic coatings on the reinforcement, wettability can be increased. As temperature rises, the rate of chemical reaction between SiC and liquid aluminum increases [2]. The literature suggests that the following factors significantly affect particle distribution in the matrix material, heating temperature, viscosity of the slurry, particle wetting, solidification rate, and minimizing gas entrapment. Stir casting is also the most cost-effective processing

technique. By applying different metallic coatings on the reinforcement, wettability can be increased. As temperature rises, the rate of chemical reaction between SiC and liquid aluminum increases [2].

Saravanan et al. [3] reported that the automotive and aerospace industries favour aluminum alloy 7075 because of its exceptional strength and durability. The following variable parameters must be considered when manufacturing the MMC by stir casting: temperature, pouring temperature, reinforcement pre-heat temperature, stirring speed, and mould temperature. The material known as the metal matrix composite demonstrates greater hardness, yield strength, and ultimate strength. The author concluded that stir casting is among the least expensive ways to make MMC. Hardness and tensile strength have been shown to rise by 30% and nearly double, respectively, compared to the base aluminum alloy [3].

Kumar et al. [155] have studied to create composite material by using graphite, SiC, and Al_2O_3 particles to reinforce with Al alloy 6061. The lowest coefficient of friction found is for the reinforcement of Al 6061+ (2.5% Al_2O_3 + 5% SiC + 6% Gr). The wear rate is decreased with the use of SiC, and Al_2O_3 additions result in a notable increase in UTS. The tensile strength of Al 6061+ (2.5% Al_2O_3 + 5% SiC + 4% Graphite) is increased by 28%. The hardness of PMAC increases as the proportion of SiC increases. This is because SiC is a hard ceramic. Al 6061+ (4% Al_2O_3 + 7% SiC) yields improvements of over 90% [155].

Sijo et al. [156] reported that the stir casting method is the most straightforward, least expensive, and most widely used of all the casting techniques. Particles are the most often used and least expensive type of reinforcement. Research on MMC fracture

toughness shows that fine-grain particle-reinforced composites are more fracture-tough than coarse-grain particle-reinforced composites. When the weight fraction of reinforcement is increased from 5% to 20%, the composites hardness, elastic modulus, fatigue behaviour, tensile strength, density, impact strength, and wear resistance all rise; on the other hand, the materials cooling rate, ductility, and forgeability all decrease. It has been seen that as holding times increases, composites ultimate strength decreases [156].

James et al. [157] have used titanium dioxide with silicon carbide reinforcement to create a hybrid aluminum metal matrix composite. According to the hardness test, adding reinforcement made of SiC and TiB_2 raises the hardness value. However, a decline in the hardness value is revealed by increasing reinforcement up to 15% weight percentage. According to the findings of tensile tests, the composite strength increased by 20% when reinforcement SiC was added to the base metal. It has also been observed that there is an abrupt drop in the hardness rating when the percentage of TiB_2 rises to 5%. Based on the experimental findings, 2.5% is determined to be the ideal TiB_2 reinforcement percentage. Wear research has demonstrated that the wear resistance behaviour of a hybrid AMC is enhanced by the presence of TiB_2 particles. The surface roughness value rises when TiB_2 reinforcement is added [157].

Kannan et al. [8] reported the manufacturing of a single reinforced nanocomposite containing 2 weight percent nano alumina particles distributed throughout the molten Al alloy of grade AA 7075. In contrast, hybrid reinforced nanocomposites containing 4 weight percent silicon carbide and 2 weight percent, 4 weight percent nano alumina particles were created. Furthermore, a squeeze-cast single reinforced nanocomposite

was produced to examine the impact of squeeze pressure on the enhancement of mechanical properties in comparison to a stir-cast nanocomposite. It was found that the base Al alloy had a lower tensile strength than the nanocomposites. Squeeze casting was used to further refine the grain and reduce the porosity in these nanocomposites. The microstructure and SEM study showed the uniform distribution of particles in the base matrix, provided that the weight percentage of nano reinforcement is maintained at 2% [8].

Tan et al. [166] conducted experimental work to make a hybrid composite of AA 2024 alloy by using reinforcement particles of SiC and SiC_p Al- composite chips prepared by the pressure infiltration method. The test result reveals that the tensile strength increased drastically from 178 to 392 MPa. Additionally, it is established that the interface between CPs and Al has been well-bonded and that CPs have been uniformly distributed throughout the composites, regardless of their dimensions. The hybrid composites made of CP/2024Al showed signs of brittle fracture, but their tensile strength was higher. For the CP/2024Al hybrid composites mechanical qualities to be further enhanced, the interfacial bonding needs to be strengthened.

Kaveripakkam et al. [167] have studied the behavior of SiC and B_4C reinforced hybrid metal matrix composite of Al-Alloy 6061 welded by friction stir process. The mechanical and microstructural properties were measured and reported. After SiC and B_4C reinforcement, the tensile qualities of friction stir welded AMMCs improved. The addition of reinforcement and the ensuing heat action during the FSW process significantly increased the hardness of the AMMCs.

Satyajeet et al. [168] have performed experimental work to study the metal matrix composite behaviors of Cu- alloy (RG-10) by using SiC in different weight % of (3%, 6%, 9%, and 12%) as reinforcement. The findings on wear characteristics and microstructural details revealed that as the proportion of reinforcement increases, the microstructure becomes more refined. It has been noted that when the percentage of SiC particles increases, so does the average hardness value. The experimental density is lower than the theoretical density and increases with increasing proportion of reinforcement because composites contain some porosity. As the reinforcement weight percentage increases, the wear weight loss decreases.

Jayashree et al. [169] have fabricated a metal matrix composite of Al-6061 by using SiC with 6 wt%. The formed composite was welded by tungsten inert gas welding by using ER 356 as filler wire. The experiment was performed by varying the current (150, 170, and 200 Amp) to weld the samples. The mechanical and wear properties were studied and concluded that as the welding current increases the wear rate decreases. For the sample with a current of 200 Amp, the hardness value increased by 29.6%.

Salmaan et al. [170] conducted an experimental investigation for the fabrication of a hybrid composite of Al-Alloy 7075, reinforced by some rare material reinforcement like Hafnium Carbide (HfC), with silicon nitride (Si_3N_4) and MoS_2 Nanoparticles. It was observed that the mechanical properties were improved along with the tribological behaviour and corrosion behavior of the fabricated metal matrix composite. The addition of silicon nitride, Hafnium carbide, and molybdenum disulfide increases the tensile strength, compressive strength, yield strength, and flexural strength, and

decreases the ductility. Hafnium carbide is a very strong material with high melting and boiling point so it can be used in all types of critical applications.

Erappa et al. [171] have investigated the mechanical, wear, and fracture behaviour of Al7075, reinforced with varying wt% of Al_2O_3 and Gr nano-particle quenched with water ice cubes. It was found that the hybrid composite's tensile strength, hardness, and wear behaviour are significantly improved by this simultaneous heat treatment. Composite quenched with ice cubes have superior properties as compared to water-quenched composite. The wear behaviour of nano-hybrid composite is better as compared to single reinforced composite. The hybrid composites compressive and tensile strengths decrease as the weight percentage of Gr nanoparticles increases.

2.5   CONCLUSIONS FROM THE LITERATURE REVIEW

A detailed literature review was conducted to get the most appropriate gaps that can affect the quality of a material as a whole like the method of composite fabrication, a compatible reinforcement selection (both in single and hybrid mode), as well as its welding through advanced welding methods. From the exhaustive literature survey, the following conclusions were made:

1.   The majority of research work has been conducted to fabricate MMCs through stir casting because of its low cost and simplicity in operations. It was observed that most melt stir-casting machines are manually operated due to that, the lack of control over the process parameters takes place.

2. It was found that a lot of work has been reported on the 2000, 5000, 6000, and 7000 series of commercially available Al-alloy but some 7000 series high-strength new alloys are yet to be explored.

3. Because existing conventional welding techniques produce a large heat input, due to this the sheet thickness has been a limiting factor. Combinations of diversified and dissimilar materials are less explored and are required to be explored through new and advanced welding methods.

4. Thus, it is necessary to use a human-machine interface (HMI)-operated, controlled stir-casting approach to create premium particulate-reinforced MMCs with the desired mechanical properties. After successfully fabricating MMCs, an advanced and new joining approach is needed to improve the weldability of selected advanced aluminum alloy and its AMMC.

2.6   RESEARCH GAPS

The following gaps are observed from the conclusions of the literature review:

1. Numerous studies have been published on the 2000, 5000, 6000, and 7000 series of commercially available aluminum alloy but some 7000 series high-strength new alloys are yet to be explored. So, the attempt is required to explore it for industrial applications or to replace some existing Al alloys.

2. Most of the reported research work is performed using single reinforcement particles. Limited work is reported using hybrid reinforcement particles.

3. Because of the high heat input required by the current standard welding methods, sheet thickness has been a limiting factor. For thin Al sheets (thickness up to 3

mm) CMT alone is a suitable method for efficient welding, whereas for thicker sheets or plates (thickness above 3mm) CMT+P welding is more suitable.

4. In most of the reported work aluminum and its alloys were successfully welded by FSW which is a solid-state welding process but for successful joining of AMMC a new welding approach is required that seems to be done by CMT as an advanced welding method.

5. Most of the investigation has been conducted using traditional welding processes. Combinations of diversified and dissimilar materials are not explored that are required to explore through new and advanced CMT welding.

2.7 PROBLEM STATEMENT AND OBJECTIVES OF THE RESEARCH WORK

2.7.1 Problem Statement

Current research works aim to fill the gaps that are observed through a literature survey to fabricate an AMMC with a combination of suitable reinforcement and its welding to form a complete structure that can solve many industrial issues. By keeping in focus to form a complete structure, the following problem statement were designed:

"MECHANICAL AND MICROSTRUCTURAL CHARACTERIZATION OF COLD METAL TRANSFER WELDED ALUMINIUM METAL MATRIX COMPOSITE JOINTS"

The problem statement focuses on fulfilling the following objectives:

2.7.2   Research Objectives

The literature survey indicated that the information/data on aluminum alloy, its MMC, and its weldability by FSW and other traditional welding processes are required to improve to some extent. Therefore, there is a need to supplement the information. The existence of a gap in the literature was used for deciding the objectives of the present research.

This study will aim to verify the results of some of the previous studies along with overcoming some of the issues encountered in previous studies. The study will have the following objectives associated with AMMC fabrication, its welding with an advanced welding approach, and industrial application in the area of automobile and aerospace:

1.   To fabricate AMMCs using suitable reinforcements on high-strength Al-alloy.

2.   To weld fabricated AMMCs using the CMT welding technique.

3.   To study the relationship between various process parameters.

4.   To study the microstructure of the CMT welded joint.

5.   To study the mechanical properties of CMT welded joints.

CHAPTER 3

METHODOLOGY FOR FABRICATION OF METAL MATRIX COMPOSITE

3.1 INTRODUCTION

Because of their outstanding mechanical qualities, which include resistance to corrosion, lightweight, high strength, high toughness, and recycling potential, alloys have grown to be among the most commonly utilized materials in applications including transportation and structural engineering. Using less expensive reinforcements, more straightforward fabrication techniques, and increased production volume can all help to reduce costs. Metal matrix composites (MMC) are gaining popularity in a study on joining techniques, because of their potential for effective engineering applications in aircraft structures and automotives. The high metal ductility and high elastic modulus of ceramics are used in aerospace applications to provide a better characteristic. The MMCs are made up of two or more macro components that are mixed with the matrix. The development of parts and components for aviation was significantly aided by the high strength-to-weight and strength-to-density ratios of the MMCs [4, 155-156].

The continuous phase of composite materials is referred to as the matrix, whereas the non-continuous, scattered phase is called the reinforcement. The material used in the reinforcing phase might take the shape of flakes, particles, or fibers. Based on the components of the matrix, composites are classified as either organic, metal matrix composites (MMCs), as well as ceramic matrix composites. When compared to other composites, MMC composites provide considerable gains in strength, specific modulus, damping capacity, stiffness, wear resistance, and weight reduction.

Metal matrix composites (MMCs) are materials, among which one is a metal, where certain properties are achieved by carefully combining different constituents. Because of their cost-effectiveness, isotropic qualities, and processing compatibility with monolithic material technologies, particle-reinforced MMCs are more appealing. Metal matrix composites can be reinforced using either of two methods, discontinuous reinforcement and continuous reinforcement [172-173].

Metal matrix composites are well suited for engineering applications due to their high strength, high elastic modulus, and strong wear resistance [1-4]. Unfortunately, the use of brittle ceramic reinforcements in Al-based composites results in low ductility and toughness, which restricts the range of applications for these materials [155-156]. Compared to monolithic materials and metal matrix composites alone, hybrid metal matrix composites have superior mechanical properties. Engineered materials that mix two or more distinct types of reinforcing particles to obtain the combined benefits of both are known as hybrid metal matrix composites [160]. It was discovered that the researchers have produced AMC for several Al alloy series using various fabrication procedures to enhance the alloy characteristics. Numerous studies have been conducted to make composites and add different materials to reinforce aluminum-based MMCs to improve their qualities.

As per the literature, not much work was reported on some advanced-grade Al alloys like the 7xxx series and especially a hybrid composite in which two or more reinforcements were added in base material to gain the properties of both reinforcements. Aluminum and its alloys are used to make metal matrix composites (MMCs) most frequently. Al alloys are very attractive due to their low density, good

resistance to corrosion, ability to withstand precipitation, high electrical and thermal conductivity, and high damping capacity [174].

The ultimate goals of MMC design can be achieved by the use of various processing techniques, reinforcement, testing, and analysis to create homogenous, isotropic, well-manufacturable, and environmentally friendly material. The reinforcement techniques used in metal matrix composites are continuous and discontinuous reinforcement. The primary drawback of MMC is typically the comparatively expensive cost of reinforcing materials and production.

3.2 STIR CASTING ROUTE FOR FABRICATION OF METAL MATRIX COMPOSITE

In the stir-casting method of creating composite materials, a dispersed phase (ceramic particles, short fibers) is mixed with a molten matrix metal by mechanical stirring. Following that, the liquid composite material is cast using standard casting methods, and it may also be handled using conventional metal forming procedures. The stir-casting process is inexpensive and comparatively easy to use.

3.2.1 Processing Techniques for Particulate Reinforced MMC

Since MMC technology is still very much in the R&D stage, the costs associated with producing MMCs are still considerable for all approaches. Melt stir casting is a popular processing technique because it is the most affordable, offers a wider range of materials and processing conditions, is versatile enough to handle large-volume production, and can be used to produce very large-sized components. The vortex technique sometimes referred to as the stir-casting technique, is the most straightforward and widely applied

method. Using the vortex process, pre-treated reinforcing particles are added to the molten alloy vortex that the rotating impeller creates.

Several factors need to be addressed during melt stir-casting, as reported by, Hashim et al. [175]:

1.   The challenge of distributing the reinforcing material uniformly.

2.   The degree of wettability of the two/more primary substances.

3.   The porosity control in the casting of metal matrix composites.

4.   Chemical exchanges that occur between the matrix alloy and reinforcing material.

To create the optimal properties of the metal matrix composite, the reinforcing material must be distributed uniformly throughout the matrix alloy and the wettability or bonding between these elements must be optimized. Requirements include minimizing porosity levels and preventing chemical interactions between the matrix alloy and reinforcing components.

To use the stir casting technique to create good-quality, particulate-reinforced MMCs with desired mechanical characteristics, careful consideration should be paid to crucial elements like:

1.   Particle size, type, and weight percentage of reinforcement.

2.   Stirrer design, location, and speed.

3.   Maintaining and adjusting temperature.

4.   Preheating temperature of the stirrer, mould, and reinforcing particles and duration.

5.   Composition of stirrer, crucible, and mould.

6.   Particle addition method.

7.   Behaviour of solidification during casting, etc.

Factors affecting the uniform distribution of the reinforcement particles: Strong variables that affect the particle dispersion in the matrix material include stirring time and speed, slurry viscosity, particle wetting, heating temperature, solidification rate, and gas entrapment minimization. The better the particle distribution, the finer the grain size of the matrix. An essential parameter is the stirrer geometry, which creates different flow patterns to achieve uniform distribution and boost the stirring force to eliminate clusters. Higher agitation speeds have produced a homogeneous particle dispersion. It is also acknowledged that optimizing the stirring duration is just as important as increasing the speed at which the particles are stirred. In general, the dispersion is more uniform with the higher the solidification rate. According to Hashim et al. [176], the soundness of the stir casting is influenced by several process variables, such as the temperature of the furnace, the speed at which stirring occurs, and the duration of stirring, holding, and the solidification process.

Wettability Between the Reinforcement Particle and Matrix Alloy: To give a high degree of mechanical characteristics, good wetting is required. Strong bonds between the matrix and the reinforcing particles result from good wetting. As described by Shorowordi et al. [177], the investigation indicates that the creation of a boron oxide layer around the particles has led to good wettability of B_4C in aluminium in the presence of air. In comparison to Al-SiC and Al-Al_2O_3 composites, it was discovered that particle distribution was superior in Al-B_4C composites [177]. To improve wettability and

87

distribution, the reinforcing particles were warmed to 200^0C and then distributed in step three into the molten Al6061 alloy vortex [178]. It was reported that semi-solid string contributed to wettability. Additionally, it has been noted that using magnesium improves wettability. However, adding more magnesium than 1 weight percent makes the slurry more viscous, which lowers the wettability [179].

Cause of formation of porosity in MMC: The churning movement created turbulence, which trapped atmospheric gas and water vapor inside the melt. Because of the high humidity, water vapor is also present at the particle surface concurrently. Hydrogen, which easily dissolves in aluminium, combines with oxygen in the liquid aluminium to generate water vapor. Water vapor increases the amount of hydrogen in the casting and encourages porosity. Hydrogen is the cause of the gas porosity in aluminium castings. Gas porosity is created when the hydrogen dissolved in the molten Al-alloy becomes trapped as the aluminium solidifies. As more particles were introduced, the porosity content rose. Reinforcement particles seemed to significantly increase the tension during solidification, which in turn affected the formation of slip bands and fissures. Numerous academic publications have discussed the formation of porosity in stir-cast discontinuous reinforced MMC. Most of these reports recognize that porosity arises from four distinct processes: (1) gas entrapment during mixing; (2) hydrogen evolution; (3) shrinkage during solidification; and (4) process parameters such as holding time, stirring speed, and impeller dimension and position. Consequently, porosity content in a stir-cast composite has been found to vary approximately linearly with particle content. According to Ahmad et al. [180], based on microanalysis findings, the solidification rate and metal feeding are the cause of porosity creation.

Techniques Used to Control the Interfacial Reaction: According to P. Gurusamy et al. [181], an interfacial thermal resistance forms between the casting and the mould at the contact interface, which is important in a metallic mould. As temperature rises, the chemical reaction rate between SiC and liquid aluminum increases. The duration of the liquid aluminum and SiC particle contact determines the Al_4C_3 reaction rate as well [180]. Additionally, it has been suggested that the SiC particle can be pre-treated by baking it for several hours at a temperature between 700 ^{0}C and 1,200 ^{0}C to prevent the creation of Al_4C_3. On the surface of the particles, a SiO_2 film forms, which can improve the wetting between the particles and the molten solution and prevent the formation of Al_4C_3. Therefore, careful consideration should be given to several crucial factors stated by [182] to fabricate high-quality particulate-reinforced MMCs with desirable mechanical properties using the stir casting technique.

3.3   STIR CASTING PROCESS PARAMETER

The following variable parameters need to be taken into account during stir casting to prepare the MMC [183]:

1.   **Rotational speed:** To avoid ripping, it is essential to rotate as quickly as possible.

2.   **Stirring speed:** One of the most crucial process variables is stirring speed because it encourages wettability or the connection of the reinforcement and matrix. The pace at which the metal is stirred directly affects how the metal flows. According to research by Rajesh Kumar et al. [184], the ideal speed range is between 300 and 600 rpm. The percentage of wettability will rise as the solidifying rate increases.

3.   **Stirring temperature:** The processing temperature has an impact on the Al matrix viscosity. The matrix particle dispersion is influenced by variations in viscosity. The viscosity of the liquid decreases as the processing temperature is raised in conjunction with an increase in the stirring holding time. The chemical reaction between the reinforcement and matrix is also accelerating. In a study carried out by Rajesh et al. [185], Al is maintained in a semisolid condition at an operating temperature of 630˚C.

4.   **Reinforcement pre-heat temperature:** Pradeep Sharma et al. [186], performed a study and reported that the reinforcement was warmed for 30 minutes at a certain temperature of 500^0C to eliminate any moisture or other gasses that may have been present. Preheating increases the wettability of the matrix reinforcement. Preheating encourages integration with the matrix.

5.   **Stirring time**: Stirring encourages uniform particle distribution throughout the liquid and a flawless interface bond between the matrix and reinforcement. The stirring time between the reinforcement and matrix during composite processing is thought to be crucial [187].

6.   **Pouring temperature:** Maximum grain refinement and an equiaxed structure are linked to low temperatures, but columnar growth is encouraged in many alloys by higher temperatures. A high pouring temperature is necessary to avoid coarse structures and to ensure metal flow and failure resistance.

7.   **Mould temperature**: In non-ferrous casting, the mould temperature should not be either too high or too low. The minimum thickness of the mould should be 25 mm, and this thickness should increase as the casting gets bigger and heavier.

Owing to its desirable characteristics and capacity to function at elevated temperatures, the Al matrix composite reinforced represents a novel class of sophisticated materials. It was discovered that the use of hybrid composites in automotive engine parts, such as drive shafts, cylinders, pistons, brake rotors, and the aerospace industry led to increased interest in researching the wear behaviour of structural components. Metal Matrix Composite (MMC) is a material with higher ultimate strength, yield strength, and hardness. Vickers hardness rose by around 35%, and ultimate tensile strength and yield strength increased by about 24% and 15%, respectively. The increased hardness values implied that the particles contributed to the higher hardness of the matrix [188].

3.4   REINFORCEMENT MATERIALS

The composite characteristics are negatively impacted by the decreased wettability. The main causes of the molten metal non-wetting of the reinforcement are oxide coatings on the metal surface and contaminants that have absorbed onto the reinforcement. Some methods to increase the wettability of metal reinforcements include applying metallic coatings to the reinforcements, adding reactive elements to the molten metal (such as calcium, titanium, or magnesium), and heat treating the particles before addition [189]. The reinforcement material can be categorized into four main groups based on its shape.

(i)   Constant strands.

(ii)   Short fibers, or cut fibers that may or may not be the same length.

(iv)   Particles.

(iii)   Whiskers.

For MMCs, there are two kinds of discontinuous reinforcement, out of it the silicon carbide is the most often used kind of whisker. There are several different types of

ceramics, such as mullite, alumina, silica, boron, alumina-silica, alumina-borosilicate, zirconia, magnesia, and boron carbide. These fibers are all made of delicate, brittle materials. Particles are the most often used and least expensive type of reinforcement. Although continuous fiber reinforcement MMCs offer the best strengthening (in a given direction), particle-reinforced MMCs are more desirable due to their cost-effectiveness, isotropic characteristics, and ability to be produced using techniques similar to those used for monolithic materials [190].

3.4.1   Effects of Alloying Elements

Magnesium and Copper together with other elements: The most significant and adaptable category of commercially available high-strength wrought aluminum-copper-magnesium (Al–Cu–Mg) alloys including manganese. In general, as magnesium and manganese levels rise independently or concurrently, tensile strength rises along with them. Magnesium and manganese additions impair the alloys ability to be fabricated, manganese also reduces ductility. As a result, manganese content in commercial alloys does not rise above 1 weight percent. After heat treatment, the tensile qualities of the wrought Al-4 wt% Cu-0.5 wt% and Mg type of alloy is improved by the additions of cobalt, chromium, or molybdenum; nevertheless, none of these elements provides a clear benefit over manganese.

Magnesium–Silicon: Three categories can be distinguished among Al–Mg_2Si alloys. Within the first category, the combined percentage of silicon and magnesium is less than 1.5 weight percent. These components have a slightly overabundance of silicon or are almost perfectly balanced. In this group, the AA6063 is commonly used for extruded sections and has a nominal Mg_2Si content of 1.1 weight percent. To boost strength in the T6 temper, the second group is said to comprise at least 1.5 weight percent of magnesium

+ silicon as well as additional additives like 0.3 weight percent Cu. Grain structure is regulated by elements like zirconium, chromium, and manganese. In the T6 temper, alloys from this group, including AA6061, achieve strengths that are roughly 70 MPa higher than those of the first group. The third group has a significant quantity of surplus silicon but also overlaps the first two groups in terms of Mg_2Si content. An alloy with 0.8 weight percent Mg_2Si gains roughly 70 MPa of strength when 0.2 weight percent Si is added. Greater surplus silicon concentrations provide fewer advantages. AA6351 and the more modern alloys AA6009 and AA6010 are common in this group. Lead and bismuth are added to an alloy in this series of AA6262 to increase its machinability [190].

Silicon: In wrought alloys, silicon, and magnesium can be combined up to 1.5 weight percent to create Mg_2Si, which is a heat-treatable alloy in the 6XXX series. Hot shortening can be observed in high-purity aluminum-silicon cast alloys up to 3 weight percent Si; the most crucial range is 0.17–0.8 weight percent Si. In alloys made of aluminum, copper, and magnesium, silicon additives (0.5–4.0 weight percent) lessen the occurrence of cracks.

Zinc–Magnesium–Copper: Copper, along with minor but significant quantities of chromium and manganese, is added to the aluminium, zinc, and magnesium system to create the strongest aluminium-base alloys of the 7XXX series that are now used as high-quality Al-alloy in important applications.

3.5 MATERIAL AND METHODS FOR FABRICATION OF METAL MATRIX COMPOSITES

3.5.1 Base Materials

For this experiment, a thick plate of Al-alloy 7475 in T7351 (solution treated + artificially aged condition) was employed, for investigation. Table 3.1 lists the chemical compositions of base metals through spectroscopic analysis. The mechanical parameters of the base aluminium alloy are shown in Table 3.2. Figure 3.1 shows a 25 mm thick plate of as received base material and sample plate for mechanical and spectroscopic analysis. Figure 3.2 depicts the load-displacement curve and microstructure of base aluminium alloy AA7475 in the T7351 temper state at a 400X magnification. With Keller solution, they were etched for 35 seconds (1.5 ml HCl, 1 ml HF, 2.5 ml HNO_3, dissolved in 95 ml of distilled water). After polishing and etching, a metallurgical optical microscope (BMI-101A) was used to study the microstructures and chemical components of the base metal. The mechanical properties of Al-alloy 7475 in T7351 as base material are analysed and given in Table 3.2.

Figure 3.1: A thick plate of base material and samples.
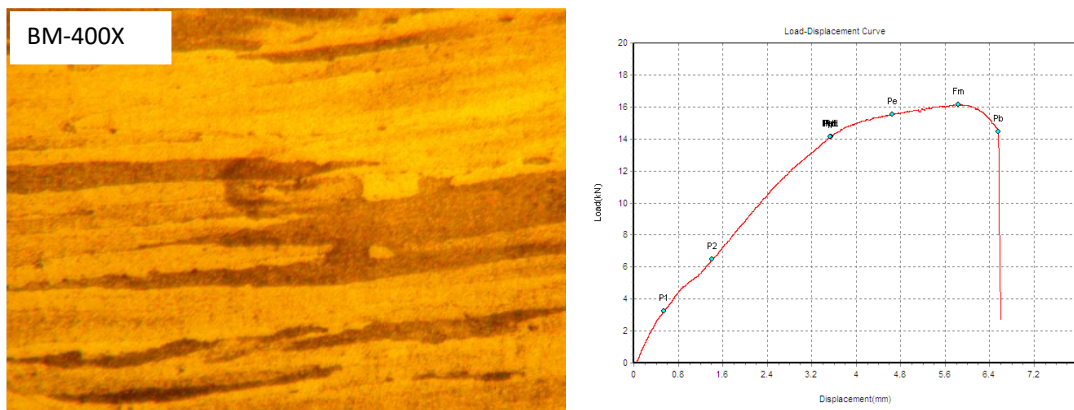
Figure 3.2: Microstructure of an AA7475-T7351 base material sample at 400X with its load-displacement curve.

Table 3.1: Chemical Compositions of AA7475-T7351 alloys.

Material	Al	Si	Mg	Cu	Fe	Mn	Zn	Ti	Cr	Others
7475-T651	91.2	0.10	2.23	1.51	0.12	0.06	5.86	0.06	0.211	0.15

Table 3.2: Mechanical properties of base AA7475-T7351 alloy

Yield Strength (MPa)	Tensile Strength Ultimate (MPa)	Fatigue Limit (MPa)	Hardness (Hv)	Elongation (%)
370	435	160	170	13.2

3.5.2 Reinforcement used

Four different types of reinforcements were used to get the improved properties of formed composites and they are SiC, B_4C, Gr, and MoS_2. These reinforcements were used in hybrid mode by keeping into consideration the desired properties of the material as per their application. The following set of combinations were tried and the mechanical properties of the formed composite are tested by following the ASTM E-8-16a guidelines and are given in Table 3.3.

95

Table 3.3: Hybrid Composites in different sets of combinations are formed through Stir-Casting

S. NO.	Reinforcement	Hybrid Combinations
1	SiC,	SiC 2% +B_4C 2% +MoS_2 2%
2	B_4C,	SiC 2 %+B_4C 3% + Gr 1%
3	Gr, M_OS_2	SiC 3% +B_4C 2% +MoS_2 1% + Gr 1%

3.6   STIR-CASTING SETUP AND PROCESS

The bottom pouring type stir casting machine has a Capacity of 850 grams to 1.8 Kg of Al or Magnesium can be used as shown in Figure 3.3. It is equipped with a heating system with a maximum temperature of 1100 ^{0}C. The top of the stir-casting furnace is where the pre-heating furnace for reinforcing (powders) is fixed. The immersion-style mold/die preheater, which has a maximum temperature of 450 ^{0}C, is included with the machine. The inert and gas mixing system (available only in magnesium casting models) has two inputs: Ar for preserving the inert gas atmosphere and SF6 for preserving the temperature if the temperature rises due to melting magnesium or any flammable materials added to the melt. One can change the gas flow rate between 0 and 10 LPM.

3.6.1   Control Panel: Human Machine Interface (HMI)

The indicator and control system, which displays, records, and stores all actions taken in real time, makes up the human-machine interface. An Android tablet or touchscreen panel that is wirelessly connected to the machine can serve as this HMI. Ten meters distant from the machine, users can use the HMI. Real-time controls over temperature, pressure, or RPM are available from this HMI. A wireless interface connects the tablet to the computer.

Figure 3.3. Bottom Pouring Type Stir Casting Machine with Squeeze Casting Attachment.

3.6.2　Squeeze Casting Attachment

The process of applying load on the molten metal after being poured on the mold is called squeeze die casting. To obtain a good sound cast in this process, there should not be a temperature drop while transferring this molten metal from the furnace. Further to avoid the loss in temperature while transferring the metal, a preheating furnace is used which maintains the temperature of the runway tube which is used to transfer the metal from the furnace to the squeeze casting setup. Also, the mold of the squeeze casting setup is preheated using an immersion-type mold heater which heats the mold from the inner side and keeps the mold at a preheated stage that is ready for the casting.

3.6.3　Hydraulic System: The squeeze casting setup is powered by a hydraulic power pack capable of generating 100 tons load which generates hydraulic pressure to press the casting.

3.7   FABRICATED COMPOSITE

3.7.1   Composite Sample with (SiC 2%+B₄C 2% +MoS₂ 2%) as reinforcement

Composite is fabricated in hybrid mode using SiC 2%, and B$_4$C 2% which is expected to provide a high hardness to the material. To control the high hardness M$_O$S$_2$ 2% is used which carries lubricating properties for the material and used to control the hardness. The samples were sliced using an EDM wire-cutting machine and are shown in Figure 3.4 a. The mechanical properties of the formed hybrid composite were tested and the values are given in Table 3.4 with the corresponding stress-strain curve.

Table 3.4: Mechanical properties of fabricated composite with its stress-strain curve.

Parameter	Result
Tensile strength (N/mm^2)	137
Yield strength (N/mm^2)	85
% Elongation	4.95
Hardness	45.5 HV
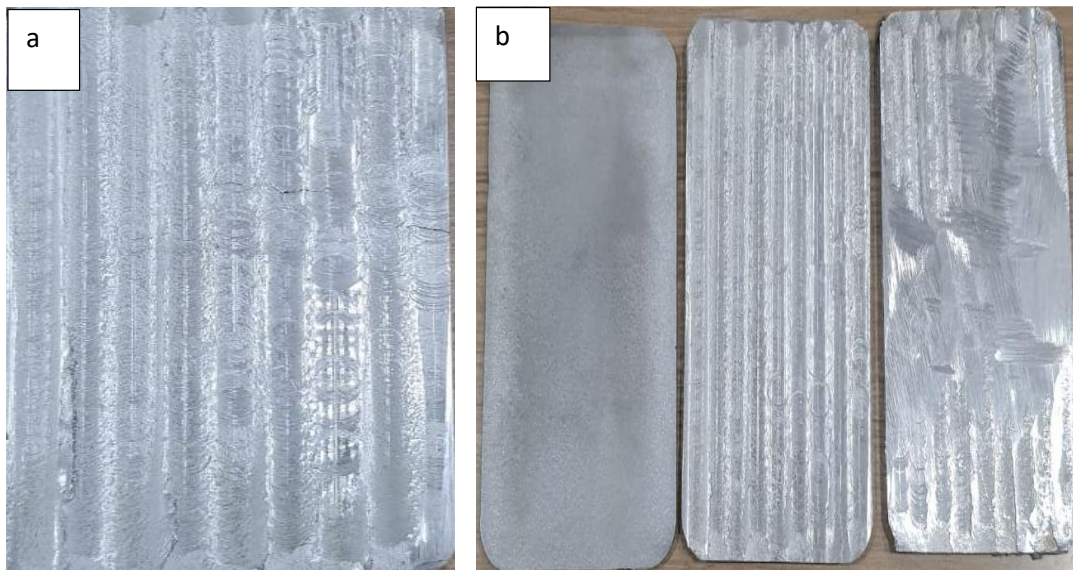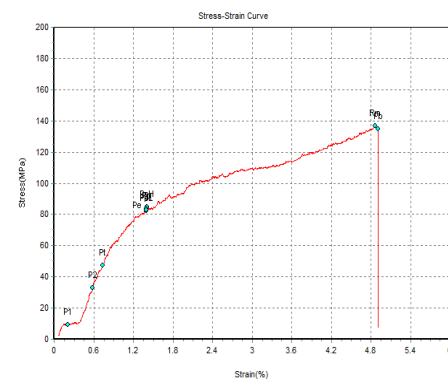
Figure 3.4: Samples with (a) (SiC 2% +B₄C 2% +MoS₂ 2%) (b) (SiC 2 %+B₄C 3% + Gr 1%)

3.7.2 Composite Samples with (SiC 2 %+B₄C 3% + Gr 1%) as reinforcement

Composite is fabricated in hybrid mode using SiC 2%, B$_4$C 3% which is expected to provide a high hardness to the base material. To control the high hardness a Gr 1% is used which carries lubricating properties for the material and used to control the hardness. The samples were sliced using an EDM wire-cutting machine and are shown in Figure 3.4 b. The mechanical properties of the formed hybrid composite were tested and the values are given in Table 3.5 with the corresponding stress-strain curve.

Table 3.5: Mechanical properties of fabricated composite with its stress-strain curve.

Parameter	Result
Tensile strength (N/mm^2)	166
Yield strength (N/mm^2)	95
% Elongation	7.5
Hardness	77.6 HV
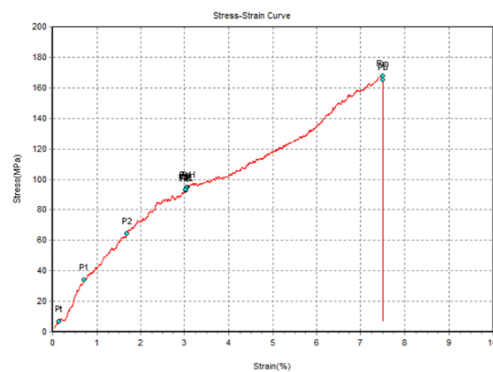
3.7.3. Composite Samples with (SiC 3% +B₄C 2% +MoS₂ 1% + Gr 1%) as reinforcement

The Composite is fabricated in another set of hybrid modes, where all four selected reinforcements are incorporated. In this by using SiC 3%, and B$_4$C 2% which are expected to provide a high hardness to the base material, and to control the high hardness M_OS_2 1% and Gr 1% are used which carry lubricating properties for the material and used to control the hardness. The samples were sliced using an EDM wire-cutting machine and are shown in Figure 3.5. The mechanical properties of the formed hybrid composite were tested, the tensile strength, yield strength, % elongation, and harness were measured and the values

are given in Table 3.6 with the corresponding stress-strain curve.

Table 3.6. Mechanical properties of fabricated composite with its stress-strain curve.

Parameter	Result
Tensile strength (N/mm^2)	80
Yield strength (N/mm^2)	66
% Elongation	2.1
Hardness	41 HV
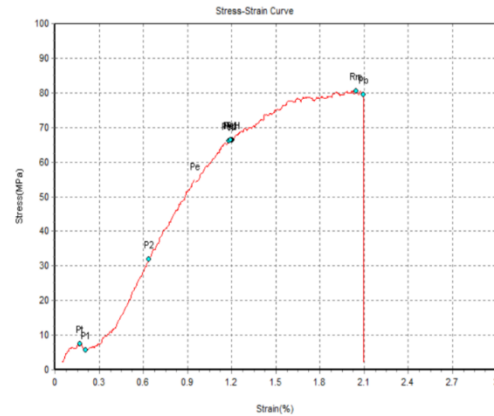
Figure 3.5: Samples with (SiC 3% +B$_4$C 2% +MoS$_2$ 1% + Gr 1%)

3.7.4 Comparative Study of Fabricated Composite

The composite was fabricated in three sets of combinations by using four reinforcements. The mechanical properties were tested and the value of tensile strength, yield strength, and % elongation, were measured and compared. The measured values

of mechanical properties are given in Table 3.7. It was observed that the mechanical properties of composite set 2 with SiC 2%, B_4C 3%, and Gr 1% showed a superior value in comparison to set 1 and set 3 of composite samples. Now, the fabricated composite with SiC 2 %+B_4C 3% + Gr 1% is taken as the best combination of reinforcement for more processing.

Table 3.7: Mechanical properties of hybrid composites in different sets of combinations.

S. No.	Reinforcements	Hybrid Combinations	Mechanical Properties of Formed Composites			
			Tensile Strength (N/mm^2)	Yield Strength (N/mm^2)	% Elongation	Hardness (HV)
1	SiC, B_4C, Gr, M_OS_2	SiC 2% +B_4C 2% +MoS_2 2%	137	85	4.95	45.5
2		SiC 2 %+B_4C 3% + Gr 1%	166	95	7.5	77.6
3		SiC 3% +B_4C 2% +MoS_2 1% + Gr 1%	80	66	2.1	41

3.7.5 Mechanical properties of Chosen composite

Out of the above set of hybrid combinations, the best combination is chosen to check the weldability of the formed composite. The maximum value of tensile strength, yield strength, and % elongation, was obtained with SiC 2 %+B_4C 3% + Gr 1% set of reinforcements. The mechanical properties of the formed composite and the values are given in Table 3.8 with the corresponding stress-strain curve.

Table 3.8: Mechanical properties of the best set of composites (SiC 2 %+B₄C 3% + Gr 1%) with its stress-strain curve.

Parameter	Result
Tensile strength (N/mm^2)	166
Yield strength (N/mm^2)	95
% Elongation	5.7
Hardness	77.6 HV
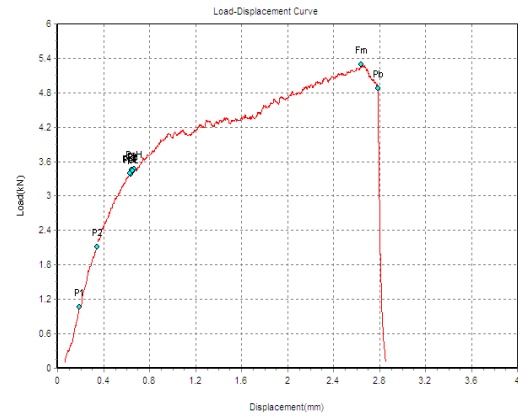
3.7.6. Final (Re-Casted) Hybrid Composites and its Mechanical Properties

Out of the above set of hybrid combinations, the best combination is SiC 2 %+B₄C 3% + Gr 1%, which provides the best mechanical property and is chosen to check the weldability of the formed composite. The new composite was formed by using a stir-casting setup combined with squeeze-casting arrangements for the selected hybrid composite which is SiC 2 %+B₄C 3% + Gr 1%. Table 3.9 provides the mechanical parameters of the newly produced composite, containing enhanced tensile strength, yield strength, and hardness values. The composite that was created has the shape of a 50 mm-diameter cylinder. The fabricated composite is sliced by using an EDM wire cutter in the form sample for welding, testing, and analysis. The fabricated composite and sample plates are shown in Figure 3.6 (a, b).

Table 3.9: Mechanical Properties of Final Hybrid Composites (SiC 2 %+B₄C 3% + Gr 1%) through Stir-Casting with squeeze-casting arrangements.

Reinforcement	Hybrid Combinations	Mechanical Properties			
		Tensile Strength (N/mm^2)	Yield Strength (N/mm^2)	% Elongation	Hardness (HV)
SiC, B₄C, Gr,	SiC 2 %+B₄C 3% + Gr 1%	168	109	5.8	114

102
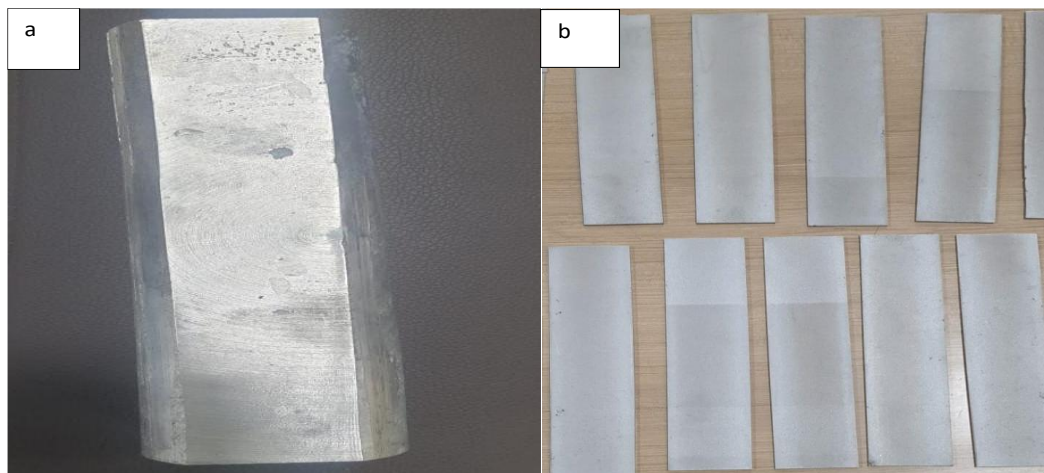
Figure 3.6: Casted composite (a) Squeeze Casted hybrid composite (b) Sample of composite.

3.7.7. Casted Base Material

The base material is cast through stir-casting with squeeze-casting arrangements. The fabricated base material is in the form cylinder of 50 mm diameter, which is sliced in the form of a sample plate using an EDM wire cutter for testing and analysis. The mechanical properties of the formed casting sample were tested and the values are given in Table 3.10 with the corresponding stress-strain curve. The casted base material in the size of the sample is displayed in Figure 3.7.
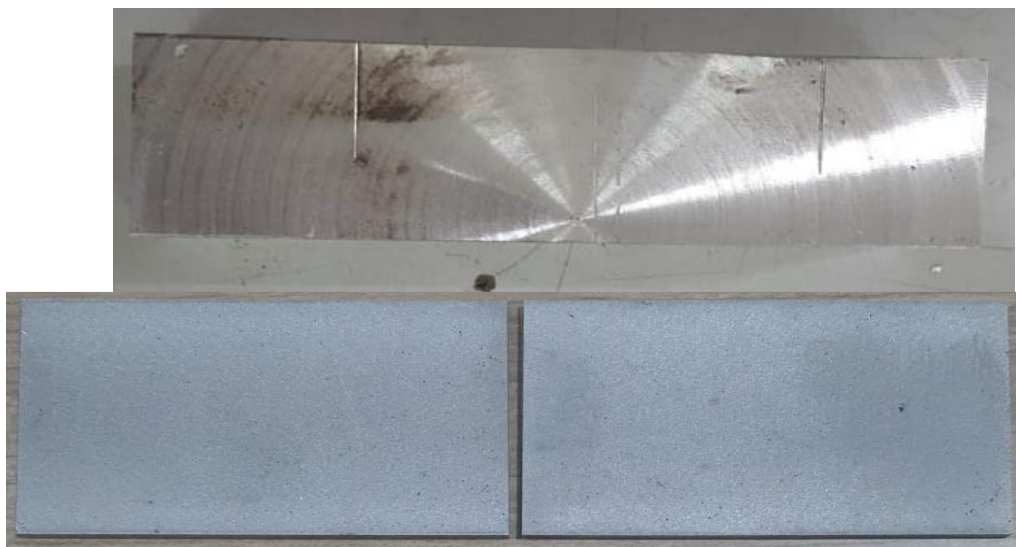
Figure 3.7. Casted base material and sample plate.

Table 3.10: Mechanical properties of fabricated base material with its stress-strain curve

Parameter	Result
Tensile strength (N/mm^2)	158
Yield strength (N/mm^2)	103
% Elongation	5.4
Hardness	104 HV1
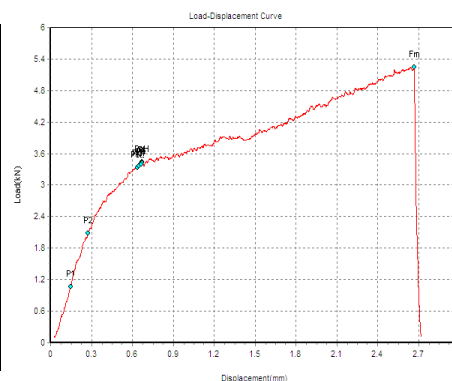
3.8. COMPARATIVE STUDY OF FABRICATED BM AND COMPOSITE

The mechanical properties of the formed composite were compared with a casted base material of Al 7475-T7351 and are given in Table 3.11. It is observed that, for the same set of conditions, there is an improvement in mechanical properties like tensile strength, yield strength, % elongation, and hardness value. The value of tensile strength is improved by 5.95 %, yield strength is improved by 5.5 % and the hardness value is improved by 8.77 %. The corresponding load-displacement curve of hybrid composite and casted base material is shown in Figure 3.8 (a, b).

Table 3.11: Mechanical Properties of Final Hybrid Composites (SiC 2 %+B$_4$C 3% + Gr 1%) and casted BM are formed through Stir-Casting with squeeze-casting arrangements.

S. NO.	Reinforcement	Hybrid Combinations	Mechanical Properties			
			Tensile strength (N/mm^2)	Yield strength (N/mm^2)	% Elongation	Hardness (HV)
1	Casted base material	Al7475 in T7351	158	103	5.4	104
2	SiC, B$_4$C, Gr,	SiC 2 %+B$_4$C 3% + Gr 1%	168	109	5.8	114
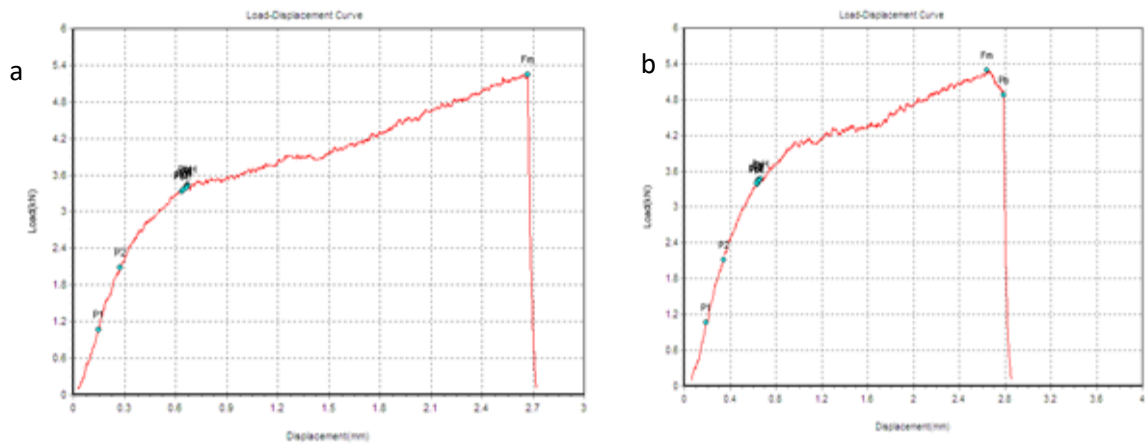
Figure 3.8: A load-displacement plot of (a) Composite Material (SiC 2 %+B$_4$C 3% + Gr 1%), (b) Casted BM.

CHAPTER 4

METHODOLOGY FOR CMT WELDING OF FABRICATED METAL MATRIX COMPOSITE

4.1 INTRODUCTION

As the need for complicated structures grows, so does the need for better connecting methods. Aluminium welding techniques are quite comparable to steel welding techniques. Welding is the most frequent connecting method for Al-alloys. Welding is a joining method that has several advantages, including high joint efficiency, ease of setup, flexibility, and cheap fabrication costs. Welding, despite its numerous advantages, entails melting the parent material, which changes the microstructural and mechanical characteristics of a substance [191]. Unlike carbon steels, which harden when heated by an arc, the basic Al-alloy softens when heated by an arc.

The Al-alloy, along with its different temper conditions, makes up a diverse and adaptable set of production materials. Understanding the distinctions between the different Al-alloys and their various performances and welding characteristics makes it critical to develop an effective welding technique for optimal product design. CMT welding is regarded as an extremely appealing and promising approach for connecting such tough-to-join Al alloys due to its reduced heat input, high gap bridging capabilities, reduced dilution, rapid operation, as well as minimal spatter compared to other welding methods [192]. Alloy 7475 sheet and plate are now being used in high-performance aviation applications for fracture-sensitive parts and components. Given these facts, it is predicted that the use of suitably treated AA7475 alloys will safely lower the total weight of aeronautical structures, which is an essential- criterion for such purposes.

106

Furthermore, it is stated that the Al7475 alloys have exceptional resistance to corrosion and fatigue behaviour. The mechanical properties that are associated with the AA7475 alloys can fulfil the needs of the aerospace and automobile industries in many applications. The increase in mechanical properties of AA7475 alloys can be obtained by suitably introducing a reinforcement material in the Al alloy. So, it is observed that as the aerospace and automobile industries require lighter and stronger materials, the need for the fabrication of newer materials leads the way for aluminium metal matrix composite (AMMC). Hard ceramic particles added to the matrix can greatly improve the tribological and mechanical characteristics of AA7475 alloys [192]. Also, an improved structure can be formed by applying a suitable welding method like CMT to weld the composite of AA7475 alloys.

4.2 CMT WELDING OF ALUMINIUM AND AMMC

Friction stir welding, or FSW is a solid-state welding technique that has shown promise in the joining of aluminum matrix composites (AMCs). The use of FSW to join AMCs is still laden with difficulties, despite significant advancements in recent years. Fusion-based welding techniques cannot produce efficient joints in terms of the strength of AMC materials because of the interaction between the matrix and reinforcements, which can result in the disintegration of reinforcements in molten metal or the development of brittle secondary states in the weld pool. Regarding welding procedures, multiple studies have demonstrated that using friction stir welding (FSW) can result in more effective joints with significantly lower porosity, cracking, distortion, and reinforcement dissolution. On the other hand, not much work has been reported about the friction stir welding of AMCs. An overview of the state of the art in AMC material welding is given in this assessment. The welded joint may have flaws including

kissing bonds and tunnel defects due to either excess or inadequate heat input in the weld zone, as seen by the macrostructure and microstructure of FSW connections in AMCs. Significant alterations have also been made to the welding zone structure and appearance. Therefore, it is important to use the right welding parameters to prevent these flaws. Microhardness, tensile strength, and fatigue are mechanical characteristics of FSW joints in AMCs that are very important, especially for crucial components. The creation of intermetallic compounds, PWHT, welding conditions, tool design, and other factors, all affect the tensile strength of AMC joints. When compared to joints made using traditional welding techniques, the efficiency of joints created with FSW is better. The intermetallic compound formation, PWHT, and strain rate are further elements that impact the FSW AMC joint's tensile strength. Studies on the fatigue characteristics of AMC joints were scarce. Under all circumstances, the FSW joints have a shorter fatigue life than the BM. As the strain amplitude declines, the fatigue life is significantly impacted by the surface roughness. Numerous parameters, including surface roughness, microstructure homogeneity, reinforcement weight percentage, and residual stresses in the weld zone, influence the fatigue strength and fatigue crack growth for FSW AMC joints. Additionally, the way reinforcement appears on aluminum matrices may influence where stress is concentrated. Consequently, further work is required to comprehend the low cycle fatigue behaviour of AMC joints using FSW.

For many kinds of AMCs, there is not a common pattern between the mechanical characteristics and welding variables. Ultimately, one of the biggest obstacles to the industry adoption of the FSW method is the wear of the FSW tools, particularly the pin, which is still a serious problem when connecting AMC.

The cold metal transfer (CMT) procedure is a recent advancement in welding technology. Its low thermal input and no-spatter welding method make it perfect for welding aluminum and its MMC [193-194]. A modified kind of metal inert gas (MIG) welding is called CMT. Since the base material melts during the process of welding, an aluminum alloy microstructure and mechanical qualities typically change after welding. It provides a lack of strength in the weld. To solve this issue, the welded portion is heat-treated to give it the appropriate mechanical qualities and to reduce any remaining tension. The primary innovation is in the integration of wire motions into the welding process and the process control system as a whole. The amount of heat input and spatter can then be significantly reduced.

4.3 EXPERIMENTATION

Experimentation starts with the proper evaluation of process parameters and its effect on output. To get this cause-and-effect relationship several pre-experiments are required. The process of developing these relationships between input parameters and output or responses is called experimentation which needs a properly designed approach.

4.3.1   Parametric analysis of weld

A measurable factor that establishes a set of criteria for how it works is called a parameter. System parameters are essential components that help determine and assess the performance of the system. To evaluate the influence of the parameter on the performance or solution of the problem, a parametric analysis or sensitivity analysis is necessary. Parametric analysis is an important tool for conducting proper experimentation, design exploration as well as influencing data examination. In this,

the parametric analysis is used to investigate how various welding factors affect both the performance and quality of the weld.

4.4 Experimental arrangements and procedure

4.4.1 Robotic CMT setup and process- The welding system contains Trans Pulse Synergic 4000 CMT welding equipment, a VR 7000-CMT 4R/G/W/F++ weld wire feed system, and a KUKA welding robot, as well as an experimental platform to construct the butt joint. The complete robotic CMT setup is shown in Figure 4.1. To make a faster welding process, the welding flame and weld were angled at 70 degrees for thin sheet welding. Argon gas was delivered through the nozzle at a rate of 15 l/min as a shielding gas during welding. A set of pre-experiments was done to optimize the welding process variables.
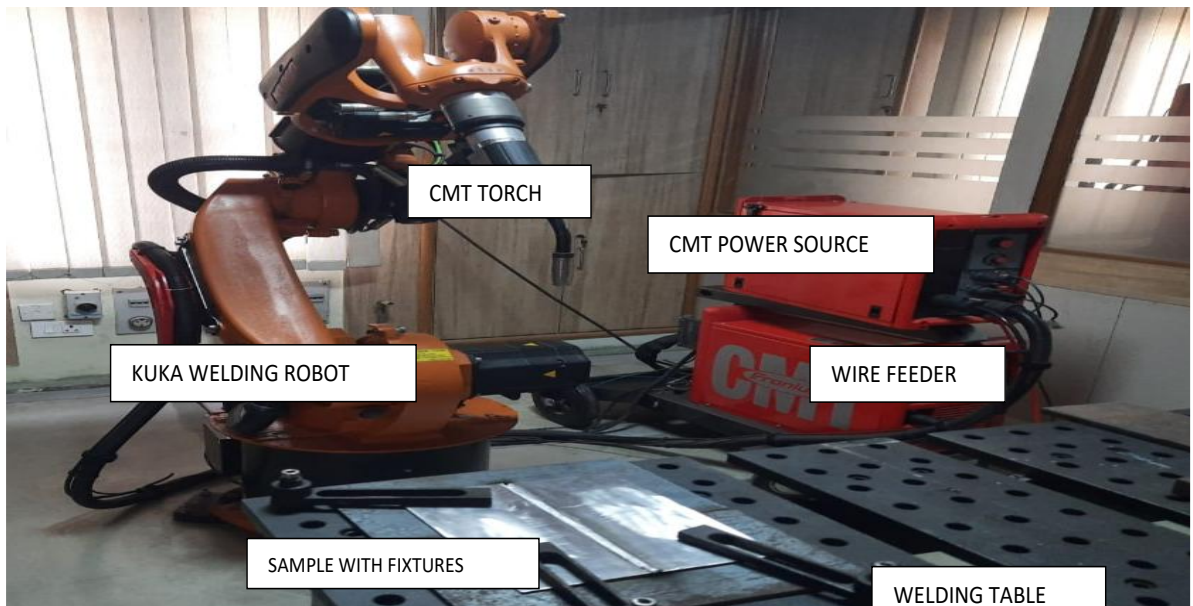
Figure 4.1: A complete robotic CMT welding setup.

4.4.2 Wire Feed System

The wire feed system is responsible for delivering the welding wire to the welding torch at a consistent and controlled rate. The 7000 CMT wire feed system is equipped with advanced features such as variable ratio (VR) functionality, allowing for precise adjustment of wire feed speed and deposition rate. This capability is crucial for maintaining uniform filler metal deposition and controlling weld bead geometry. The VR functionality of the wire feed system enables operators to optimize the deposition rate based on the welding parameters and material properties. By adjusting the wire feed speed in real-time, operators can achieve the desired weld penetration, bead profile, and fusion characteristics [195-197]. Furthermore, the wire feed system incorporates features for wire spool management, wire tension control, and wire feeding reliability, ensuring uninterrupted welding operation.

4.5   Experimental trials and determination of welding parameters

The welding process parameters were decided through trial to get the best weld bead. For this, a large number of trial experiments were conducted to identify the contributing welding parameters. Out of all input parameters, the most contributing welding parameters were decided through parametric analysis that directly affected the weld quality and weld performance.   The most contributing input parameters are voltage, welding speed, and wire feed rate. Trial experiments were performed by varying these parameters for their minimum to maximum value and the range of contributing welding parameters is given in Table 4.1. Figure 4.2 shows the welded plate used for trial experiments.

Figure 4.2: Welded sample and plate used for trial experiments.

Table 4.1: Welding Parameters Range

Welding Process Parameters	Symbols	Range	
		Minimum	**Maximum**
Voltage (V)	A	14	18
Welding Speed (m/min)	B	0.36	0.48
Wire Feed Rate (m/min)	C	6	8

After getting the range of contributing welding parameters, three levels of each parameter were selected to perform the final experiments. The symbols A, B, and C are given to each contributing welding parameter and they are welding voltage, welding speed, and wire feed rate respectively. The three levels of each contributing factor that are, welding voltage, welding speed, and wire feed rate are given in Table 4.2.

Table 4.2: Welding Parameters and Their Levels.

Input Parameters	Symbols	LEVELS		
		1	**2**	**3**
Voltage (V)	**A**	14	16	18
Welding Speed (m/min)	**B**	0.36	0.42	0.48
Wire Feed Rate (m/min)	C	6	7	8

4.6 EXPERIMENTAL DESIGN

An experimental design is a test/investigation or a sequence of tests in which the planned variation is applied to the input parameters to check the variations in the output variables. For this, a systematic approach called design of experiment (DoE) is available to investigate the effect of change in input variables on output. In DoE the input parameters are also known as independent variables and the output is called dependent variables or responses. It provides all possible combinations of input parameters and its effect on responses or output. The right choice of experimental design will maximize the amount of information for experimentation and analysis. The DoE has different types, out of which the Taguchi Method is one of them for proper experimental design.

4.6.1 Taguchi Design

The Taguchi analysis is based on the idea that the desired result will be attained at the planned stage prior to the experiment. Reducing the variability around the target value of the product attributes is the primary goal of Taguchi analysis. This can be obtained by identifying the most controllable component causing the variability and designing the process around it. A methodical use of experimental design (DoE) to enhance the caliber of the experimental outcomes is known as Taguchi analysis. Taguchi L9 orthogonal array is very useful to effectively test two to four variables at three levels. Taguchi L9 orthogonal array will be sufficient without the need to conduct an excessively large number of experiments. So, the Taguchi L9 orthogonal array is used for three variables at three levels [198-199].

4.6.2   Plan of Experimentation

To get a fruitful experimental result a suitable experimental plan is necessary. The experimental plan starts with the selection of welding parameters that directly or indirectly affect the quality of results expected from the experiments. The parameters that directly affect the results in welding are welding voltage, welding speed, and wire feed rate. To check the effect of these three parameters on weld quality three levels of each parameter were selected and for this, a standard Taguchi's Orthogonal array L9 is available to conduct the planned experimentation. Taguchi's Orthogonal array L9 arrangement of experimentation is given in Table 4.3, with three variables and three levels of each variable.

Table 4.3: Experimental plan according to Taguchi's Orthogonal array of L9.

Experiment No.	Voltage (V) A	Welding Speed (m/min) B	Wire Feed Rate (m/min) C
1	1	1	1
2	1	2	2
3	1	3	3
4	2	1	2
5	2	2	3
6	2	3	1
7	3	1	3
8	3	2	1
9	3	3	2

4.6.3 Input Parameters to Weld AMMC Samples as per the Experimental Design

As per Taguchi's Orthogonal array L9, the welding parameters wire feeding rate, welding speed, and voltage values were decided according to the range. Nine runs were conducted as per the experimental design and the corresponding values of parameters are given in Table 4.4.

Table 4.4: Input Parameters for welding as per the experimental design

Experiment No.	Voltage (V)	Welding Speed (m/min)	Wire Feed Rate (m/min)
1.	14	0.36	6
2.	14	0.42	7
3.	14	0.48	8
4.	16	0.36	7
5.	16	0.42	8
6.	16	0.48	6
7.	18	0.36	8
8.	18	0.42	6
9.	18	0.48	7

4.7 PREPARATION OF TEST SAMPLES

The final composite is fabricated through stir casting with a squeeze casting arrangement to get the best quality composite. In squeeze casting a pressure of 40 KN is applied through the piston over the molten metal in cylindrical die, which reduces the chances of a defect in the casting and also simultaneously refine the grain size of casted composites. The casted composite and base material are in the form cylinder of 50 mm in diameter. They are sliced in the form of sheets of 3 mm in thickness and about 38.50 mm in width through an EDM wire cutter. Now the formed samples were welded by using a robotic CMT set-up. The test samples were prepared for mechanical and microstructural analysis by following the ASTM E-8-16a standard and are shown in Figure 4.3.
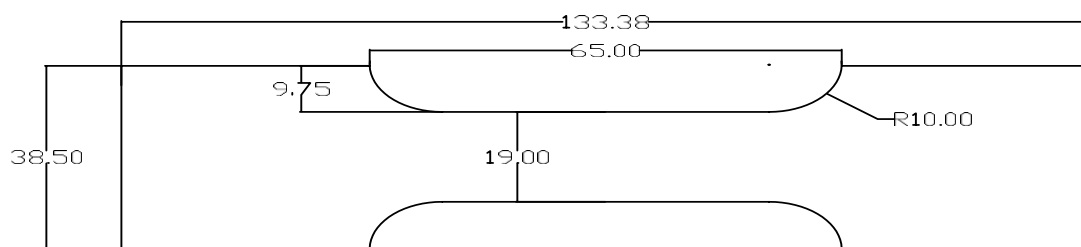
Figure 4.3: Tensile Sample Particulars of Composite as per ASTM E-8-16a Standard, all dimensions are in mm.

4.7.1 Welding of AMMC Sample and used filler metal

For this experiment, a stir-casted composite of Al-alloy 7475 was employed, for investigation. Coupons measuring 66 mm x 38.50 mm x 3 mm were cut by using wire EDM and put in a butt joint arrangement with no space between the samples. The mechanical properties of the composite material were analyzed and summarized in Table 3.11. The filler metal is made of 1 mm-diameter UNI-ER 4043 (AlSi5) wires. For optimal weld bead, robotic CMT welding techniques were used. Three seconds before the arc was struck, pure argon shielding gas was turned on at a flow rate of 15 l/min. Following an experimental design, the suitable welding parameters were chosen and are listed in Table 4.4. As per the Taguchi L9, the sample plates are welded, and tensile samples are prepared and shown in Figure 4.4. Table 4.5 lists the chemical compositions of the filler metal and composite materials.

Table 4.5: Chemical composition (Wt.-%) of the used filler metal and fabricated composite.

Material	Al	Si	Mg	Cu	Fe	Mn	Zn	Ni	Ti	Cr	Others
ER4043	92.6	5.6	0.05	0.3	0.8	0.05	0.12	0.047	0.02	<0.004	<0.05

Element	Results %
Si	0.079
Fe	0.689
Cu	1.546
Mn	0.041
Mg	2.285
Cr	0.182
Ni	0.0047
Zn	6.308
Ti	0.032
Cd	<0.00010
Co	0.0028
Pb	0.0011
Sn	<0.0004
Al	88.68
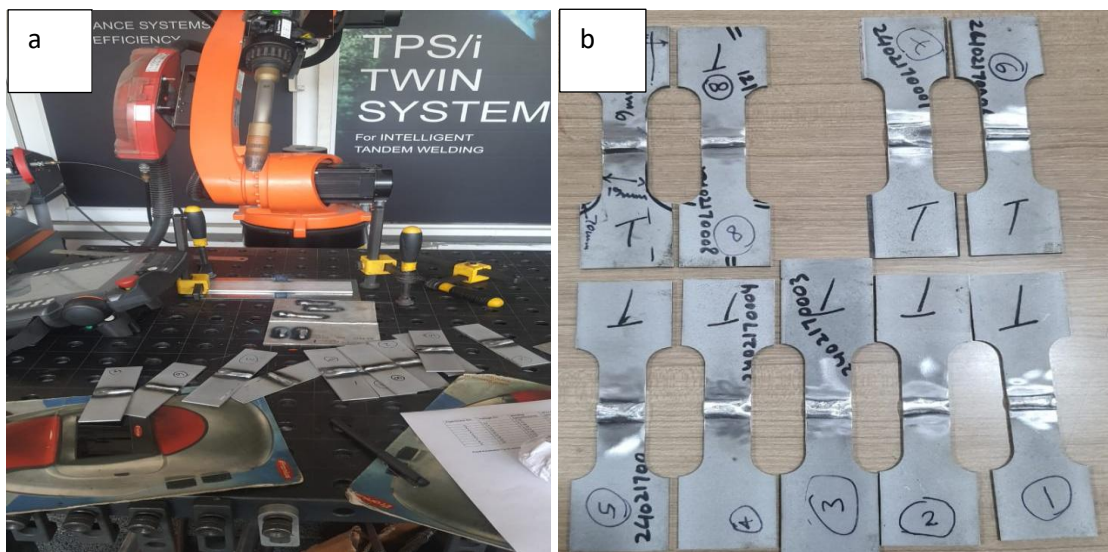
Figure 4.4: A schematic of (a) welded plate using CMT setup and process (b) welded tensile test samples.

4.7.2 Mechanical testing of the CMT joints of AMMC

After ocular inspections, a non-destructive test was performed to discover the flaws created on the weld surface. After performing an LPT (liquid penetrant test) on all of the samples, it was discovered that the welding was free from serious flaws. A Microhardness test was carried out on the transverse section of the welded specimen with a 0.2 mm separation and a weight of 300 g imposed for 15 seconds using a digital Vickers hardness tester (VH-1000B). Tensile testing was used to evaluate the elongation, yield strength (YS), as well as tensile strength (TS) of the test section. The micrographs were taken from different locations of the welded samples like WM, HAZ, and BM. The microstructural analysis was conducted to characterize the weld.

CHAPTER 5

RESULT AND DISCUSSION

5.1   INTRODUCTION

The stir-casting method is used and described in detail to form hybrid composites. The AA7475 alloy is taken as a matrix material and SiC, B_4C, MoS_2, as well as Gr, are used as reinforcement to fabricate a hybrid composite. The fabricated composites are in hybrid form and in three different sets of combinations. Mechanical tests were done to check the properties of each composite. Based on the tensile strength result and micro-hardness test values the best composite is re-casted using a bottom pouring type stir-casting machine with a squeeze casting arrangement. The final fabricated composite is sliced in the form of samples and is welded by using a robotic CMT welding process. The welding parameters ranges were decided as per the trial experiments and then experimental design was applied. The Taguchi L9 orthogonal array is used as per the three welding variables at three levels. The nine samples were welded as per the experimental design. The mechanical properties like tensile strength, hardness, and microhardness as well as microstructure were measured and reported. The mechanical and microstructural properties of the formed composite as well as the weld sample were analysed. The obtained results were analysed and discussed in detail. The SEM with EDX is used to discuss the composition of the formed weld. The results were analysed and discussed in detail. Based on the results and discussion, the best welding parameters were chosen and the confirmatory test was performed to check the weldability of fabricated composite as well as base AA7475 alloy. The mechanical properties were tested, microstructure analysed and reported to confirm the findings through confirmatory tests for industrial applications.

118

5.2 TESTING AND ANALYSIS OF ALUMINIUM METAL MATRIX COMPOSITE WELD

5.2.1 Mechanical testing of the CMT welded joints

Following visual examinations, a non-destructive test was run to identify the flaw left on the weld surface. All of the samples were subjected to a liquid penetrant test (LPT), which revealed that there were no significant welding flaws. Using a digital Vickers hardness tester (VH-1000B), a microhardness test was performed on the transverse portion of the welded specimen with a 1 mm separation and a weight of 300g applied for 15 seconds. The tensile testing samples were prepared following ASTM E-8-16a guidelines. A welded test specimens are given in Figure 5.1. Elongation, yield strength, and tensile strength of the test section were all assessed by tensile testing.

Figure 5.1: welded samples for tensile test.

5.2.2 Macrostructures of Weld

Even at low magnification, it is clear to see that there is no contact between the fusion zone and the HAZ in Figure 5.2. There is no discernible difference in composition between the weld metal and the base metal, except for a small concentration of Si in the melted zone owing to the presence of filler wire material. Due to its low heat input characteristics and the lack of surface porosity and other imperfections on the weld surface, CMT welding eliminates the possibility of hot cracking.

5.2.3 Weld defects- Because it is a low heat input welding process and the lack of surface porosity and other imperfections on the weld surface, CMT welding eliminates the possibility of hot cracking. Small surface porosities are seen on the joined weld surface, but they do not affect the weld quality. As demonstrated in Table 5.1, there are no hot cracks, blowholes, or other dangerous faults on the weld according to the test results for all samples.

Figure 5.2: Macro-structure of CMT welded Sample at 10X.

Table 5.1: Weld Structure Test.

Parameter			
Welding Point No.	**Welding Height**	**Welding Length**	**Cracks/Blow hole/Harmful Defect**
1.	3.251 mm	6.258mm	Not observed at the weld area

5.3   TENSILE TESTING OF WELDED COMPOSITE SAMPLES

The tensile test was performed to assess the tensile strength (TS), yield strength (YS) as well as percentage elongation of the welded composite samples.   The test was conducted using a universal tensile testing machine and is shown in Figure 5.3. The corresponding values of tensile strength, yield strength, and % elongation is given in Table 5.2.
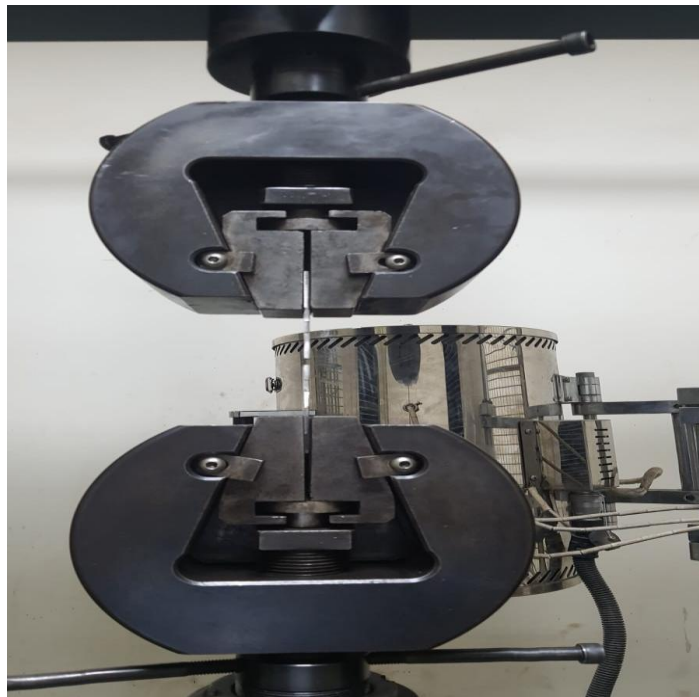
Figure 5.3: Universal tensile testing machine for tensile test.

5.3.1 Tensile properties of the welded samples

Tensile testing was done to examine the weldment's performance, and the results (TS, YS, and elongation values) are displayed in Table 5.2. Comparing the tensile strength of the casted base metal standard alloy, which is 158 MPa, with the composite formed which shows the tensile strength of 168 MPa. An improvement in TS, YS, and % elongation was observed in the casted composite. Now the formed composite was welded as per the Taguchi L9 of DoE, the TS, YS, as well as percentage elongation, were analyzed and the values were tabulated in Table 5.2. The corresponding load-displacement curves for all the samples from L1-L9 are shown in Figure 5.4. It was observed that the maximum TS of the WM is 111.98 MPa which is 66.65 % of the composite for sample 1 and shows similar patterns for the YS. The tensile specimen of the CMT welded junction does not deform plastically, yielding the lowest WM elongation of 3.2 percent. All the welded samples fail at the weld metal. As per the performance of HAZ and BM, the WM is the welding joint's weakest link.

Table 5.2: Welding Input and Output Parameters

Experiment No.	Voltage (V)	Welding Speed (m/min)	Wire Feed Rate (m/min)	TS (N/mm^2)	Yield Strength (N/mm^2)	% Elongation
1.	14	0.36	6	111.98	67.92	3.2
2.	14	0.42	7	96.32	68.90	1.5
3.	14	0.48	8	90.01	77.80	5.2
4.	16	0.36	7	101.26	55.80	1.56
5.	16	0.42	8	82.30	53.60	7.0
6.	16	0.48	6	104.36	63.40	4.6
7.	18	0.36	8	78.20	46.80	3.88
8.	18	0.42	6	95.24	50.00	13.6
9.	18	0.48	7	84.66	55.48	6.0
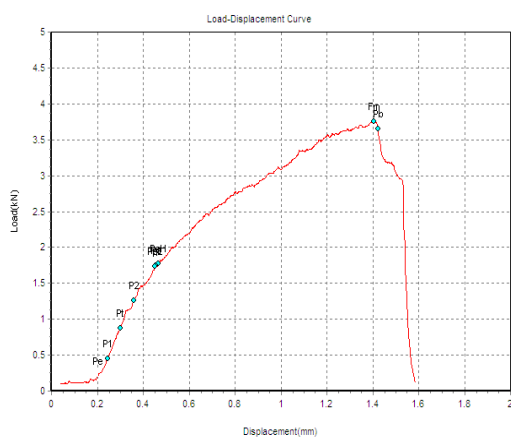
Sample-1
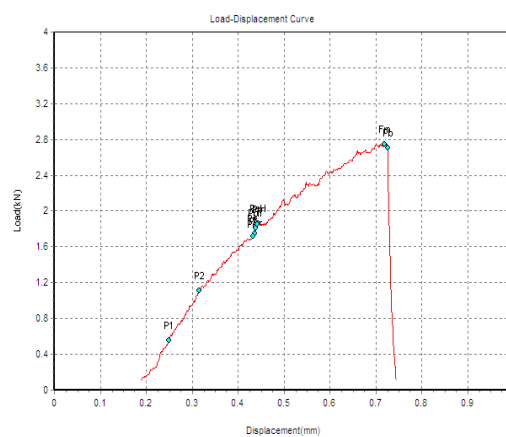
Sample-2
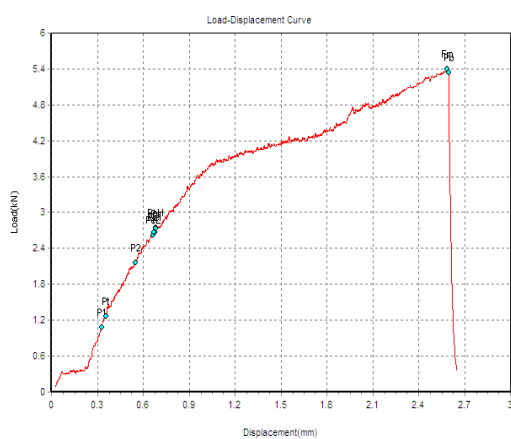
Sample-3
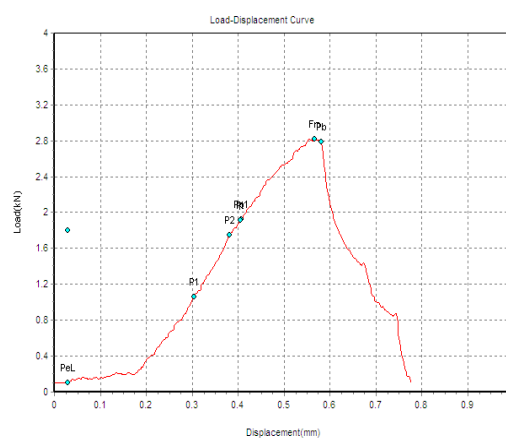
Sample-4

Sample-5

Sample-6

123
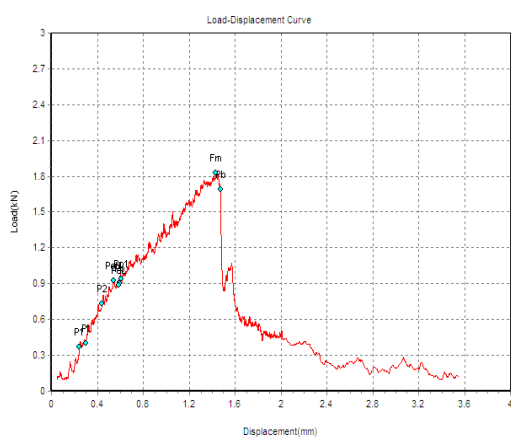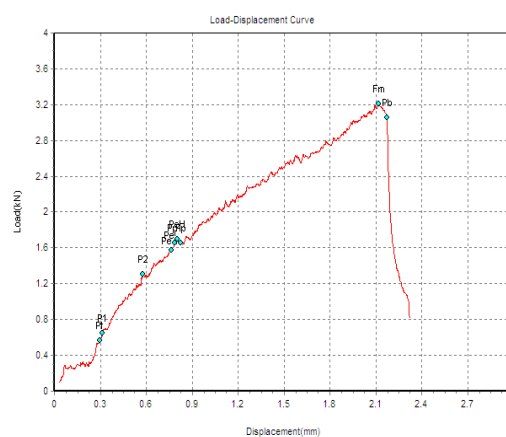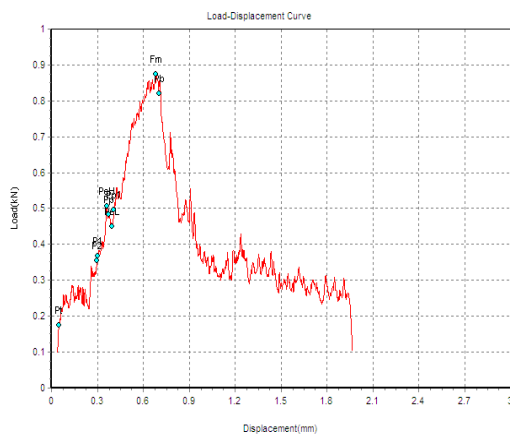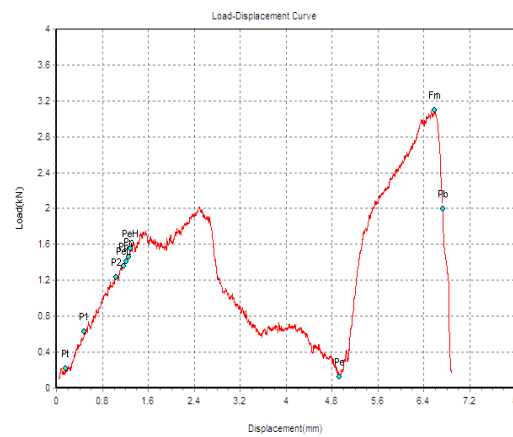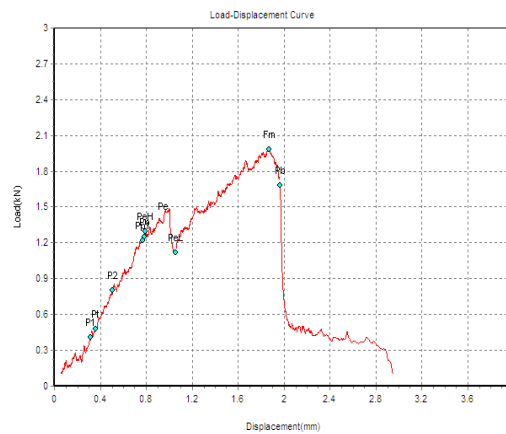
Sample-7

Sample-8

Sample-9

Figure 5.4: Load-displacement curves of weld sample L1-L9.

5.4   MICROHARDNESS ANALYSIS

5.4.1 Microhardness Analysis of Fabricated Base Metal and Composite Material

The Vickers microhardness test was conducted to check the hardness value of casted base metal as well as composite. The Cross-sectional image of the casted Al-alloy and composite sample is given in Figure 5.5. It was found that the average hardness value for the fabricated composite is 151.18 HV and for the casted base metal is 138.8 HV which is given in Table 5.3.
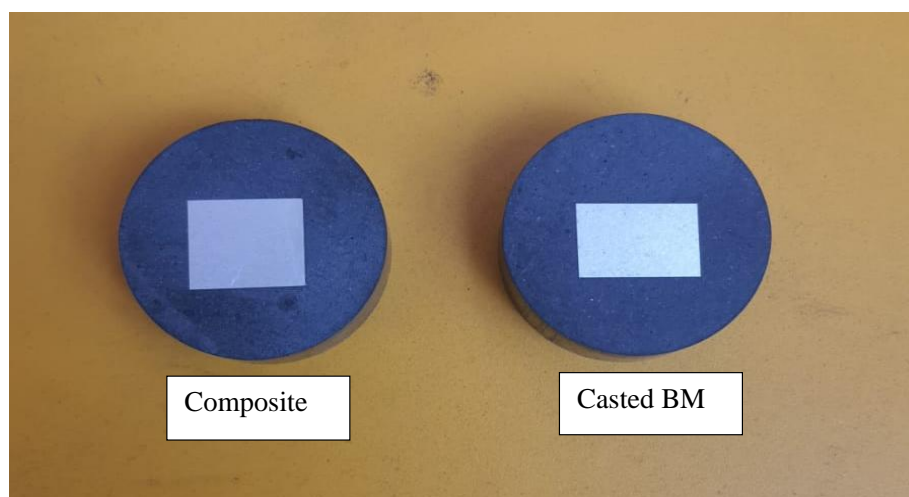
Figure 5.5: Cross-sectional image of casted base metal and composite material.

Table 5.3: Hardness Test.

Parameter	Result (Avg.)
Hardness Test (Composite BM)	151.18 HV
Hardness Test (Casted BM)	138.8 HV

A significant improvement in the hardness value was observed for composite material.

The hardness plot for composite and casted base material is shown in Figure 5.6.
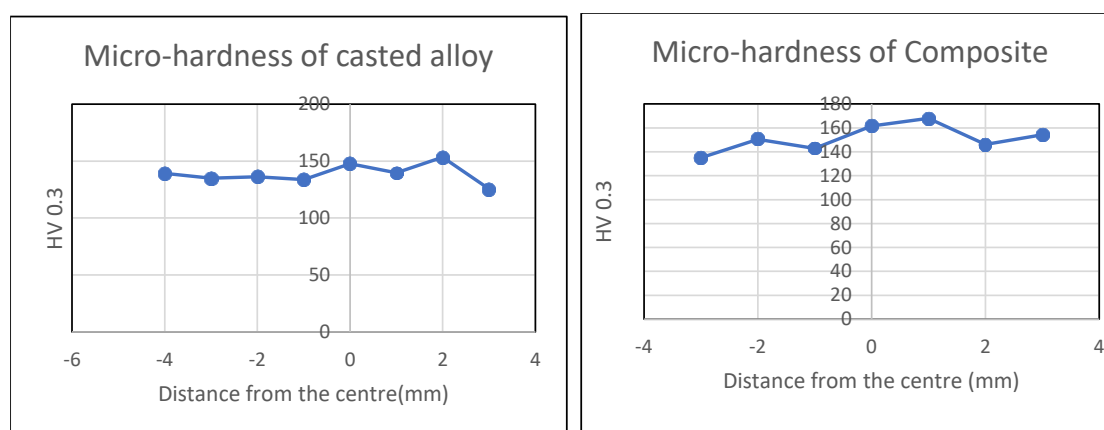
Figure 5.6. Micro-hardness Plot of (a) Casted Al-alloy (b) Casted Composite.

5.4.2   Microhardness Analysis of the Welded Samples

Weld cross-section flaws and macrostructure of the welded connection of composite have already been studied and it was observed that there are no significant flaws on the weld surface that can affect the weld quality. The results of the Vickers microhardness test for the CMT welded samples are shown in Figure 5.7. The variations in the values of hardness are shown in the plot for the different samples from L1- L9, and from different locations like WM, HAZ, and BM. The hardness variation from the weld center towards BM is plotted and shown in Figure 5.7.

The average hardness values of WM and HAZ are given in Table 5.4. The average hardness values of WM and HAZ are 98.21 HV and 115.4 HV respectively. The hardness value increases from weld metal to composite base. The weld metal shows the lowest hardness which is 64.69% of composite whereas the HAZ shows 76.33% hardness of the composite base metal. The lowest hardness was recorded at the WM and is only 64.69% of the composite metal in the CMT sample due to the weld's heterogeneous structure, which is primarily made up of filler metal. Similar outcomes were seen by [140] in Al5.5Zn2.5Mg2.2Cu welded joints, where the WM is the weakest component and only possesses a 56% hardness of the base material. This is because the alloy components move toward the grain boundaries during solidification, softening the WM. This might also be because AA4043, a softer filler material than AA7475-T7351, was used. The HAZ, which is essentially a transition zone created by the welding heat input, results in the formation of the recrystallization strengthening phase and partial hardness restoration. So, the HAZ shows a better hardness value than weld metal. The cross-sectional image of the welded sample for L1-L9 is shown in Figure 5.8.

The combined plot for welded samples L1-L9 is shown in Figure 5.9. The combined

plot shows the average WM hardness is lower as compared to HAZ and BM.
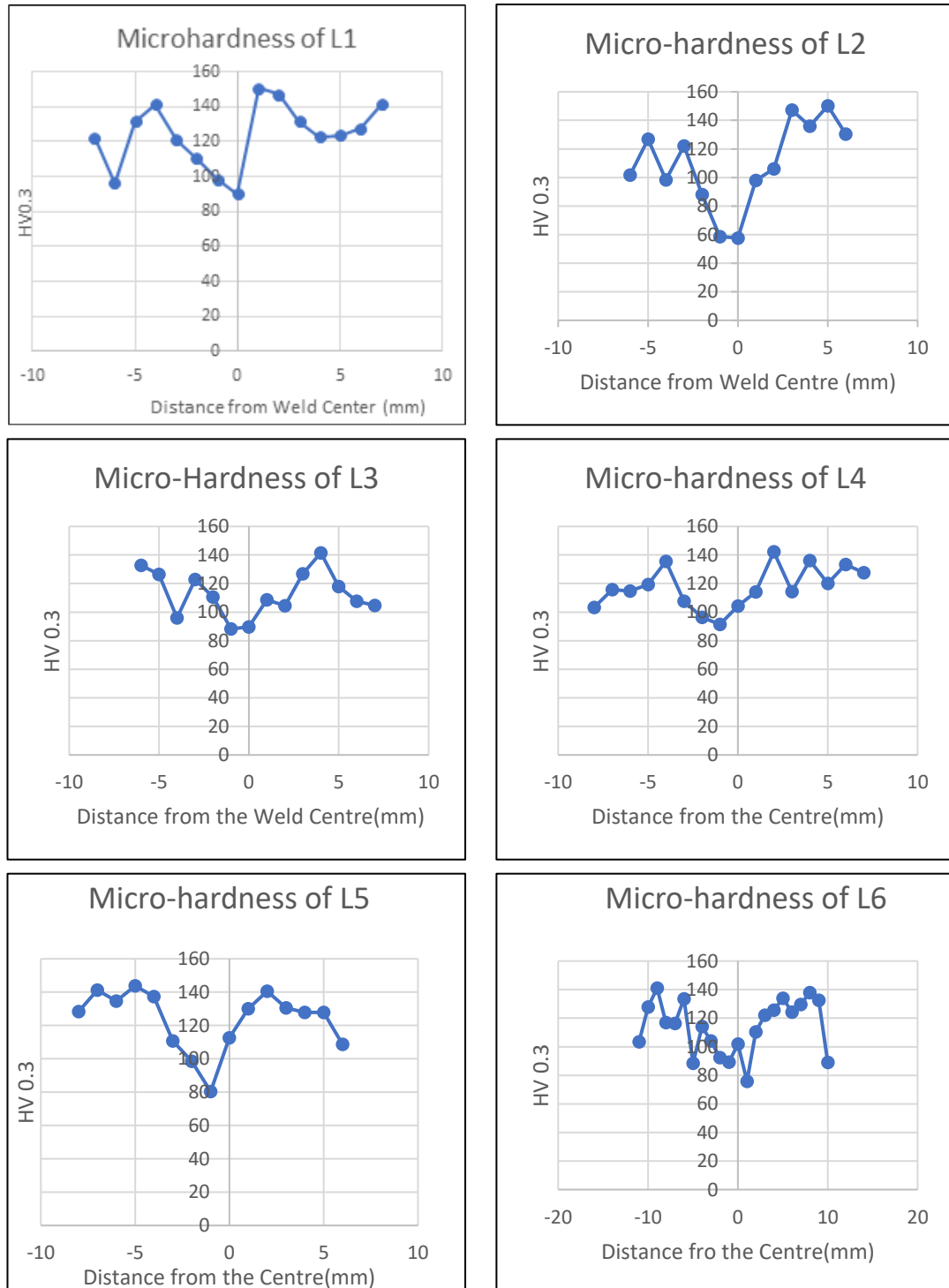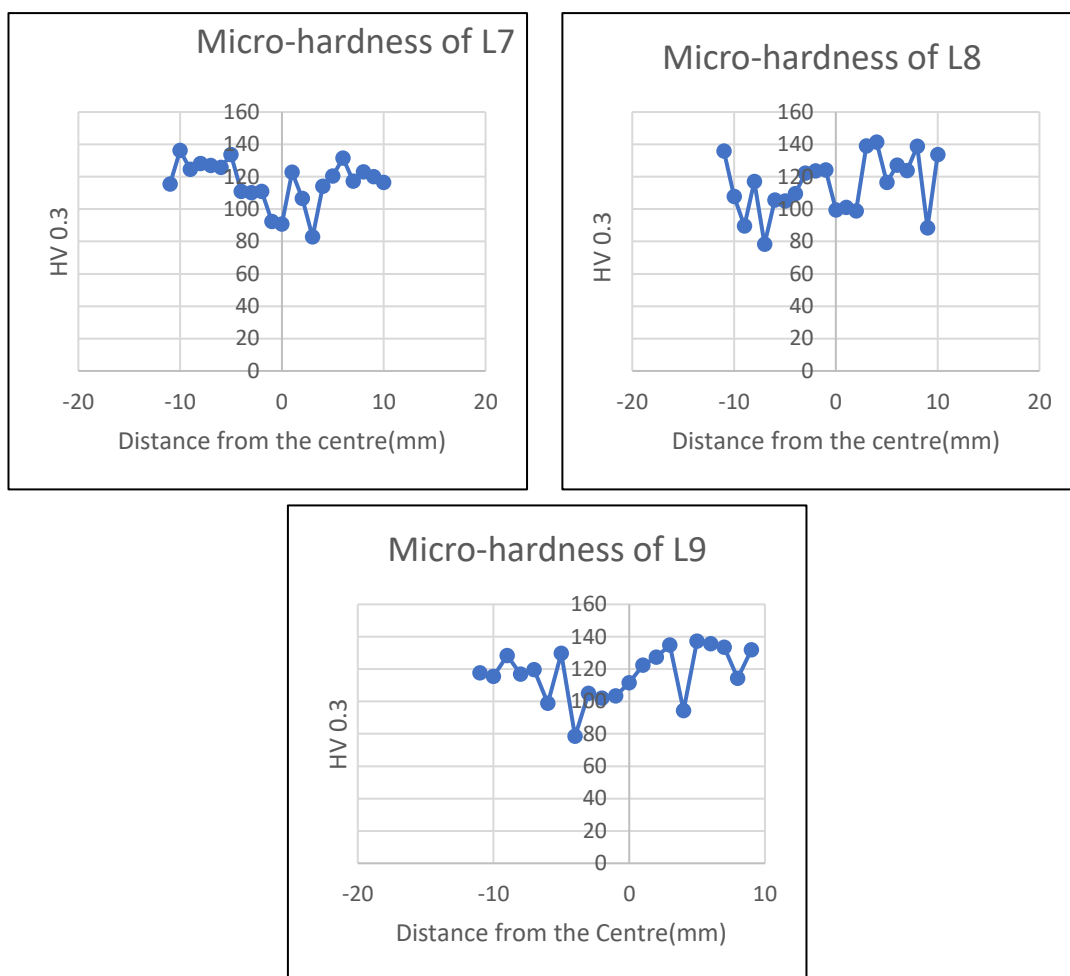
Figure 5.7. Micro-hardness Plot of Composite sample L1-L9.
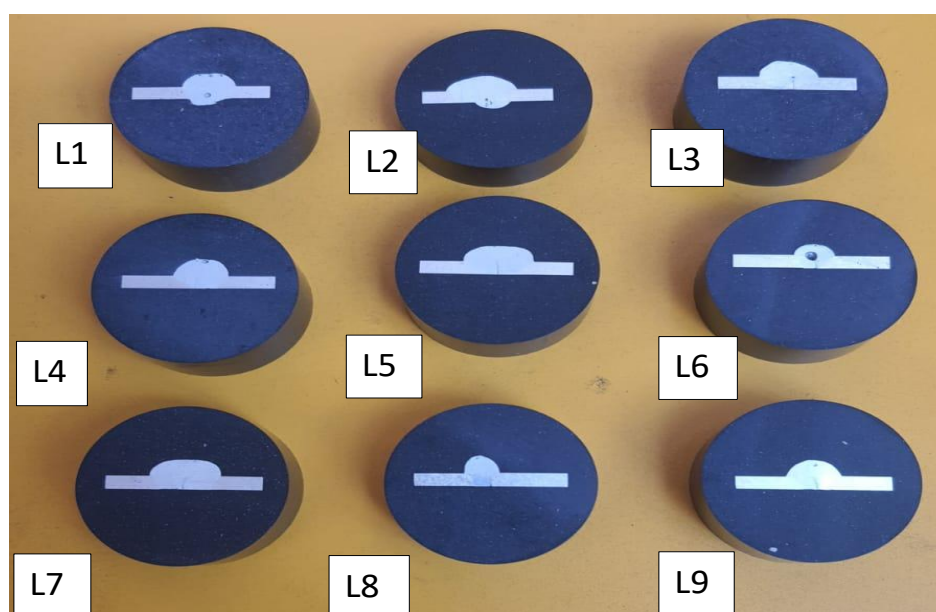
Figure 5.8. Cross-sectional image of weld samples L1-L9.
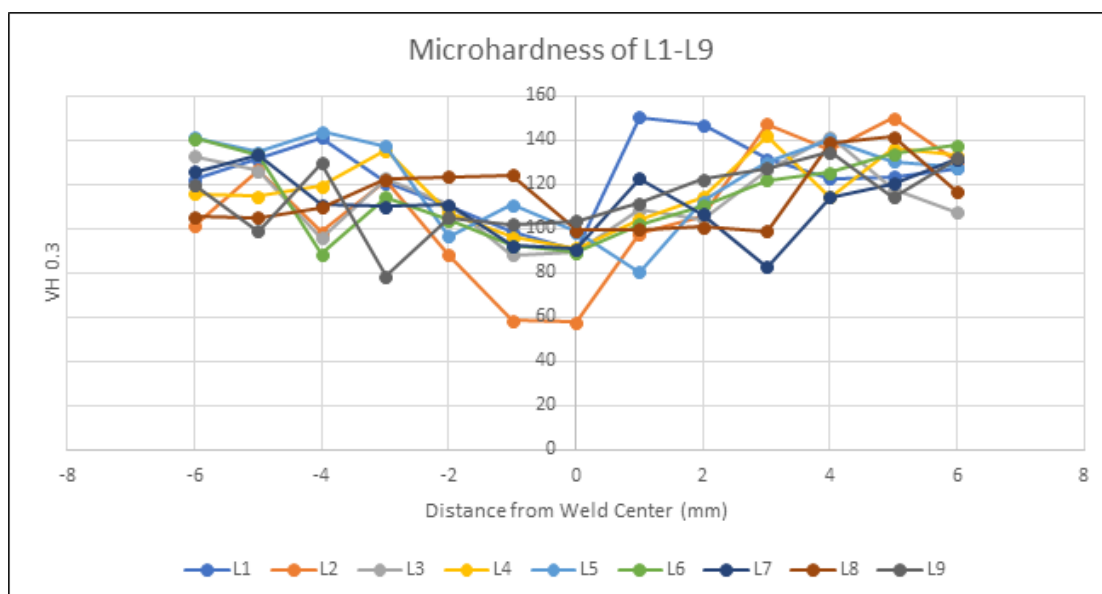
Figure 5.9: Combined micro-hardness plots of weld samples.

Table 5.4: Hardness Test.

Parameter	Result (Avg.)
Hardness Test (Weld Metal)	98.21 HV
Hardness Test (HAZ)	115.4 HV

5.5   Microstructural Observations

A microstructural study is performed by extracting a specimen from a weld cross-section as shown in Figure 5.10. The specimen was etched in Keller solution of 1.5 ml HCl with 1 ml HF and 2.5 ml HNO_3 dissolved in 95 ml of distilled water for 35 seconds. After polishing and etching, a metallurgical optical microscope (BMI-101 A) was used to study the different weld bead aesthetics and morphologies as well as the microstructure of the joint. The micrographs were taken and analysed. The fractured surface was analysed with an SEM equipped with EDX to evaluate the compositions of a weld after performing tensile tests. BM, and WM, as well as the generation of the secondary phase in the HAZ, were studied from SEM micrographs and corresponding phase composition with EDX.

Figure 5.10: A metallurgical optical microscope for the microstructure of the weld sample.

5.5.1 Microstructural Analysis of Casted Base Metal and Composite Material

The metallographic image of casted base Al-alloy and casted composite is shown in Figure 5.11 (a, b). The composite micrography shows a uniform distribution of reinforcement throughout the matrix. A very negligible agglomeration is visible in the composite material. The typical metallographic representations of casted base and composite samples obtained at various locations along the surface show similar microstructure and are displayed in Figure 5.11. A dendritic grain structure and tiny grains make up the structure.
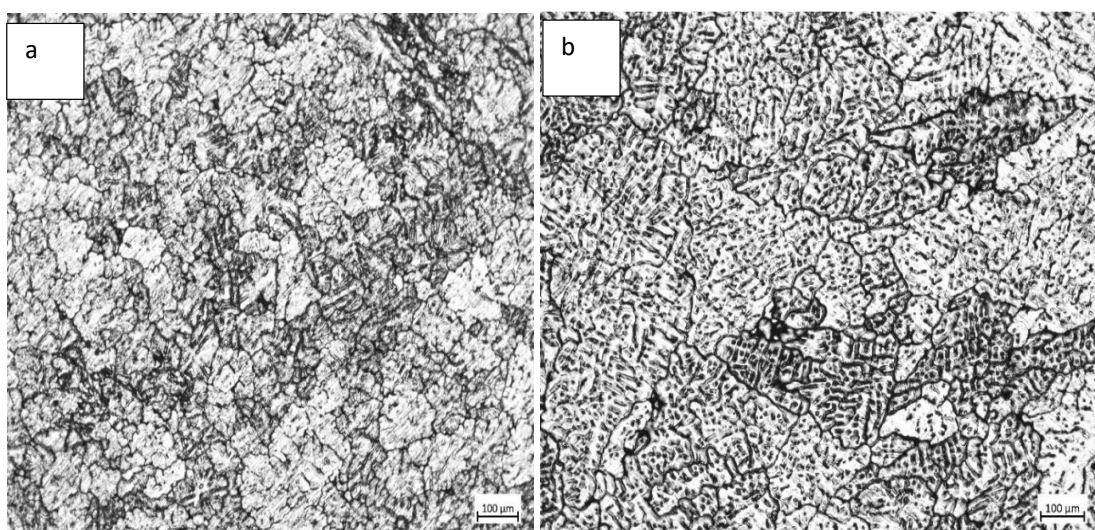
Figure 5.11. Microstructure of (a) Casted base material and (b) Composite material.

5.5.2   Microstructural Analysis of Weld

The typical metallographic representations of CMT welded samples obtained at various locations along the joint are displayed in Figure 5.12. Figure 5.11. shows the microstructure of the casted BM and composite material, a dendritic grain structure, and tiny grains make up the structure. The microstructure of the sample L1-L9 was taken from BM, weld metal interface, and WM are shown in Figure 5.12. The dendritic structure that is not equally distributed throughout the matrix is visible in the general microstructure. A uniform dendritic grain structure at WM and a nonuniform dendritic structure at base metal are shown in Figure 5.12 (a, c) for all the samples L1-L9. The minimum heat input and the high cooling rate at the weld interface near the fusion zone produced dendritic microstructure through the weld interface was observed [200-201]. Larger and coarser grains were found in the HAZ compared to WM because of the rapid cooling of WM stated by [202] in his findings. The structure consists of dendritic grains and prolonged grains. The weld interface is visible in Figure 5.12-b for all the samples. In the foundation structure, full penetration welding is visible in the general microstructure. Thermal cycling causes the molten pool to crystallize as columnar crystals, exhibiting typical eutectic crystallization traits from the partially melted BM surface to the weld center.

5.5.3   Microstructural Characterization of Weld Sample L1-L9

A nonuniform dendritic structure at base metal makes the structure as shown in Figure 5.12-a for all the samples. The micrograph of the samples from the composite base shows a uniform distribution of reinforcement throughout the matrix. A small agglomeration of reinforcements takes place at some discrete locations and is visible in samples L2, L6, and L7. A small agglomeration of reinforcements is visible at the weld metal interface for

sample L2. The Larger and coarser grains make the structure at HAZ and the uniform dendritic structure at the WM for all the samples. Some defects like blow holes and porosities are visible on the weld surface of samples L2, L3, L5, and L7. These samples show minimum hardness and tensile strength at the weld portion compared to the other sample. It can be concluded that the defects on the weld surface seriously affect the mechanical property. The metallography taken from the WM interface and WM for sample L8 reveals that some small porosities are visible at the WM interface and WM but they cannot seriously affect the hardness and tensile strength of the samples at the weld and HAZ. A nonuniform and uniform dendritic structure at base metal makes the structure. Sample L1 shows the best mechanical properties because there were no flaws on WM, HAZ, and BM visible in the microstructure.
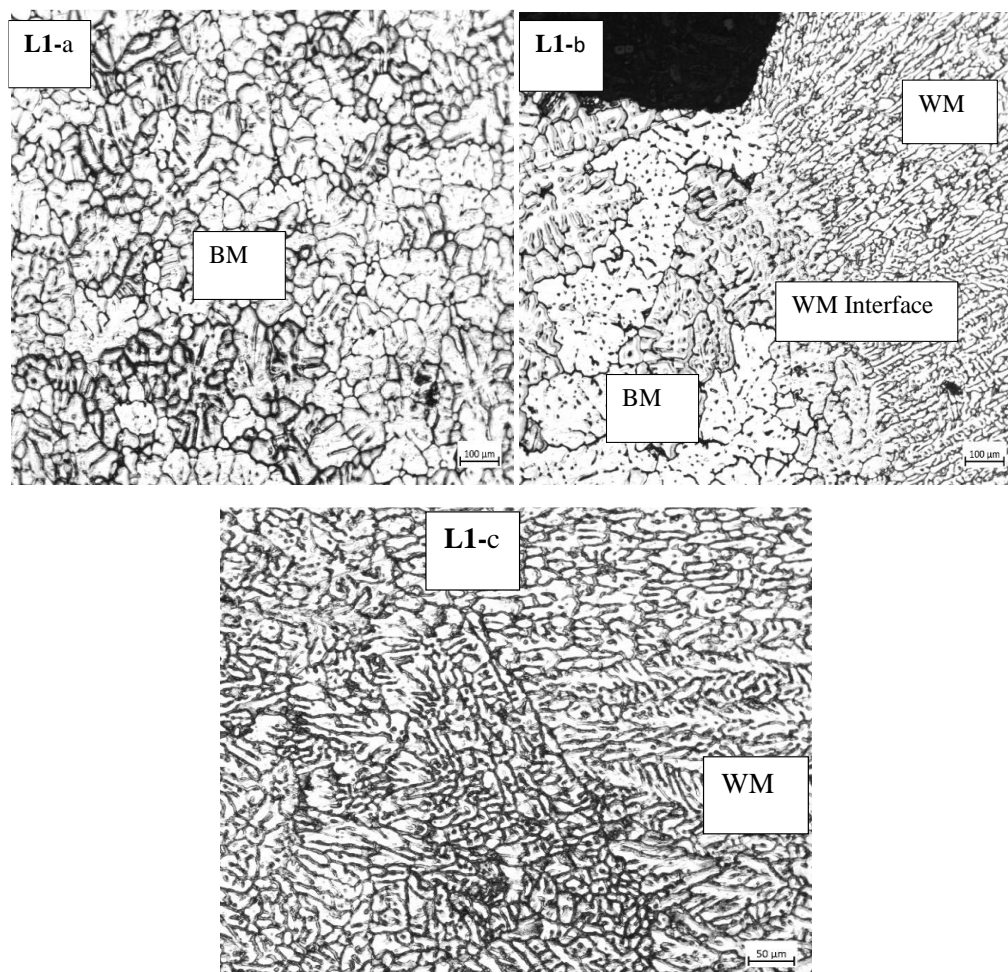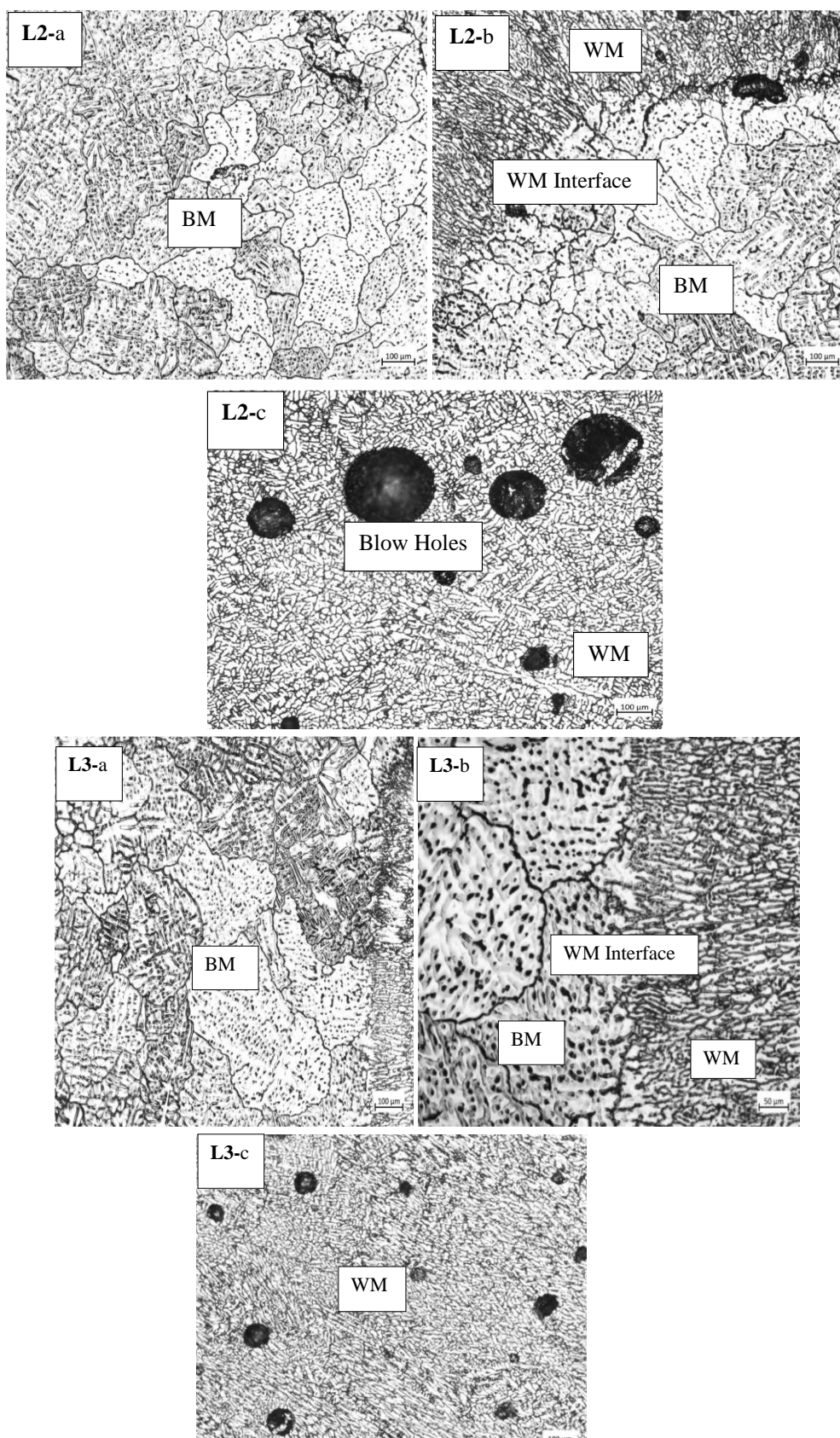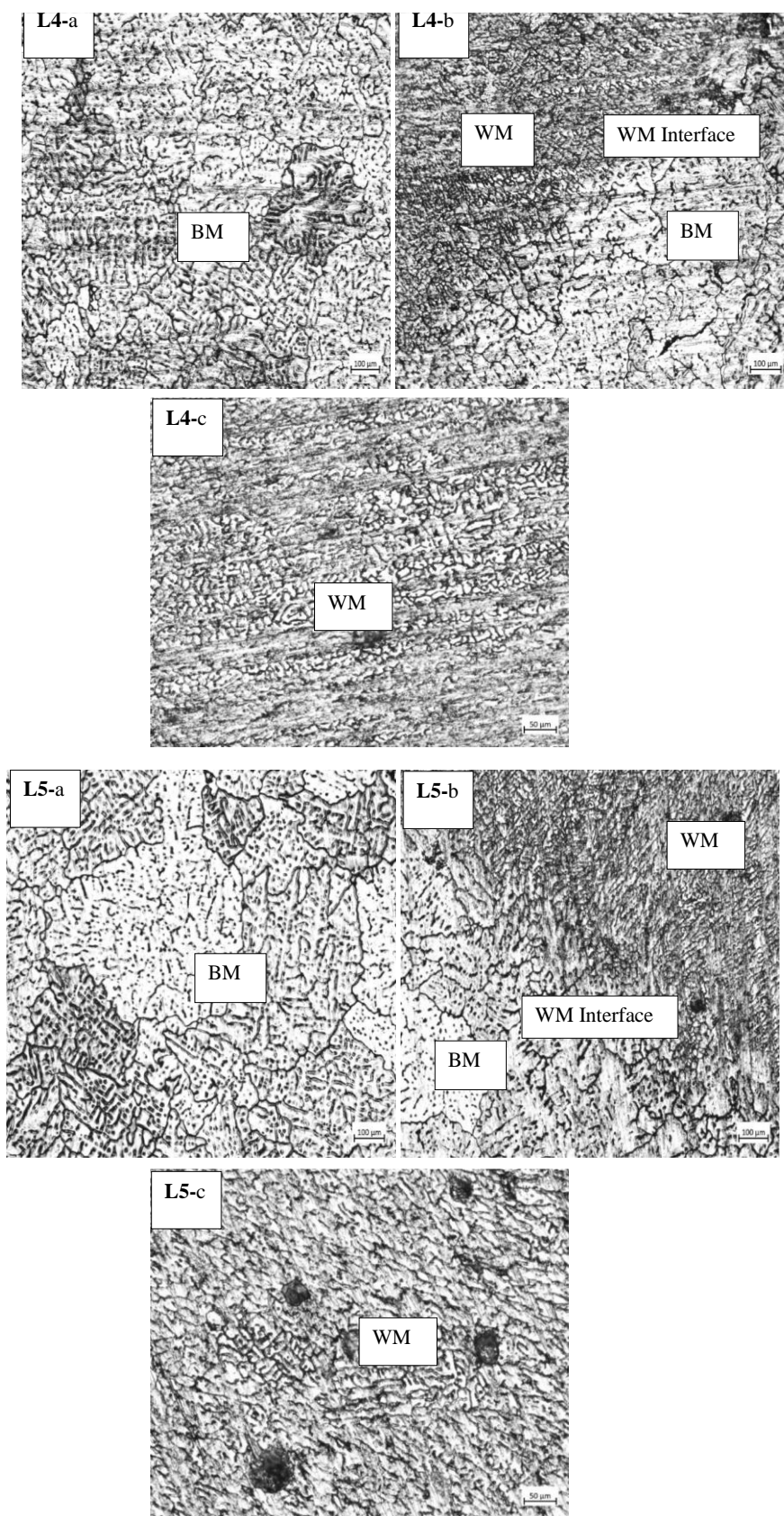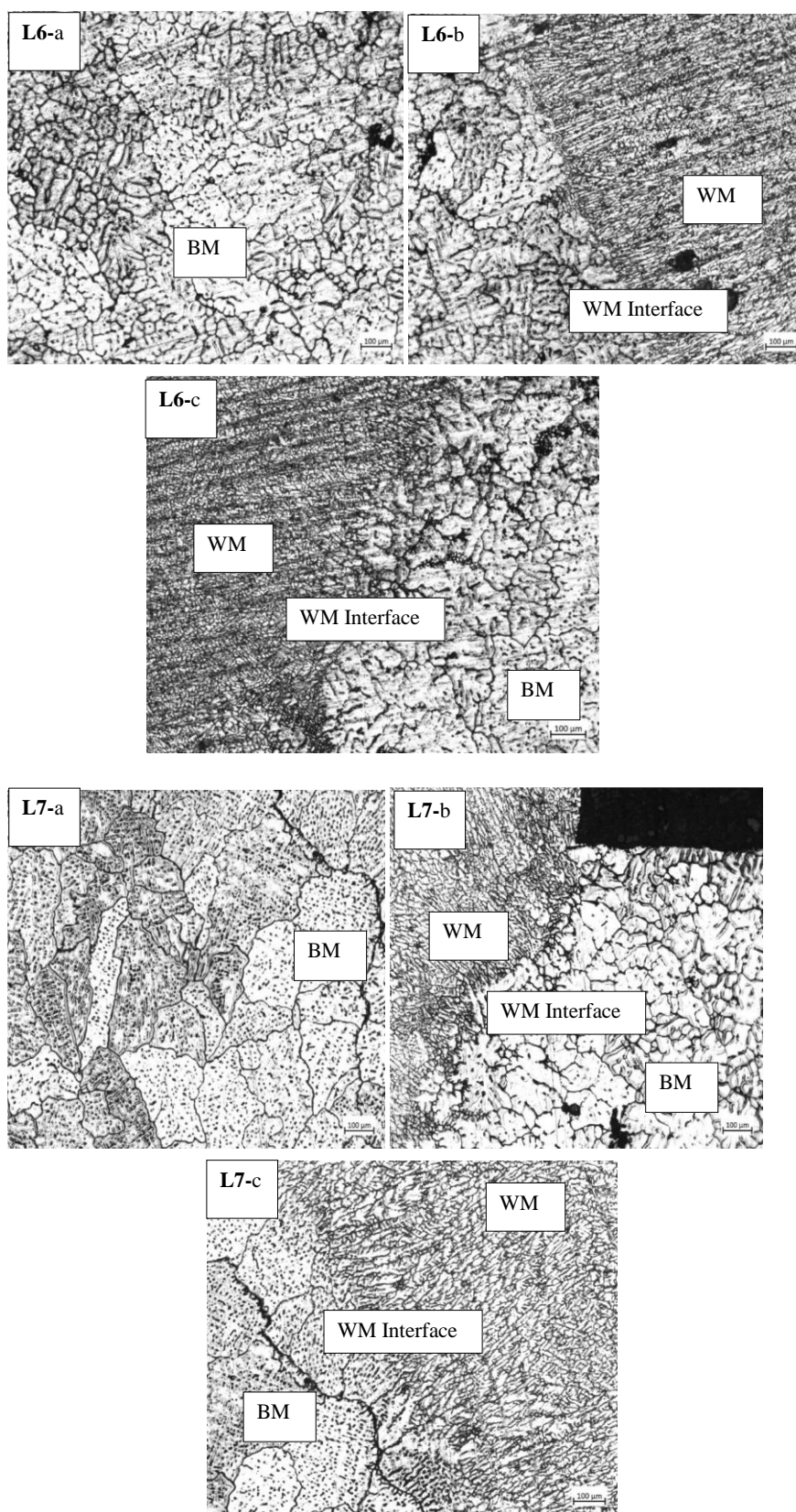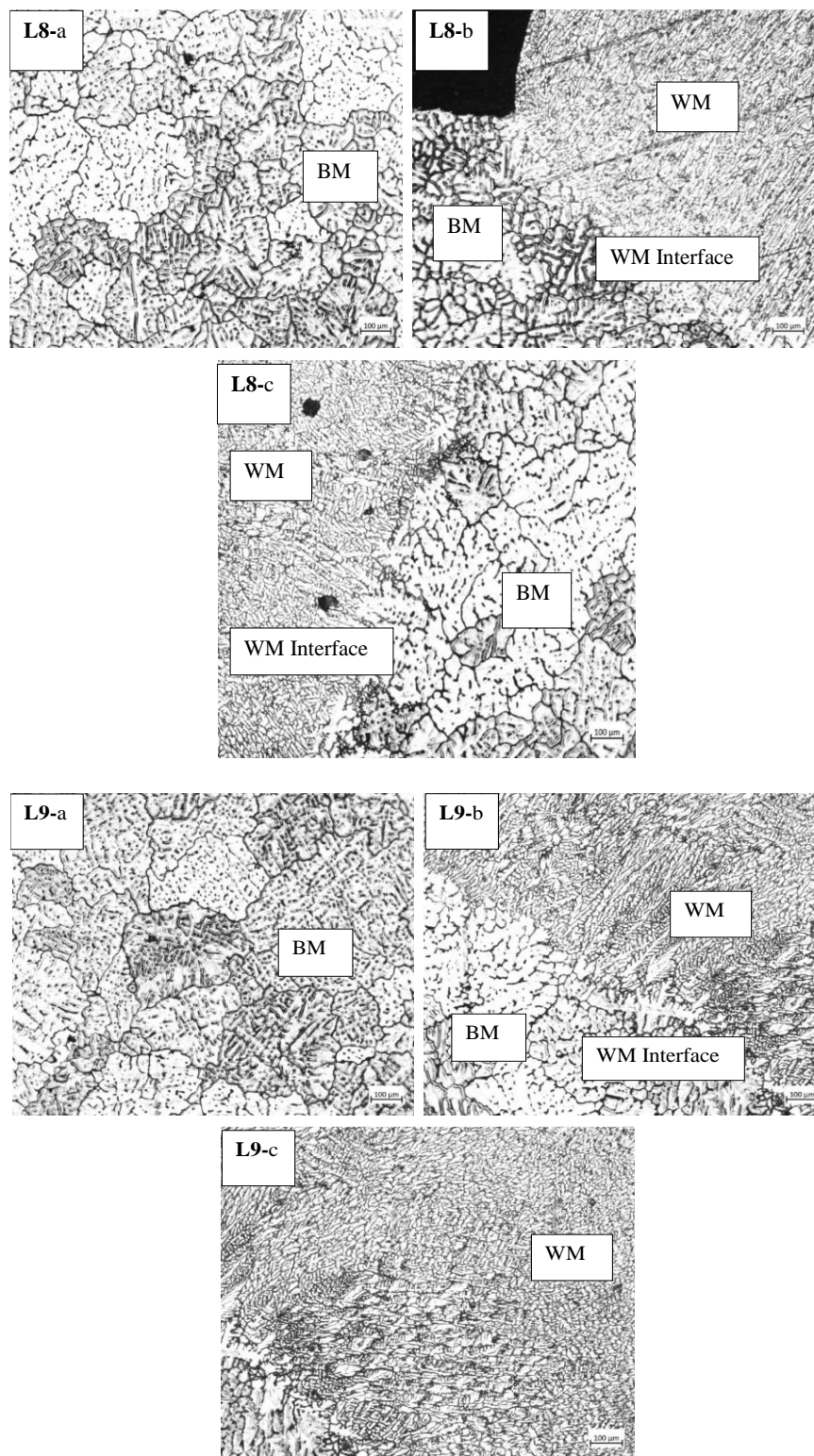
Figure 5.12: Welded Sample microstructure of L1-L9 at (a) Base composite (B) WM interface and (c) WM.

5.6 Taguchi Analysis

Taguchi uses statistical performance measures that are denoted as the S/N ratio and used previously in electrical control systems to analyse the performance [203]. Taguchi develops the S/N ratio as a performance criterion to get the best level of control variable that minimizes the effect of uncontrolled variables. Simply, the ratio of the mean (signal) to the standard deviation (noise) is called the S/N ratio.

5.6.1 Tensile Strength (MPa) versus A, B, C

The ideal set of parameter values is indicated by a higher S/N ratio. The S/N ratio is used to determine the process parameter's ranking. The delta values were compared to establish the ranking order. The difference between the highest and lowest values for the level of each factor is the delta score. The ranking of the parameter begins with the larger value of the delta and ends with the minimum value of the delta.

Response Table for Signal-to-Noise Ratio

Level	A	B	C
1	39.91	39.65	40.31
2	39.60	39.19	39.45
3	38.66	39.34	38.42
Delta	1.25	0.47	1.89
Rank	2	3	1

5.6.2 Response for Means

Although Taguchi suggested a variety of S/N ratios, the main three are, the smaller-best, larger-best, and nominal-best which are the most commonly adopted. In this analysis, the larger best is used and the larger best signal-to-noise ratio (S/N) is given by the following relation:

$$\frac{S}{N} = -10 \, * \log\left(\frac{1}{n}\sum_{i=1}^{n}\frac{1}{y_i^2}\right)$$

The variables $\bar{Y}$, s^2, and n represent the mean, variance, and number of observed assessments, respectively.

Response Table for Means

Level	A	B	C
1	99.44	97.15	103.86
2	95.97	91.29	94.08
3	86.03	93.01	83.50
Delta	13.41	5.86	20.36
Rank	2	3	1

5.6.3 Analysis of Means and S/N Ratio Analysis

In S/N ratio analysis, the larger the better is followed, and it is observed the maximum value is carried by parameter C which is wire feed rate, the second maximum value is for parameter A which is voltage and the third is for parameter B which is welding speed and are shown in Figure 5.13. As per the rank of the matrix that is 2,3,1, the first rank is for wire feed rate, the second rank is for voltage and the third rank is for welding speed. So, as per the analysis of means and analysis of S/N ratio the effect of the welding parameter is in the order of C, A, and B, and their corresponding values are chosen as the first set of welding parameters.
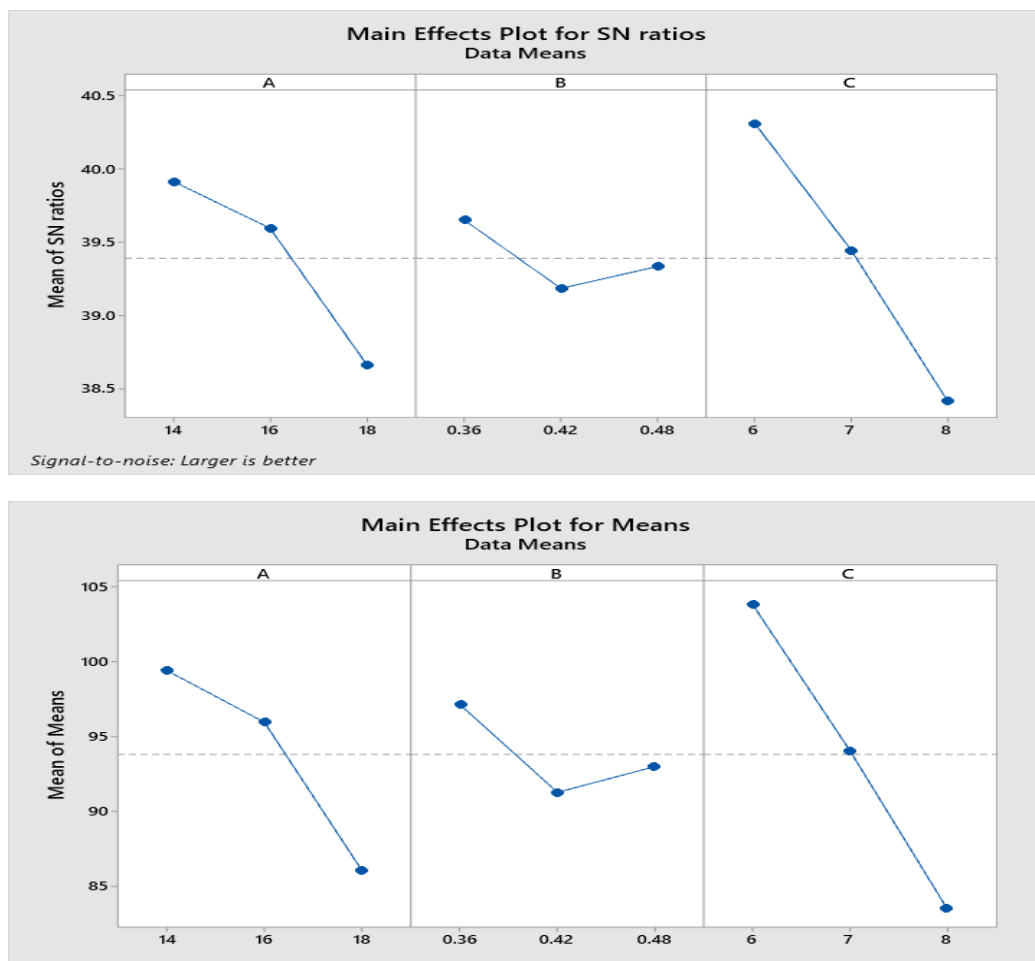
Figure 5.13: A plot of (a) S/N Ratio Analysis and (b) Analysis of Means.

5.6.4   Regression Analysis

As per the regression analysis, C is the most prominent parameter, the second is A and the third is B. So, as per the P-value of coefficients and variance the order of most contributing parameters is wire feed rate, Voltage, and welding speed respectively.

Tensile Strength (MPa) versus A, B, C

Regression Equation

Tensile Strength (MPa)	=	233.2 - 3.352 A - 34.5 B - 10.18 C

139

Coefficients

Term	Coef	SE Coef	T-Value	P-Value	VIF
Constant	233.2	18.5	12.63	0.000	
A	-3.352	0.724	-4.63	0.006	1.00
B	-34.5	24.1	-1.43	0.212	1.00
C	-10.18	1.45	-7.03	0.001	1.00

Model Summary

S	R-sq	R-sq (adj)	R-sq (pred)
3.54603	93.58%	89.73%	84.26%

5.6.5 Analysis of Variance (ANOVA)

Data obtained from the experiments should be analysed and for this, variance analysis is used. The percentage of contributions represents the rate of variability for each significant factor and interaction in the experiment. The percentage contribution is determined by multiplying each major factor with the squared total. The strength of the components is represented by their percentage contribution. Error variance is included in the variance of a factor or interaction, as is well known. If the error contribution is 15% or below, it indicates that the experiment does not miss any important components. If the experimental error contribution percentage is 50% or higher, it indicates that certain significant factors are being overlooked [204].

Source	DF	Adj SS	Adj MS	F-Value	P-Value
Regression	3	917.02	305.67	24.31	0.002
A	1	269.59	269.59	21.44	0.006
B	1	25.70	25.70	2.04	0.212
C	1	621.73	621.73	49.44	0.001
Error	5	62.87	12.57		
Total	8	979.90			

5.6.6   Probability and Fit Value Plot

The probability plots of responses have been represented in Figure 5.14, which indicates that all the data are normally distributed with a 93.58% confidence level. The scatter plot of fitted values on the X-axis and residuals on the Y-axis is called a fit value plot. It represents the line of best fit with confidence limits. Figure 5.14 shows the fit value plot which is used to detect non-linearity, outliers, and variances. Figure 5.15 represents the histogram and observation order plot for tensile strength.
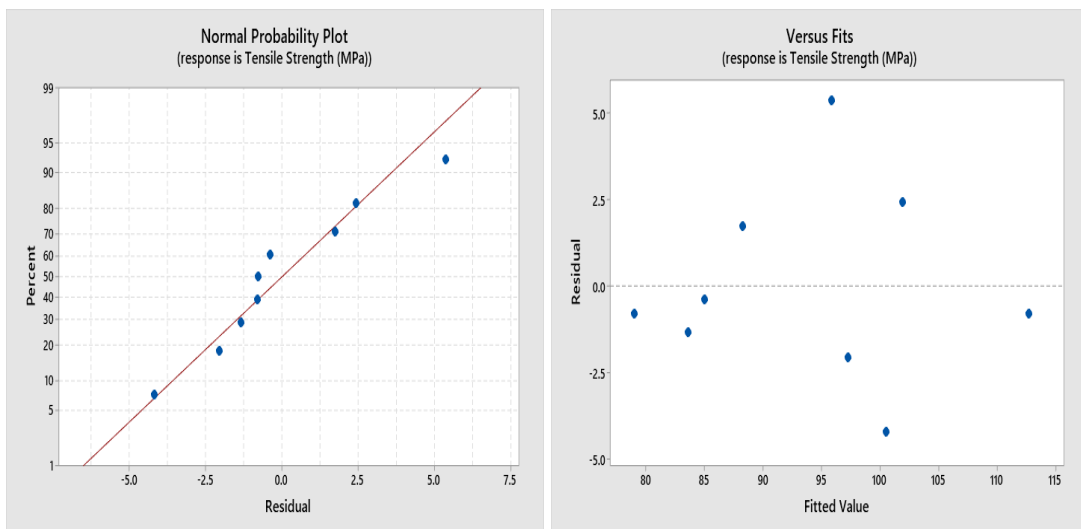
Figure 5.14: The Probability plot and Fit value.
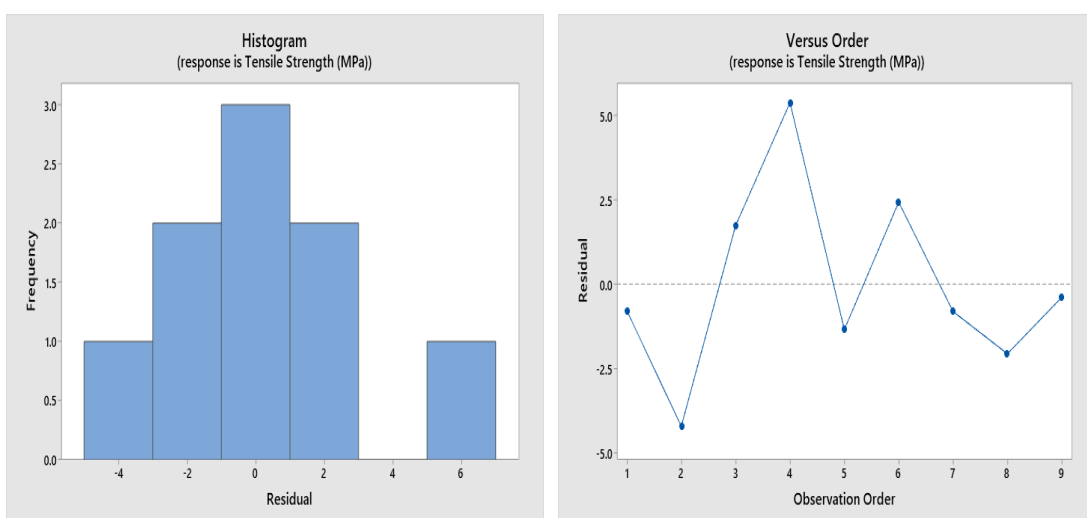
Figure 5.15: The Histogram and observation order plot.

5.6.7 Contour Plot

The contour plot shows the contribution of parameters for maximum tensile strength. In this, the contribution of three variables, welding voltage, welding speed, and wire feed rate is measured for the maximum value of tensile strength. In the tensile strength contour plot, the two independent variables, welding parameters were displayed along the X and Y axis, while contour lines and bands on the Z axis represent the dependent variable which is tensile strength. Here out of three welding variables one variable is kept as a hold value and the effect of the other two variables on the value of tensile strength was measured and is shown in Figure 5.16. The holding value of a variable and the range of the other two variables for the maximum value of tensile strength for a set of contour plots are given in Table 5.5.

Table 5.5: Hold values of variables and range of variables.

Welding Parameters	Hold Value	A	B	C
Voltage (V) (A)	A-16		0.360-0.380	6
Welding Speed (m/min) (B)	B-0.42	14.2		6.3
Wire Feed Rate (m/min) (C)	C-7	14.0-14.4	0.360-0.375	
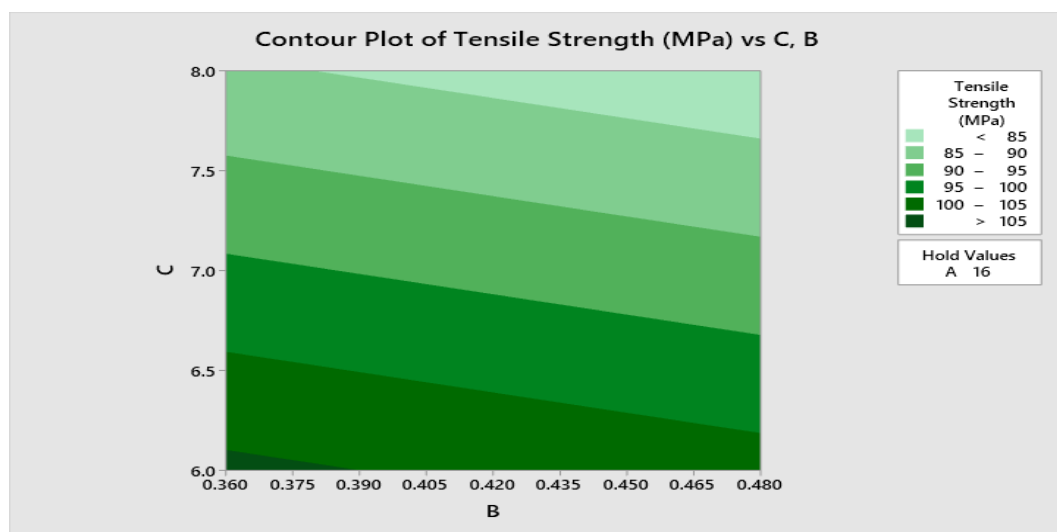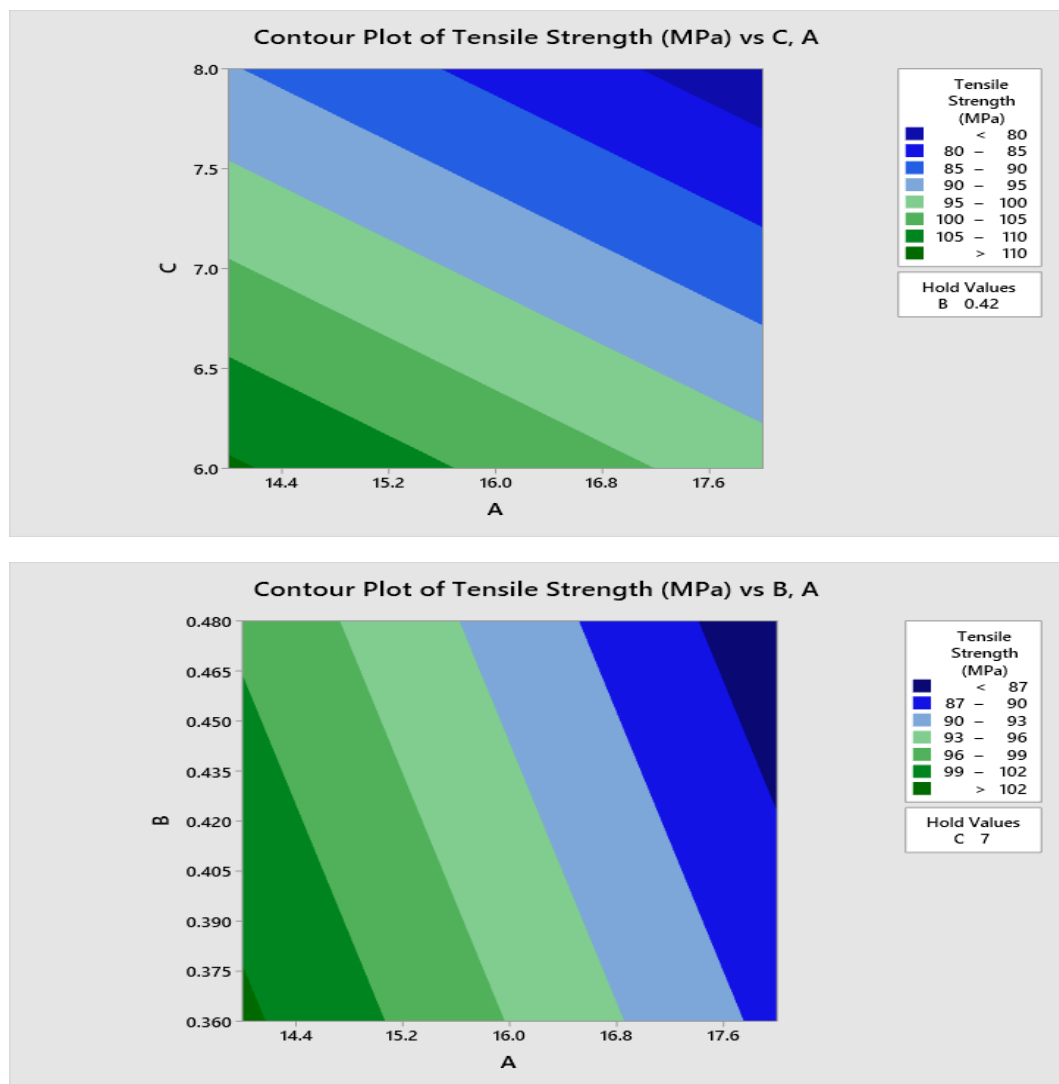
Figure 5.16: The Contour Plot of tensile strength.

5.6.8 Surface Plots of Tensile Strength

A surface plot is a functional relationship between two independent variables that are on the X and Z axis with a designated dependent variable on the Y axis by keeping the third independent variable as a hold value at a time. It is used to distinguish between a dependent variable and an independent variable. In Figure 5.17. voltage, welding speed, and WFR as independent parameters were plotted for the maximum value of tensile

143

strength as a dependent parameter by keeping one independent welding variable as a hold value at a time.
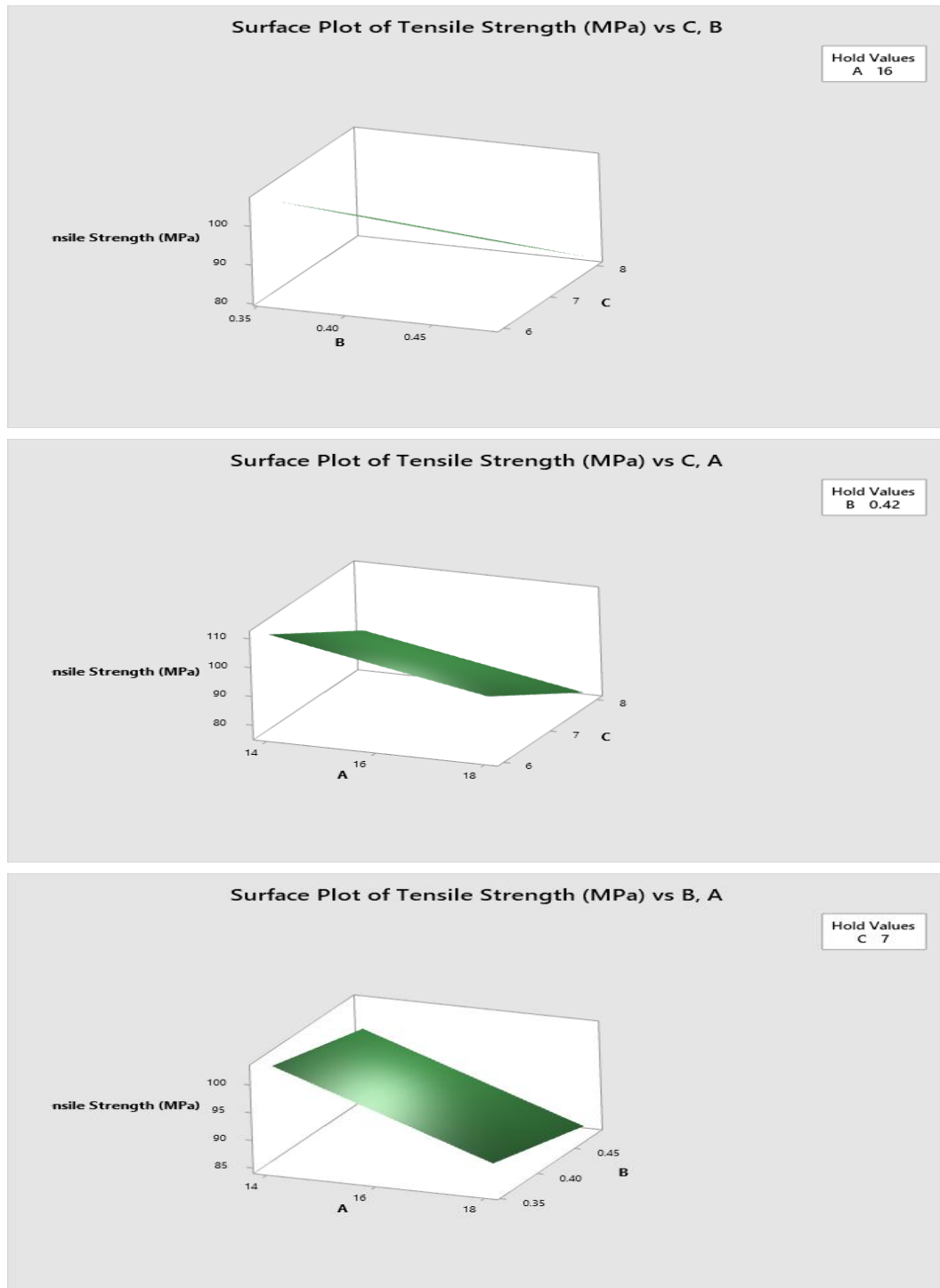
Figure 5.17: The Surface Plots of Tensile Strength.

5.7 Optimized Welding Parameter

The final welding parameters were decided through experimental design are given in Table 5.6. The most prominent parameter is wire feed rate and having rank 1, rank 2 is for welding voltage, and rank 3 is for welding speed. The corresponding values of wire feed rate are 6 m/min, voltage is 14 volts and welding speed is 0.36 m/min.

Table 5.6: Optimized Welding Parameter: Based on ANOM, S/N ratio, P-value, and Rank.

S. NO.	Voltage (V)	Welding Speed (m/min)	Wire Feed Rate (m/min)
Rank	2	3	1
1	14	0.36	6

5.8 Confirmatory Test

5.8.1 Parameters for Confirmatory Test

A confirmatory test was conducted for the most appropriate set of welding parameters which are welding voltage, welding speed, as well as wire feed rate. As per the experimental design rank 1 shows the most influencing welding parameter which is wire feed rate. The other experiments are conducted for the adjacent upper and lower values of WFR by keeping the values of parameters of rank 2 and rank 3 constants. The confirmatory test parameters are given in Table 5.7.

Table 5.7: Welding parameters for confirmatory test.

S. No.	Voltage (V)	Welding Speed (m/min)	Wire Feed Rate (m/min)
1	14	0.36	5
2	14	0.36	6
3	14	0.36	7

5.8.2   Confirmatory tests for composite weld

Confirmatory tests were conducted and it was observed that the results of the tests were similar to those of the previous experimental values. The best welding parameters are the wire feed rate with rank 1 and its corresponding value is 6 m/min, rank 2 is given to welding voltage with the value of 14 Volt, and rank 3 is for welding speed with the value of 0.36 m/min. Figure 5.18 shows the welded plate for a confirmatory test.

Figure 5.18: Welded plate for a confirmatory test.

5.9   Mechanical properties of weld

5.9.1   Tensile Properties of Weld

A tensile test was conducted to examine the weld performance, at optimized welding parameters, and the results of TS, YS, as well as % elongation values are displayed in Table 5.8. The results of the tensile test show almost similar values of TS, YS, and % elongation with some marginal improvements corresponding to optimized welding parameters whereas the upper and lower values of wire feed rate show decreased value of mechanical properties. The load-displacement curve for all confirmatory test samples is shown in Figure 5.19 (a, b, c).

Table 5.8: Input and Output Welding Parameters of confirmatory test

Experiment No.	Voltage (V)	Welding Speed (m/min)	Wire Feed Rate (m/min)	TS (N/mm²)	Yield Strength (N/mm²)	% Elongation
1.	14	0.36	5	92.32	65.20	4.0
2.	14	0.36	6	112.6	71.90	3.5
3.	14	0.36	7	98.4	67.80	3.0
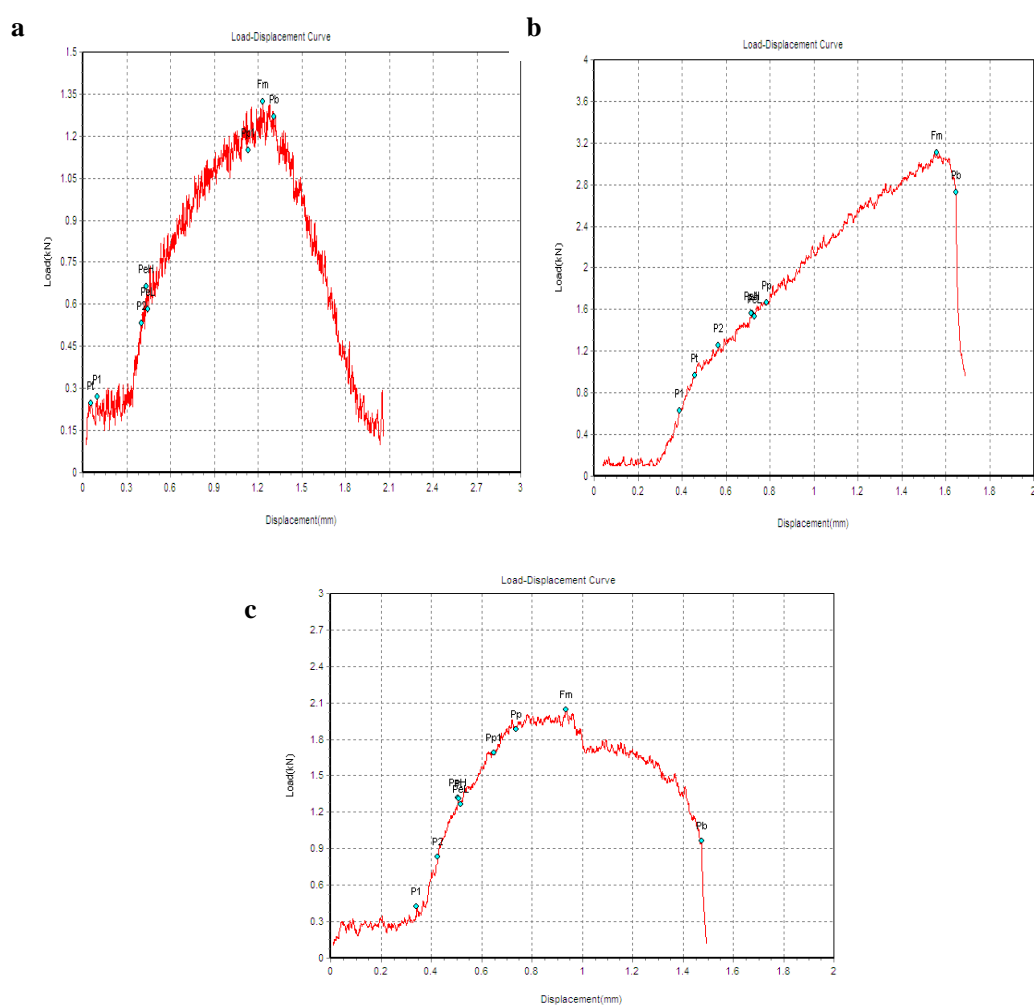
Figure 5.19: A load-displacement curve of confirmatory test sample (a) Sample-1 (b) Sample-2 (c) Sample-3.

5.9.2   Microhardness analysis of weld

The microhardness test was performed for a welded sample at optimized welding parameters and the hardness values are shown in Table 5.9. The result shows almost similar values of hardness at WM and HAZ with marginal variations. The hardness value of WM is less than HAZ and BM. The hardness of WM is 64.16 % of the BM.

Table 5.9: Hardness Test of optimized test Sample.

Parameter	Observed Value (HV0.3)	Result (Avg.)
Hardness Test (Weld Metal)	98,96,97	97HV 0.3
Hardness Test (HAZ)	117,119,115	117HV 0.3

So, the confirmatory test results confirm the welding parameters corresponding to the best mechanical properties of composite welds.

5.9.3   Microstructure Analysis of Optimized Test Sample

The micrographs were taken for the optimized confirmatory test sample-2 from BM HAZ and weld metal interface and are shown in Figure 5.20. The general microstructure shows eutectic silicon grains in dendritic structure observed throughout the matrix. The microstructure taken from WM at 600X shows a uniform dendritic structure throughout the weld and is shown in Figure 5.20-a. The BM microstructure taken at 600X shows fine & uniform, recrystallized grains throughout the matrix and is shown in Figure 5.20-b. Figure 5.20-c shows the micrograph of the WM interface. The weld metal interface shows a clear separation between the base metal weld area.

Microstructure (Weld)	Microstructure (Base)
Magnification – 600X	Magnification – 600X
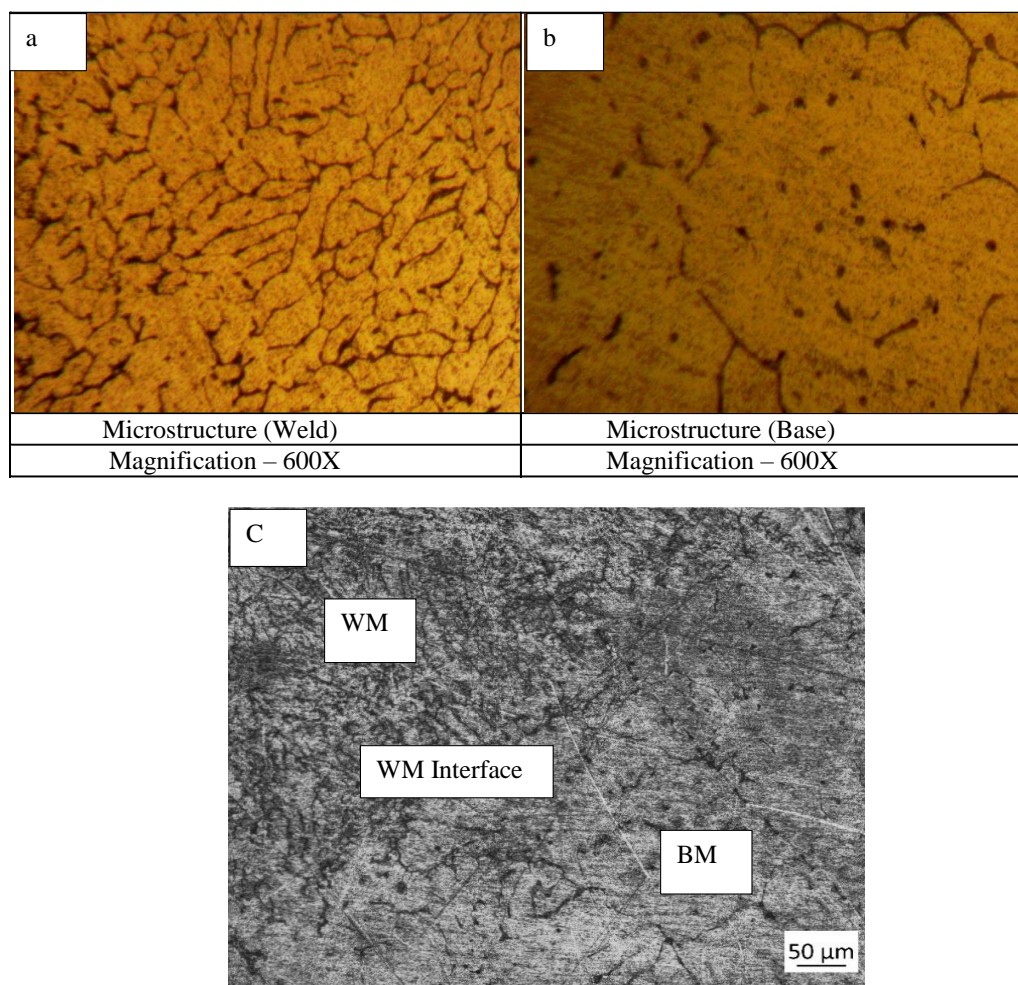
Figure 5.20: Microstructure of confirmatory test sample (a) WM (b) BM (c) WM interface.

5.10 WELDING AND ANALYSIS OF AL-ALLOY 7475 IN T7351 TEMPERED CONDITION FOR CONFIRMATORY TEST

5.10.1 Welding and Analysis of AA7475 alloy in T7351 Temper using Optimized Welding Parameters

Now the set of optimized welding parameters is applied to weld the Al-alloy 7475 in T7351 (solution treated + artificially aged condition) tempered conditions, as a confirmatory test, and the mechanical and micro-structural properties were analysed and the outcomes are discussed in detail.

5.11 Material and Methods

5.11.1 Preparation of test sample

A thick sheet having a thickness of 25 mm of Al-alloy 7475 in T7351 (solution treated + artificially aged state) is used for this investigation, as illustrated in Figure 5.21-a. Then it is sliced with a power hacksaw and finished by using an Ace-Microsmatic CNC machine, as illustrated in Figure 5.21- (b, c). As illustrated in Figure 5.21-d, the prepared samples have a thickness of 3 mm, and then buffing is applied to the finished samples to eliminate the imperfections over the samples. The final samples are used to perform the welding by using optimized welding parameters and are displayed in Figure 5.21-e.
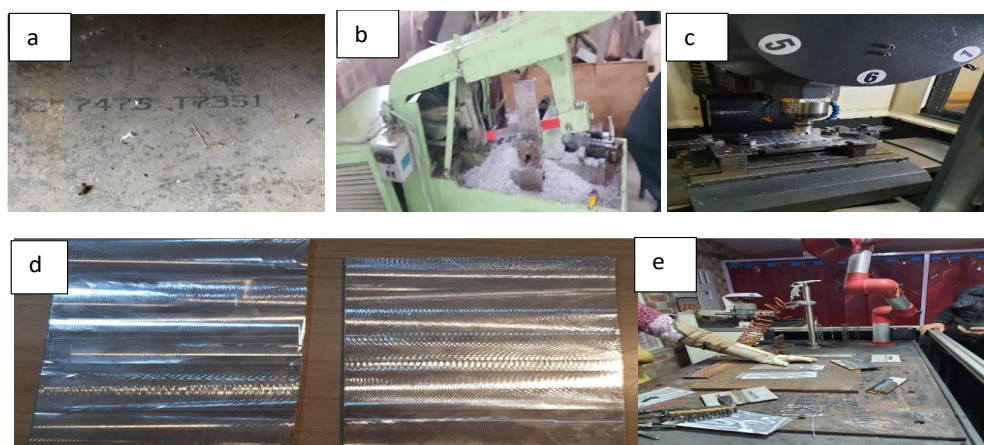
Figure 5.21: (a-e)-Represents the process of sample preparation for welding and investigation from as-received material.

5.12 WELDING PROCESS AND USED FILLER METAL

The experimentation starts with the welding of a plate of Al-alloy 7475 in T7351 (solution treated + artificially aged condition) by using optimized welding parameters through experimental design. Coupons measuring 203 mm x 65 mm x 3 mm were cut and put in a butt joint arrangement with no space between the plates. The chemical composition of the base and filler metals is shown in Table 5.10. In Table 5.11, the mechanical characteristics of the Al7475 in T7351 alloy are examined and reported. Table 5.12, includes the sample size, tensile strength, and other details. ER 4043 (AlSi5) wires with a diameter of 1 mm are used as the filler metal. The optimized welding parameters were used for the best weld bead and weld quality after numerous experiments. The oxide layers have been removed with emery paper and acetone before welding. Welding was performed by using optimized welding parameters and the welded plate as well as the sample is shown in Figure 5.22.

Table 5.10: Chemical Composition (Wt.%) of AA7475-T7351 alloy and filler metal.

Elements	Si	Fe	Cu	Mn	Mg	Ni	Zn	Ti	Cd	Co	Pb	Sn	Cr
AA7475 T7351	0.0507	0.0291	1.51	0.0072	2.23	0.0042	5.86	0.0188	<0.00010	<0.0010	0.0112	0.0022	0.211
ER4043	5.4	0.8	0.055	0.32	0.76	0.047	0.12	0.018	-	<0.010	<0.012	-	<0.004

Table 5.11: Mechanical Properties of Base Al alloy.

Yield Strength (MPa)	Ultimate Tensile Strength (MPa)	Fatigue Strength (MPa)	Hardness (Hv)	Elongation (%)
370	435	160	170	13.2

Table 5.12: Sample Particulars: AA7475-T7351 Aluminium Plate.

Specimen	Size (mm)	Area (mm^2)	GL (mm)	UT Load (KN)	T/S (N/mm^2)	0.2%PS Load (KN)	0.2%PS (N/mm^2)	Final	% E/L
1.	12.35 X 3.00	37.05	50.0	16.124	435	14.116	381	53.75	13.2
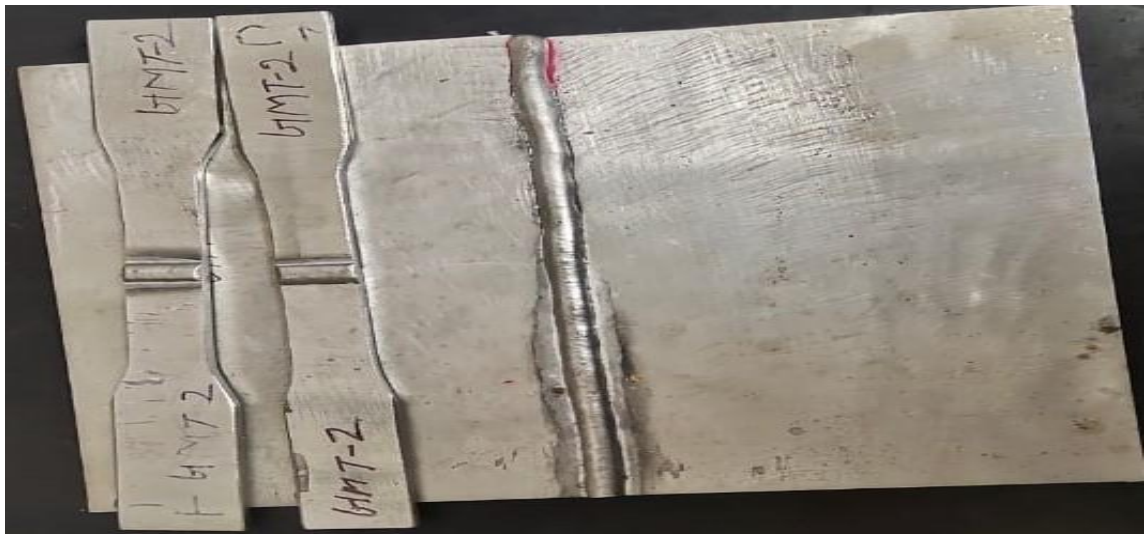
Figure 5.22: Schematic of the robotic CMT welded plate and samples for tensile test.

5.12.1 Weld defects- In CMT welding, the chances of hot cracking are erased as a result of its minimal heat input characteristics. Small surface porosities are observed on the weld surface which can not affect the weld quality. According to the test findings for all samples, there are no hot cracks, blowholes, or other hazardous flaws on the weld surface.

5.12.2 Mechanical testing of the CMT joint's local zones - After ocular inspections, a non-destructive test was performed to discover the fault created on the weld surface. After performing an LPT (liquid penetrant test) on all of the samples, it was discovered that the welding was free from serious flaws. A Microhardness test was carried out on the transverse section of the welded specimen with a 0.2 mm separation and a weight of 1000 g imposed for 15 seconds using a digital Vickers hardness tester (VH-1000B). The ASTM E-8-16a procedure was used to prepare the tensile testing samples. Tensile testing was used to evaluate the elongation, yield strength (YS), as well as tensile strength (TS) of the test section. The welded plate and tensile-tested samples are shown

in Figure 5.23 (a, b). The characteristics of fractured surfaces of the tensile tested sample were examined by applying SEM with EDX.

Figure 5.23: Al-alloy 7475 in T7351 (a) CMT welded plate and (b) Tensile-tested weld samples.

5.13 TENSILE PROPERTIES OF THE BM, HAZ, AND WM

Tensile testing was done to examine the weld performance, and the results (TS, YS, and % elongation values) are displayed in Table 5.13. Comparing the TS of the base metal standard alloy, which is 435 MPa, with the WM and HAZ, it was found that both WM and HAZ have the lowest TS, at 256 MPa and 266 MPa, respectively, and show similar patterns for the YS. The tensile specimen of the CMT welded junction does not deform plastically, yielding the lowest WM elongation of 6.2 percent. All joint samples fail in the welded zone. HAZ has substantially lower tensile and yield strengths than BM. Since the precipitated phases were solid solutions, coarsening occurred inside the HAZ; its elongation was 8.4% as compared to 13.2% for the BM. As a result, there would be a significant softening, a loss of strength, and an increase in flexibility.

According to the performance of the BM and HAZ, the WM is the welding joint's weakest link.

The load-displacement curve of the HAZ is very different from that of the BM and is shown in Figure 5.24-b. With increasing stress, the regional sliding distortion between the grains of the tensile specimen changes as stressed by [205]. The specimen exhibits plastic slip deformation as the stress rises. In the meantime, the material starts to quickly give up and deform before breaking. The WM elongates substantially less than the BM and HAZ up until the fracture point, which is when plastic deformation ceases. The load-displacement curve of the WM is shown in Figure 5.24-a. To determine the percentage of elongation, the average value of elongation was employed, as indicated in Table 5.13. The phenomena would be justified by the uniform and clean distribution of precipitates at the welding sites as well as by the benefits of the CMT process, such as a less spatter welding process and increased gap-bridging capabilities with lower heat input. The joint performance of the CMT technology was examined [206] and found that the CMT welds had a smaller dilution ratio and a more constrained composition range. According to earlier studies by [207-208], the increase in tensile strength and hardness value of the material is due to the fine dimples. A strengthening effect can come from precipitate production interfering with the dislocation's mobility [209]. The TS, YS, and elongation values for the welds are therefore found to be much lower than those for the base metal.

Table 5.13: Tensile Strength and % Elongation.

Specimen	Size (mm)	Area (mm²)	GL (mm)	UT Load (KN)	T/S (N/mm²)	% E/L	Location of Fracture
1.	12.40 X 3.20	39.68	50.0	10.148	256	6.2	WM
2.	12.45 X 3.30	41.08	50.0	10.936	266	8.4	HAZ

Mechanical Test Graph of WM   Mechanical Test Graph of HAZ
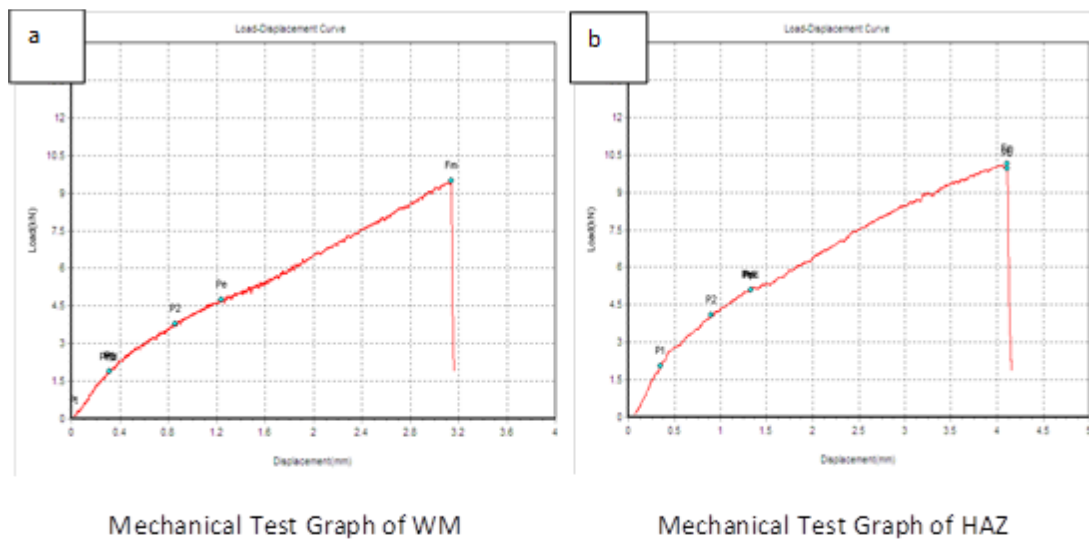
Figure 5.24: A Load-Displacement curves of AA7475-T7351 CMT welded joint: (a) WM (b) HAZ.

5.14 MICROSTRUCTURAL OBSERVATIONS

CMT joint specimen was taken out from the weld X-section and then finished with 180 to 2000-grit sandpaper for microstructural analysis. Following the polishing and etching, a Metallurgical optical microscope (BMI-101A) was used to study the various aesthetics and morphology of welds, as well as the microstructures of the joints.

5.14.1 Microstructure of the BM, HAZ, and WM

The typical metallographic representations of CMT samples obtained at various locations along the AA7475-T7351 joint are displayed in Figure 5.25. Figure 3.2 shows the

microstructure of the AA7475-T7351 BM at 400X; the BM is made up of elongated grains. The microstructure of the HAZ region of the CMT joint at the fusion border is shown in Figure 5.25- (a), at 100X and 200X. Both the semi-molten HAZ grain and the WM columnar crystal are visible in Figure 5.25- (b). The dendritic structure that is not equally distributed throughout the matrix is visible in the general microstructure. Figure 5.25 (c) shows the WM's microstructure at a magnification of 400X and demonstrates complete penetration welding in the base metal. A dendritic grain structure and tiny grains make up the structure. In the foundation structure, full penetration welding is visible in the general microstructure. Figure 5.25- (d), depicts the structure, which comprises a non-uniform dendritic grain structure and coarse grains. The minimum heat input and the high cooling rate at the weld interface near the fusion zone produce dendritic microstructure through the weld interface was observed by [200-201]. Thermal cycling causes the molten pool to crystallize as columnar crystals, exhibiting typical eutectic crystallization traits from the partially melted BM surface to the weld center. As can be observed from the overall microstructure, the dendritic structure is constant throughout the matrix. With secondary phases that are segregated at grain boundaries and dendritic branching because of the modest temperature difference between the liquid state at the center of the molten material, the WM is mostly composed of uniform dendrites and columnar crystals. New crystal nuclei that can spontaneously develop in the liquid state can emerge when a greater supercooling degree is reached in the liquid phase, as reported in [210]. Grain formation and coarsening of the fibrous tissues are visible in the HAZ, in contrast to the BM's morphology. Larger and coarser grains were found in the HAZ compared to WM because of the rapid cooling of WM stated by [202] in his findings**.** Increased welding heat input is the cause of this. The structure consists of dendritic grains and prolonged grains. On the other side, precipitate density steadily drops, leading to "phase coarsening." Near the same

time, a zone devoid of precipitation developed at the grain boundary. The primary causes of the mechanical property loss are the coarsening of microstructural precipitates and the expansion of the precipitate-free zone. The basic metal granules are broad and extended. The non-uniform and uniform dendritic structures in the HAZ and WM of CMT joints may be induced by the different rates at which base metal heats up during welding and cools quickly afterward. The dendritic structure was reported by [211] during welding due to melting and solidification in the fusion zone and the base metal showed elongated grain. The HAZ-fusion zone interface's grain coarsening zone, which is discernible even at low magnification, can be seen in metallographs. Sample-2, which is at an optimum welding setting and is shown in Figure 5.26 (a-d), shows similar findings.

HAZ Microstructure	HAZ Microstructure
Mag- 100X	Mag- 200X
Weld Metal Microstructure	Weld Metal Microstructure
Mag- 100X	Mag- 200X

| Weld Metal Microstructure | HAZ Microstructure |
| Mag- 400X | Mag- 400X |
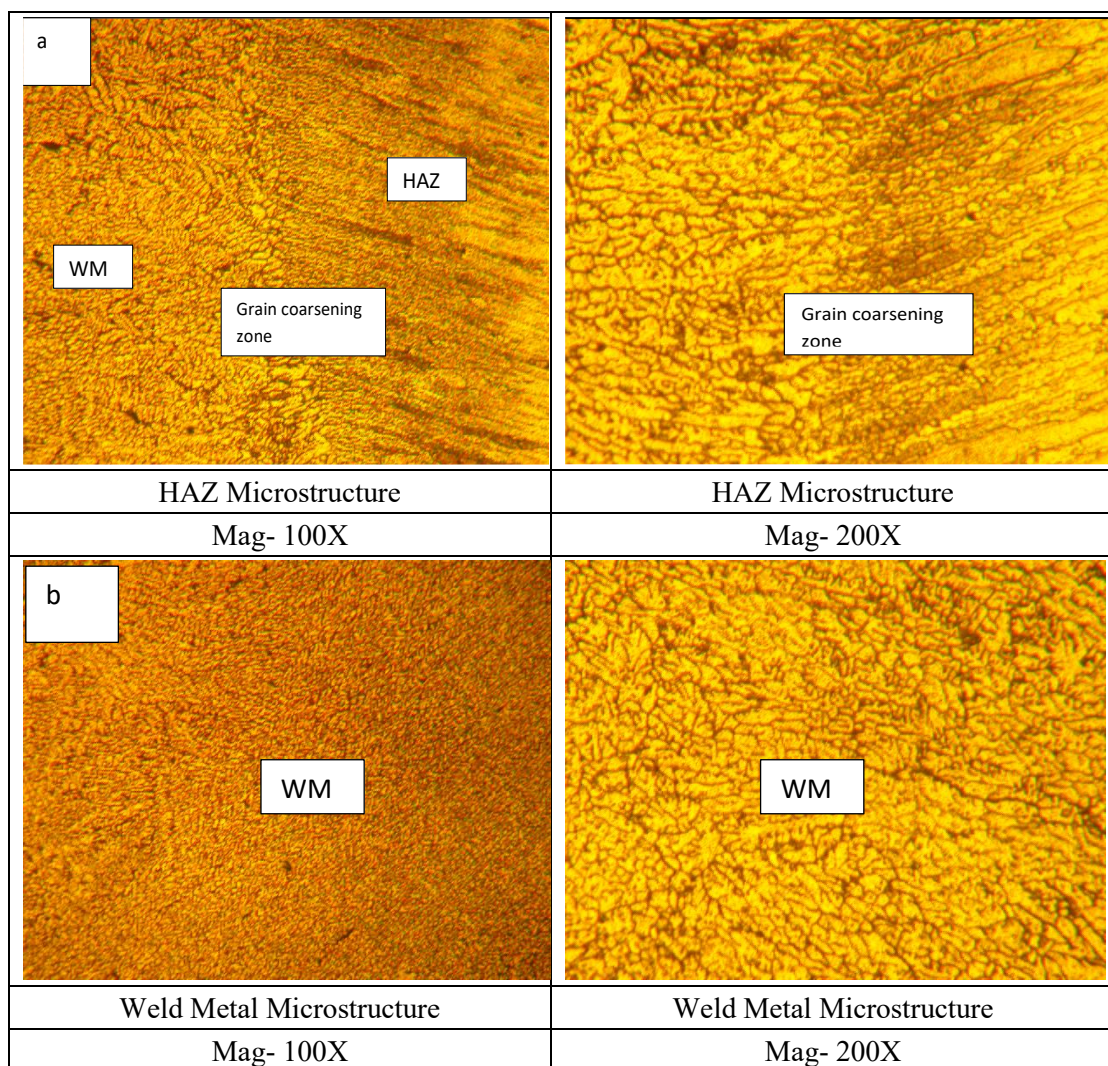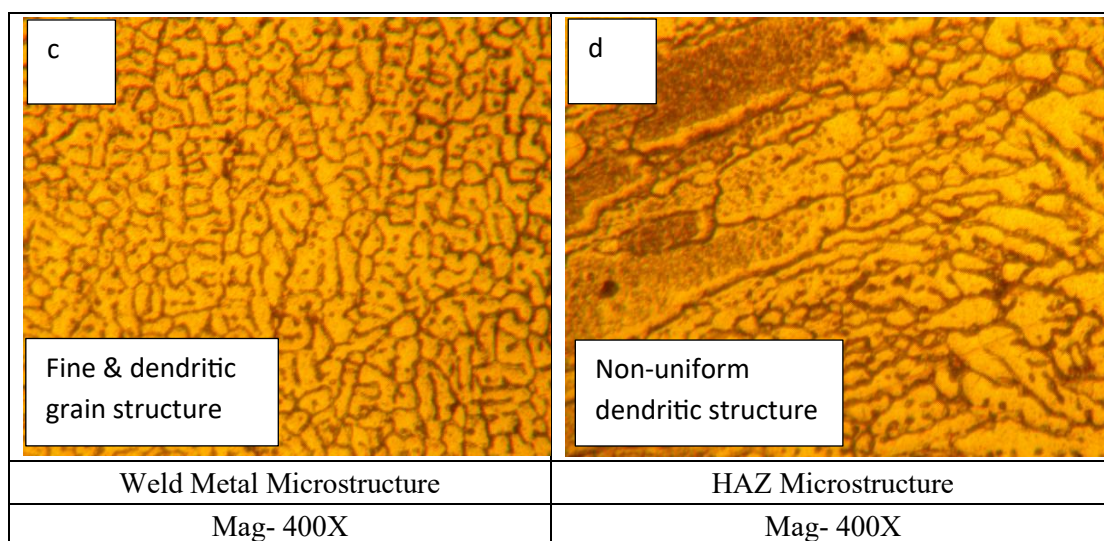
Figure 5.25: Metallography images of the CMT Welded sample-1, (a) HAZ (b) WM (c) WM, and (d) HAZ, at different magnifications.

| HAZ Microstructure | HAZ Microstructure |
| Mag- 100X | Mag- 200X |

Weld Metal Microstructure	Weld Metal Microstructure
Mag- 100X	Mag- 200X
Weld Metal Microstructure	HAZ Microstructure
Mag- 400X	Mag- 400X
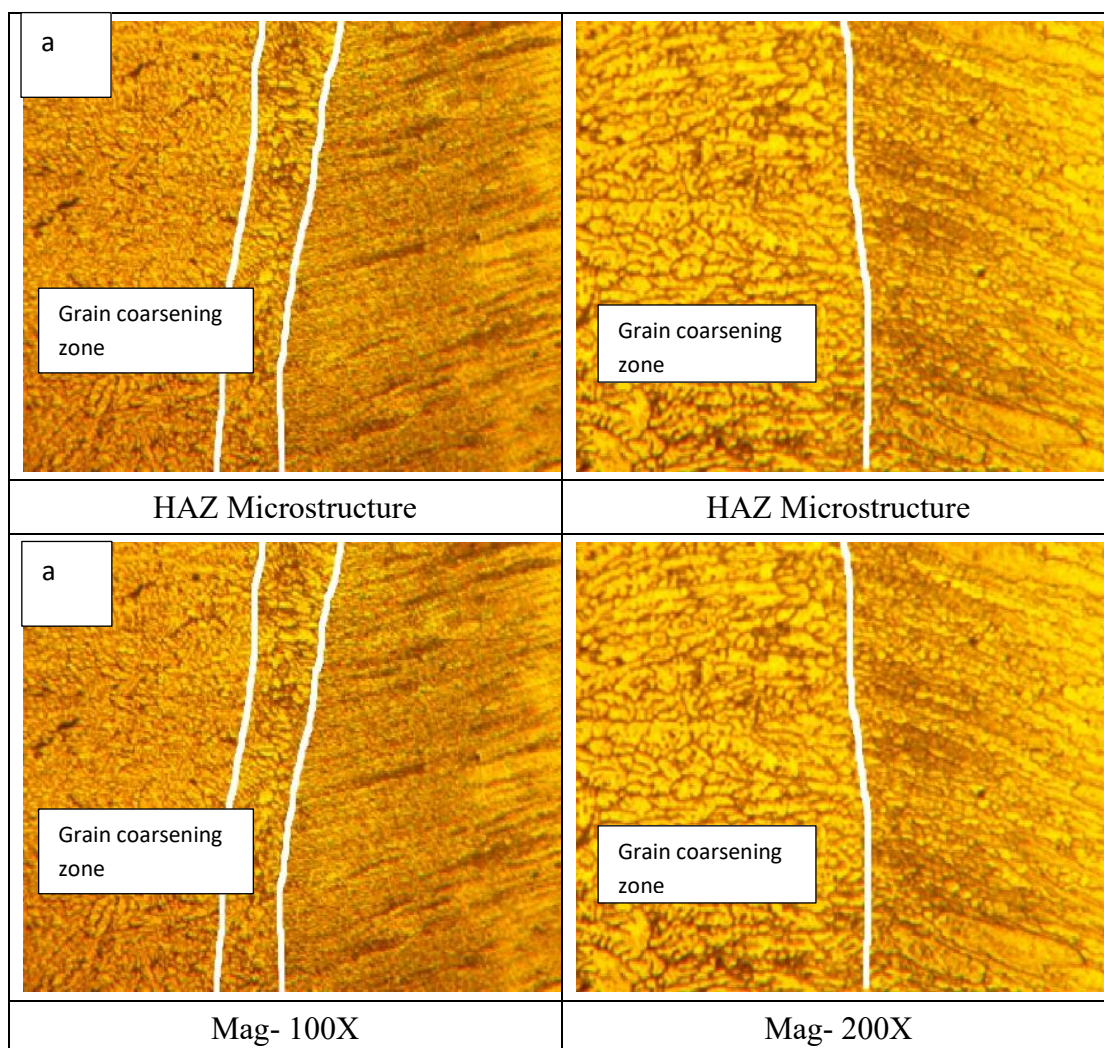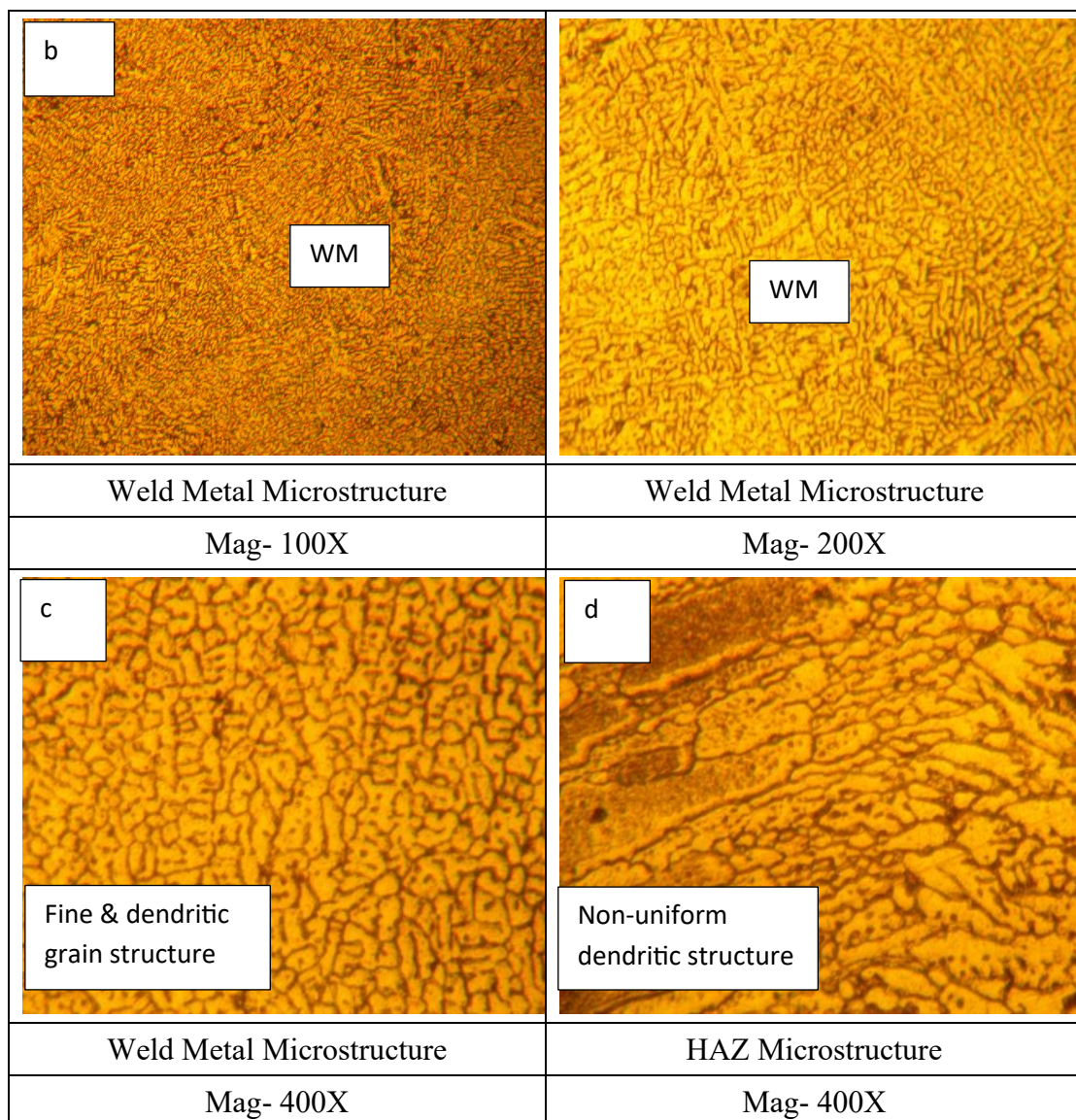
Figure 5.26: Metallography images of CMT Welded sample-2, (a) HAZ (b) WM (c) WM, and (d) HAZ, at different magnifications.

5.15 MICROHARDNESS OF THE BM, HAZ, AND WM

Weld cross-section, flaws, and macrostructure of the welded connection of AA7475-T7351 have already been studied. The results of the Vickers microhardness test for the CMT sample on the HAZ and the weld cross-section are shown in Table 5.14. The BM has a hardness value of 170 HV and is higher than both the WM and HAZ. The lowest hardness, 99 HV, was recorded at the WM and is only 58.24% of the BM in the CMT

159

sample due to the weld's heterogeneous structure, which is primarily made up of filler metal. Similar outcomes were seen by [212] in Al5.5Zn2.5Mg2.2Cu welded joints, where the WM is the weakest component and only possesses a 56% hardness of the base material. This is because the alloy components move toward the grain boundaries during solidification, softening the WM. This might also be because AA4043, a softer filler material than AA7475-T7351, was used. Given that the HAZ is composed of semi-molten BM, it has a hardness value of 145 HV. The HAZ, which is essentially a transition zone created by the welding heat input, results in the development of a recrystallization strengthening phase and partial hardness restoration. Hardness distribution in the material has the inverse proportion of the size and distribution of precipitates and also on the size of grains. Weld metal and HAZ have a lower hardness in comparison to the base metal. According to the findings, HAZ, which is close to the fusion zone, receives a high heat input followed by a sluggish rate of cooling [213]. A similar microstructure was observed in the microhardness analysis of weld sample-2.

Table 5.14: Hardness Test.

Parameter	Observed Value (HV1)	Result (Avg.)
Hardness Test (Weld Metal)	99,98,100	99HV1
Hardness Test (HAZ)	143,145,146	145HV1

5.16 MICROSTRUCTURAL COMPOSITIONS OF WELD

The WM is the weakest zone in comparison to the BM and HAZ, according to the above findings. Therefore, a weld composition analysis is necessary. To do this, an SEM micrograph was taken, and an associated EDX analysis was performed at the top, center, and root portions of the weld samples. The results are shown in Figure 5.27. In the top, middle, and root of the joint, the constituent linear scanning profiles for Mg,

Cu, Fe, Zn, and other elements are shown in Figure 5.27. Scanning Electron Microscope (SEM) micrographs from the top, center, and root of the CMT weld sample are shown in Figure 5.27 (a-c), along with matching EDX analyses. Figure 5.27-(a) illustrates how elements Mg, Zn, and Cu migrate from the BM to the WM even during welding, because the ER4043 welding wire had substantially less Mg, Cu, and Zn than the BM. Figure 5.27- (a) shows that the EDX result from the top of the weld had components with percentages of 56.74 percent Al, 34.55 percent Cu, and 5.60 percent O, indicating that the solid solution was Al-Cu based. Figure 5.27- (b) displays the EDX result from the weld's center. The Cu element decreased to 32.00%, whereas Al increased to 58.83% and O elements increased to 6.16%, showing that this location had not yet been completely made up of an Al-based solid solution. However, the diffusion of other content, such as Zn, Mg, and Fe from BM to WM had improved. In Figure 5.27- (c), the EDX result from the weld's root is displayed. With 88.16% Al, 8.37% O components, and an increased proportion of Zn and Mg in the phase composition at the weld's root, which creates a pure Al-based solid solution, the diffusion of the Cu element was greatly decreased. The solute accumulation layer in the welding pool appears to form in variable degrees as stated by [214], based on the solidification theory, in the vicinity of the solid-liquid contact. Figure 5.27 (a, b) displays the EDX results for the top and middle regions of the weld, which were 56.74% Al, 34.55% Cu, 1.45% Mg, and 58.83% Al, 32.00% Cu, 1.38% Mg, respectively. This indicated that the region must be made up of an Al-Cu-based solid solution. As per the work performed by [215], Cu_2Mg made up the majority of the Al/Cu reaction particle phase. Brittle alloying elements that were continuously disseminated in the top and middle of the fusion zone are what led to the fracture.

Almost similar results were observed from the SEM micrograph and EDX analysis of sample 2, which is presented in Figure 5.28. Figure 5.28 (a, b), which is from the top and centre of the weld shows the Al-based Al-Cu solid solution with other content which is diffused from the BM to WZ. Figure 5.28c shows the phase composition at the root of the weld which forms a pure Al-based solid solution, diffusion of the Cu element was reduced significantly.
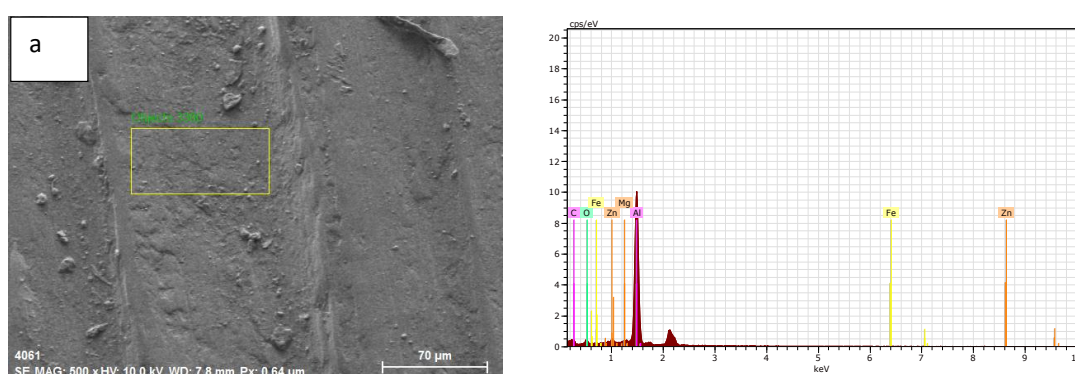
Spectrum: Objects 3380				
El AN Series unn. C norm. C Atom. C Error (1 Sigma)				
	[wt.%]	[wt.%]	[at. %]	[wt.%]
Al 13 K-series	26.76	70.51	56.74	1.29
C 6 K-series	7.25	19.11	34.55	2.37
O 8 K-series	1.57	4.13	5.60	0.63
Zn 30 L-series	0.93	2.45	0.81	0.13
Fe 26 K-series	0.83	2.18	0.85	0.25
Mg 12 K-series	0.61	1.62	1.45	0.09
Total:	37.95	100.00	100.00	

Spectrum: Objects 3381				
El AN Series unn. C norm. C Atom. C Error (1 Sigma)				
	wt.%]	[wt.%]	[at.%]	[wt.%]
Al 13 K-series	29.39	72.00	58.83	1.42
C 6 K-series	7.12	17.43	32.00	2.46
O 8 K-series	1.83	4.47	6.16	0.72
Zn 30 L-series	1.29	3.15	1.06	0.16
Mg 12 K-series	0.62	1.52	1.38	0.09
Fe 26 K-series	0.58	1.43	0.56	0.21
Total:	40.82	100.00	100.00	

Spectrum: Objects 3382				
El AN Series unn. C norm. C Atom. C Error (1 Sigma)				
	[wt.%]	[wt.%]	[at.%]	[wt.%]
Al 13 K-series	30.46	89.36	88.16	1.47
O 8 K-series	1.71	5.03	8.37	0.70
Zn 30 L-series	1.32	3.88	1.58	0.17
Mg 12 K-series	0.59	1.73	1.89	0.09
Total:	34.09	100.00	100.00	

Figure 5.27: EDX analysis with the corresponding SEM micrograph of the different micro-zones of weld for Sample-1: (a) top, (b) Centre, and (c) root of the weld.

163
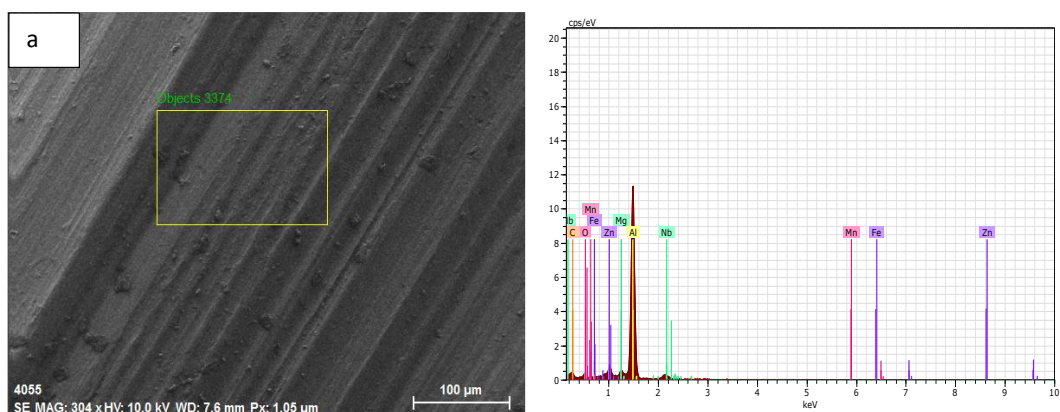
Spectrum: Objects 3374			
El AN Series	unn. C [wt.%]	norm. C [wt.%]	Atom. C [at.%]	C Error (1 Sigma) [wt.%]
Al 13 K-series	40.89	64.82	56.64	1.90
C 6 K-series	10.04	15.91	31.23	2.62
Nb 41 L-series	5.07	8.03	2.04	0.32
O 8 K-series	2.74	4.34	6.40	0.80
Zn 30 L-series	2.11	3.35	1.21	0.20
Mg 12 K-series	1.13	1.80	1.74	0.11
Fe 26 K-series	0.77	1.23	0.52	0.25
Mn 25 K-series	0.33	0.52	0.22	0.14
Total:	63.09	100.00	100.00	
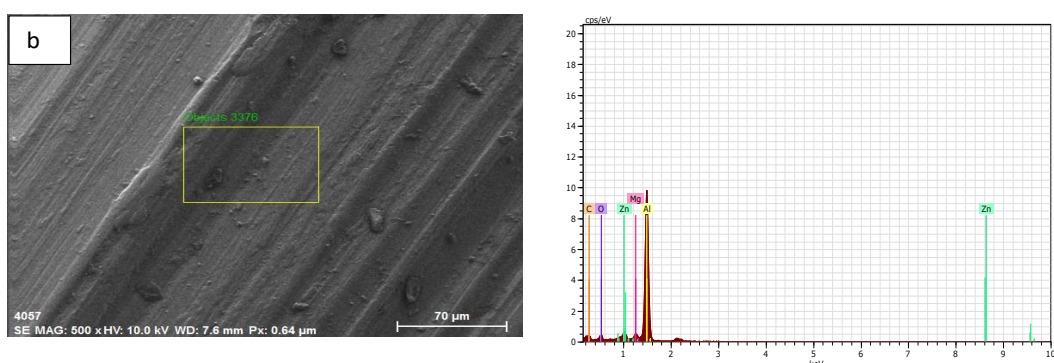
Spectrum: Objects 3376			
El AN Series	unn. C [wt.%]	norm. C [wt.%]	Atom. C [at.%]	C Error (1 Sigma) [wt.%]
Al 13 K-series	28.29	67.30	52.93	1.39
C 6 K-series	8.59	20.44	36.10	2.98
O 8 K-series	2.47	5.86	7.78	0.95
Zn 30 L-series	1.83	4.36	1.42	0.21
Mg 12 K-series	0.86	2.03	1.78	0.11
Total:	42.04	100.00	100.00	

| Spectrum: Objects 3375				
El AN Series unn. C norm. C Atom. C Error (1 Sigma)				
	[wt.%]	[wt.%]	[at.%]	[wt.%]
--				
Al 13 K-series	38.65	90.84	90.01	1.57
O 8 K-series	2.99	6.66	8.47	0.70
Fe 26 K-series	0.44	1.04	0.41	0.23
Mg 12 K-series	0.43	1.00	0.92	0.07
Mn 25 K-series	0.20	0.46	0.19	0.14
--				
Total:	42.71	100.00	100.00	
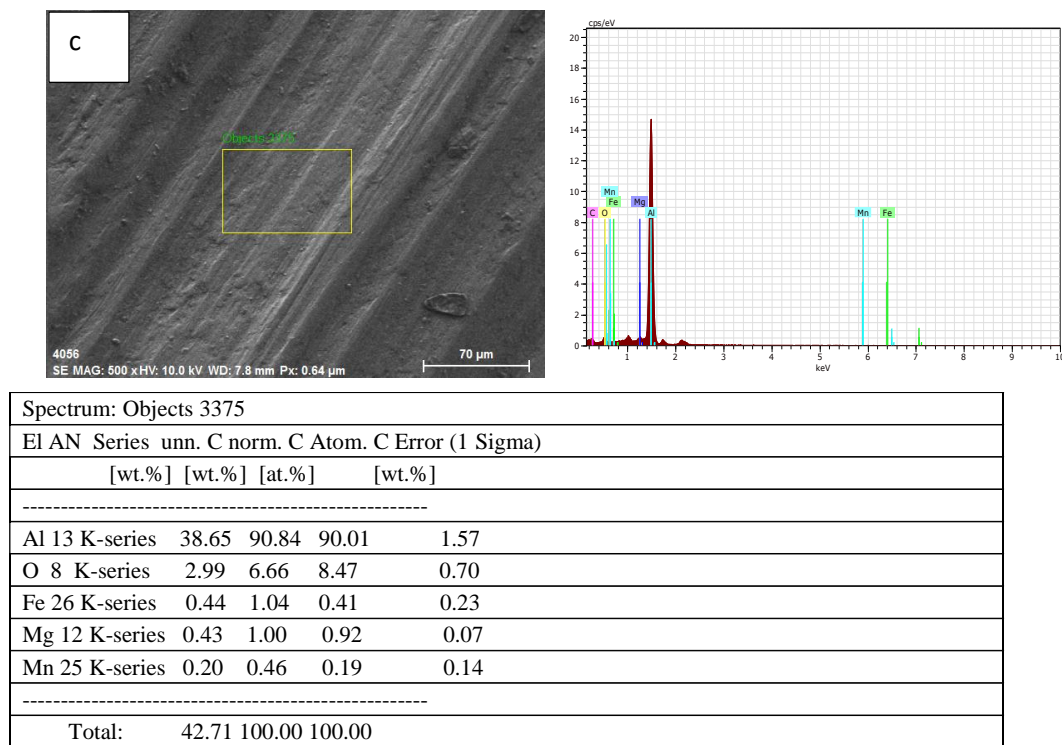
Figure 5.28: EDX analysis with the corresponding SEM micrograph of the different micro-zones of weld for Sample-2: (a) top, (b) Centre, and (c) root of the weld.

5.17 FRACTURE MECHANISM OF THE CMT JOINTS

To thoroughly characterize the failure patterns of the welded connection, SEM was used to analyse the fractured surface of the tensile samples. SEM fractography from the top surfaces, middle surface, and bottom (root) regions of the joints were taken. Figure 5.29 displays the fractography of shattered WM surfaces following failure under tensile loading. The sample clearly shows fracture to the weld metal, yet the fracture surface appears to be free of porosities and inclusions. The CMT welded sample shows a fracture with a high number of evenly distributed equiaxed dimples as seen from the top of the weld in Figure 5.29- (a). The spacing between the grains determined how ductile the welded joint was. The fractography collected from the center of the tensile fracture sample is shown in Figure 5.29- (b). The fracture surfaces of CMT specimens at the center of the weld had nearly extremely fine dimples. The fracture surfaces'

165

predominance of dimples suggests that ductile fracture was the primary factor in most of the failures. The solution heat-treated samples showed several micro dimples, as reported in [210], which lends more credence to this conclusion. A sign of ductile failure is fine dimples. Before necking, voids show up in ductile material that is being tested for tensile strength. However, if a neck develops early, as seen in Figure 5.29-(b) by the coarse and extended dimples, the void growth is much more obvious. On the other hand, some dimples and some flat portions show both ductile and brittle fractures [216]. Poor welding results in insufficient metal consolation at the weld zone's root; the weldment was unable to adequately penetrate the parent metal, which may be the cause of the bottom-area fracture that has a brittle appearance [217]. Figure 5.29-(c) illustrates the patterns of cleavage failure that were found. The cleavage facets in CMT, from the root portion of the joints had smaller cleavage facets than the top and center areas of the welded joints. The first finding is that the fracture of the welded specimens always took place within the welded zone. Viewed in another manner, a joint's strength and ductility are better when its dimple size is less, and vice versa. A ductile failure is indicated by fine dimples. Void formation usually occurs before necking in ductile material undergoing tensile testing. Moreover, this is corroborated by [218], which found long and coarse dimples in PWHT pulsed-current GMAW weld. The fractography of sample -2, which was obtained from the root section of the joints as well as the top surfaces and center, revealed similar failure patterns, which are displayed in Figure 5.30.
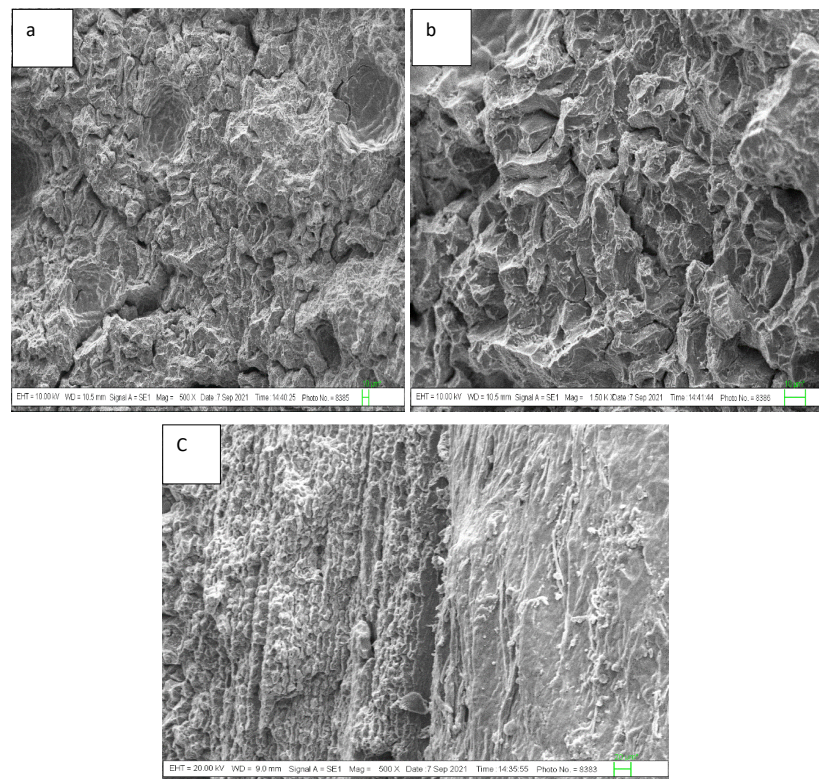
Figure 5.29: The SEM fractography of CMT welded tensile tested specimens-1; (a) top regions; (b) center regions (c) root region of the weld.
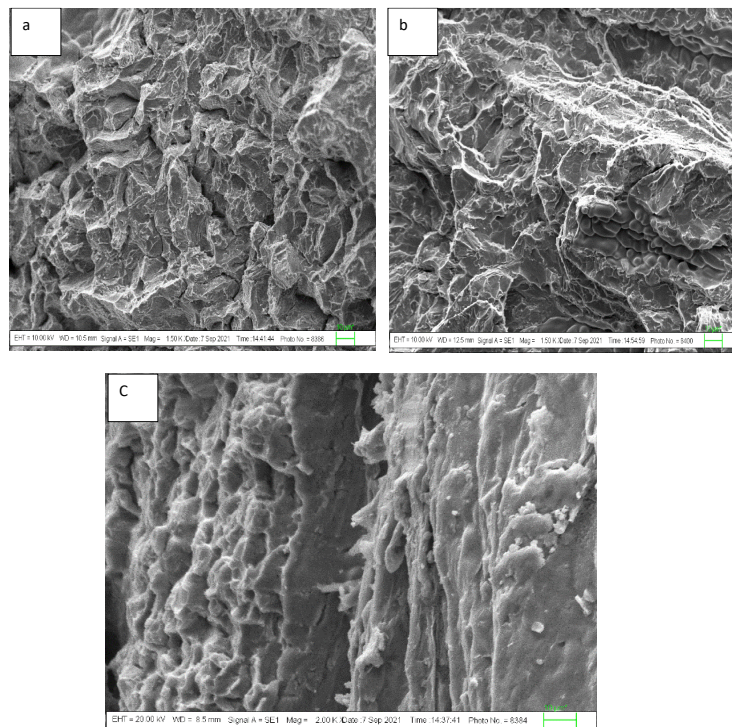
Figure 5.30: The SEM fractography of CMT welded tensile tested specimens-2; (a) top regions; (b) center regions (c) root region of the weld.

167

CHAPTER 6

CONCLUSIONS AND FUTURE SCOPE

6.1 CONCLUSIONS

In this study, the robotic CMT is used to weld the hybrid composite AA7475-T7351 alloy. The composite was fabricated in hybrid mode by the application of a bottom-pouring stir-casting setup. SiC, B_4C, MoS_2, and Gr micro-particles are used to fabricate the composite. The composite samples were welded and the joints were produced without spatter, cracks, and very low surface porosity. The welds were performed over the hybrid composite incorporated with the reinforcements of SiC 2%+B_4C 3% + Gr 1%. The casted composite was welded through the robotic CMT welding setup, and the mechanical properties were tested and microstructural were analysed. Also, the samples of AA7475 alloy in T7351 temper conditions were welded by utilizing the optimized welding parameters as a confirmatory test. The analysis was done and results were compared based on microstructural analysis, hardness distribution, tensile properties, and fractography. Based on the above analysis, the following conclusions have been summarized as given below:

1. The fabricated composite has a TS of 168 MPa showing an improvement in tensile strength as compared to the cast Al-alloy having a TS of 158 MPa. The maximum TS of CMT welded composite WM is 66.65% of composite base metal, showing significant improvement in welding efficiency. Similar improvements were observed in YS and elongation. WM is the weakest link and all the samples failed at WM.

168

2. Composite base metal shows an average hardness value of 151.18 HV compared to 138.8 HV of cast Al-alloy. A significant improvement in hardness value was found in the formed composite. The hardness of WM as well as HAZ are 64.69% and 76.33% of the composite base metal respectively. It is concluded that the composite base metal is the hardest portion of the weld samples.

3. The micrograph of the weld sample is taken from the different regions of the weld and reported. The base metal shows the non-uniform elongated grain whereas the weld portion shows the dendritic grain structure uniformly distributed throughout the weld. Larger and coarser grains were found in the HAZ compared to WM.

4. The confirmatory test was conducted by utilizing the optimized welding parameters to weld the composite. The test results show marginal improvements in the mechanical and microstructural properties of the weld, which validates the optimized welding parameters for the chosen weld.

5. Similar findings were observed when AA7475 alloy in T7351 temper conditions was welded by utilizing the CMT welding processes as a confirmatory test by utilizing optimized welding parameters. It is found that in comparison to the performance of the BM and HAZ, the WM is the weakest portion. The tensile strength and elongation value show a significant decrement at HAZ and WM compared to BM for welded samples. WM has 6.2 % elongation, which is slightly less than 8.4% of HAZ and significantly less than 13.2% of the BM. It is found that in terms of % elongation, TS, and YS, the weld metal is the weakest link of the weldments formed and all the samples failed in the WM.

6. The BM is the hardest, with a hardness of 170 HV, much greater than the WM and HAZ, and the lowest hardness, 99 HV, was recorded in CMT at the WM and is only

58.24 percent of the BM. The BM is the hardest, and the lowest hardness was recorded at the WM.

7. A metallographic image taken from BM shows that it is made up of elongated grains whereas an ununiform dendritic structure was observed in the HAZ throughout the matrix. The general microstructure of WM shows full penetration welding in the base structure. The structure consists of fine & uniform dendritic grain structure.

8. EDX analysis is done for the top, center, and bottom portion of the weld, and it was observed that the Zn, Mg, and Cu contents diffuse from BM towards the WM and vary from the top of the weld to the root of the weld. The phase composition of the root is mainly an Al-based solid solution.

9. The fractography from the top of the weld reveals that the fracture has a considerable number of equiaxed dimples that are equally distributed. The dimples at the top of the weld are wider and deeper than the dimples on the fracture surface of the Centre and root of the weld, indicating better ductility of the top region of the weld compared to the Centre and root of the weld and a typical mode of toughness fracture. The dimples on the fracture surfaces of CMT specimens were nearly fine. The dimples predominated on the fracture surfaces, indicating that ductile fracture was the cause of the majority of the failure. Cleavage failure patterns were observed at the root of the weld.

6.2 FUTURE SCOPE

Based on research work conducted and observed findings, some future directions of the work on this most applicable material are required to be explored. The following works in this noble material that need to be carried out are as follows:

1. Alloys in the 7XXX Series are, Al-Zn base alloys with 0.8-12 %, of Zn and they are among the strongest Al alloys. The major applications of these alloys are in, aircraft industries and in making professional goods for sports, also use these alloys. A hard-to-weld and heat-treatable 7xxx series aluminum alloy like Al-7475 is a precipitation-hardened Al-alloy and can be heat-treated at different ranges one of them is T7351 tempered condition. The strength of these alloys in their age-hardened condition is metastable and very sensitive to temperature. Its strength is exposed during processing at elevated temperatures. During high temperatures casting or melting, it is required to maintain its tempered condition otherwise precipitation takes place and the strength gets dissolved. Controlled casting is the future direction to maintain the tempered condition and properties during the fabrication of the composite of the Al-7000 series.

2. The composite is made by using micro-reinforcement particles in a hybrid form, a nanocomposite with micro-particle or pure nanohybrid combination may be used to enhance the properties of high-application Al-alloy.

3. To get better properties of aerospace Al-alloy some new reinforcements like carbon nanotubes and some rare material reinforcement need to be tried by checking the compatibility may be the future direction of research.

REFERENCES

1. Mavhungu, S. T.; Akinlabi, E. T.; Onitiri, M. A.; Varachia. F. M. Aluminium Matrix Composite for Industrial Use: Advances and Trends: International Conference on Sustainable Material and Manufacturing, Procedia Manufacturing 2017, 7, 178-182.

2. Baisane, V. P.; Sable, Y. S.; Dhobe, M. M.; Sonawane, P. M. Recent development and challenges in the processing of ceramics reinforced Al matrix composite through stir casting process: International Journal of Engineering and Applied Sciences (IJEAS) 2015, ISSN: 2394-3661, Volume-2, Issue-10.

3. Saravanan, C.; Sbramanian, K.; Krishanan, V. A.; Narayanan, R. S. Effect of Particulate Reinforced Aluminium Metal Matrix Composite Mechanics Mechanical Engineering Lodz University of Technology 2015, Vol. 19, No. 1 23–30.

4. Rambabu, P.; Prasad, N. E.; Kutumbarao, V. V.; Wanhill, R. J. H. Aluminium Alloys for Aerospace Applications, Chapter 2, © Springer Science+Business Media Singapore 2017, 10.1007/978-981-10-2134-3_2.

5. Miller, W. S.; Zhuang, L.; Bottema, J.; Wittebrood, A. J.; Smet, P. D.; Haszler, A.; Vieregge, A. Recent development in aluminium alloys for the automotive industry, Journal of Materials Science and Engineering A 2000, 280, 37–49.

6. Kumar, D. S.; Suman, K. N. S.; Sasanka, C. T.; Ravindra, K.; Poddar, P.; Siva, S. V. V. Microstructure, mechanical response and fractography of AZ91E/Al2O3 (p) nanocomposite fabricated by semi-solid stir casting method, Journal of Magnesium and Alloys 2017, 5, 48–55.

7. Harichandran, R.; kumar, N. S. Effect of nano/micro B_4C particles on the mechanical properties of aluminium metal matrix composites Fabricated by ultrasonic cavitation-assisted solidification process, Journal of Materials Processing Technology 2015, 86, 61–71.

8. Kannan, C.; Ramanujam, R. Comparative study on the mechanical and microstructural characterisation of AA 7075 nano and hybrid nanocomposites

produced by stir and squeeze casting, Journal of Advanced Research 2017, 8, 309–319.

9. Baradeswaran, A.; Perumal, A. E. Study on mechanical and wear properties of Al 7075/Al$_2$O$_3$/graphite hybrid composites. Compos Part B – Eng; 2014, 56, 464–71.

10. Baradeswaran, A.; Perumal, A. E. Wear and mechanical characteristics of Al 7075/graphite composites. Compos Part B - Eng; 2014, 56, 472–76.

11. Ahamed, H.; kumar, V. S, Experimental investigation on newly developed ultrafine-grained aluminium based nano-composites with improved mechanical properties. Mater Des; 2012, 37, 182–92.

12. Soleymani S., A. Abdollah-zadeh∗, S.A. Alidokht, Microstructural and tribological properties of Al5083 based surface hybrid composite produced by friction stir processing (2012) Wear 278– 279 (2012) 41– 47 doi: 10.1016/j.wear.2012.01.009.

13. Zhanh, Q.; Wu, G.; Jiang, L. Tensile deformation behavior of a sub-micrometer Al$_2$O$_3$/6061Al composite, Materials Science and Engineering A 2008, 483, 281–284.

14. Alidokht S. A., Abdullah-Zadeh A., S. Soleymani, H. Assadi, Microstructure and tribological performance of an aluminium alloy-based hybrid composite produced by friction stir processing, Mater. Des. 32 (2011) 2727–2733.

15. Baradeswaran A, Perumal AE. (2014) Wear and mechanical characteristics of Al 7075/graphite composites. Compos Part B - Eng; 56: 472–6.

16. Ahamed H, Senthilkumar V. (2012) Experimental investigation on newly developed ultrafine-grained aluminum-based nano-composites with improved mechanical properties. Mater Des;37: 182–92.

17. Zhanh Q., G. Wu, L. Jiang, (2008) Tensile deformation behavior of a sub-micrometer Al2O3/6061Al composite, Materials Science and Engineering A 483 281–284.

18. Yalda Afkhama, et al. (2018) Enhanced mechanical properties of in situ aluminium matrix composites reinforced by alumina nanoparticles, Archives of civil and Mechanical Engineering 18, 215–226.

19. Boostani A. F., S. Tahamtan, Z. et al., (2015) Enhanced tensile properties of aluminium matrix omposites reinforced with grapheme encapsulated SiC nanoparticles, Composites Part A: Applied Science and Manufacturing 68, 155–163.

20. Ma Z., S. Tjong, (1997) In situ ceramic particle-reinforced aluminium matrix composites fabricated by reaction pressing in the TiO2 (Ti)-Al-B (B2O3) systems, Metallurgical and Materials Transactions A 28, 1931–1942.

21. Baradeswaran A, Perumal AE. (2014) Study on mechanical and wear properties of Al 7075/Al2O3/graphite hybrid composites.Compos Part B – Eng ;56: 464–71.

22. Imaizumi, S, Welding of aluminium to dissimilar metals, Weld. Int. 1996, 10, 593–604.

23. Huang, J.; He, X.; Yanning, G.; Zhang, Z.; Shi, Y.; Fan, D. Joining of aluminum alloys to galvanized mild steel by the pulsed DE-GMAW with the alternation of droplet transfer, Journal of Manufacturing Processes 2017, 25, 16–25.

24. Peyre, P.; Sierra, G.; Deschaux-Beaume, F.; Stuart, D.; Fras, G, Generation of aluminium–steel joints with laser-induced reactive wetting, Mater. Sci. Eng., A 2007, 444, 327–338.

25. Sierra, G.; Peyre, P. F.; Beaume, D.; Stuart, D.; Fras, G. Galvanised steel to aluminium joining by laser and GTAW processes, Mater. Charact. 2008, 59, 1705–1715.

26. Rathod, M.; Kutsuna, M. Joining of aluminum alloy 5052 and low-carbon steel by laser roll welding, Weld J. 2004, 83, 16s–26s.

27. Sproesser, G.; Pittner, A.; Rethmeier, M. Increasing performance and energy efficiency of Gas Metal Arc Welding by a high-power tandem process, Procedia CIRP 2016, 40, 643 – 648.

28. Bai, P.; Wang, Z.; Shengsun, H.; Shangwen, M.; Liang, Y. Sensing of the weld penetration at the beginning of pulsed gas metal arc welding, Journal of Manufacturing Processes 2017, 28, 343–350.

29. Verma, B. B.; Atkinson, J. D.; Kumar, M. Study of fatigue behaviour of 7475 aluminium alloy, © Indian Academy of Sciences, Bull. Mater. Sci., 2001, Vol. 24, No. 2, pp. 231–236.

30. Jacob, A.; Maheshwari, S.; Siddique, A. N.; Gangil, N. Improvements in strength and microstructural behavior of friction stir welded 7475 aluminium alloy using in-process cooling, Mater. Res. Express 2018, 5, 076518, 1591-2053.

31. Dursun, T.; Soutis, C, Recent developments in advanced aircraft aluminium alloys, Journal of Materials and Design 2013, 56, 862–871.

32. Rajan, R.; Kah, P.; Mvola, B.; Martikainen, J. Trends in aluminium alloy development and their joining methods Rev.Adv.Mater 2016, Sci.44383–97.

33. Feng, J.; Zhang, H.; He, P. The CMT short-circuiting metal transfer process and its use in thin aluminium sheets welding. Material Design. 2009, 30(5), 1850–1852. Available from: http://dx.doi.org/10.1016/j.matdes.2008.07.015.

34. Jana, S.; Hovanski, Y.; Grant, G.J. Friction stir lap welding of magnesium alloy to steel: a preliminary investigation. Metall. Mater Trans A 2010, 41A, 3173–82.

35. Shang, J.; Wang, K.; Zhou, Q.; Zhang, D.; Huang, J.; Li, G. Microstructure characteristics and mechanical properties of cold metal transfer welding Mg/Al dissimilar metals. Material Design. 2012, 34, 559–565. Available from: http://dx.doi.org/10.1016/j.matdes.2011.05.008.

36. Yong, Y.; Da-tong, Z.; Cheng, Q.; Wen, Z. Dissimilar friction stir welding between 5052 aluminium alloy and AZ31 magnesium alloy. Transactions of Nonferrous Metals Society of China 2010, 20, 619 – 623.

37. Kwon, Y. J.; Shigematsu, I.; Saito, N. Dissimilar friction stir welding between magnesium and aluminium alloys. Mater Lett 2008, 62, 3827–9.

38. Yan, J. C.; Xu, Z.W.; Li, Z.Y.; Li, L.; Yang, S.Q. Microstructure characteristics and performance of dissimilar welds between magnesium alloy and aluminium formed by friction stirring. Scripta Mater 2005, 53, 585–9.

39. Zhao, L. M.; Zhang, Z. D. Effect of Zn alloy interlayer on interface microstructure and strength of diffusion-bonded Mg–Al joints. Scripta Mater 2008, 58, 283–6.

40. Mahendran, G.; Balasubramanian, V.; Senthilvelan, T. Developing diffusion bonding windows for joining AZ31B magnesium–AA2024 aluminium alloys. Mater Des 2009, 30, 1240–4.

41. Liu, P.; Li, Y. J.; Geng, H. R.; Wang, J. Microstructure characteristics in TIG welded joint of Mg/Al dissimilar materials. Mater Lett 2007, 61, 1288–91.

42. Wang, J.; Feng, J. C.; Wang, Y. X. Microstructure of Al–Mg dissimilar weld made by cold metal transfer MIG welding. Mater Sci Technol 2008, 24(7), 827–31.

43. Borrisutthekul, R.; Miyashita, Y.; Mutoh, Y. Dissimilar material laser welding between magnesium alloy AZ31B and aluminium alloy A5052-O. Sci Technol Adv Mater 2005, 6, 199–204.

44. Liu, L. M.; Wang, H. Y.; Zhang, Z.D. The analysis of laser weld bonding of Al alloy to Mg alloy. Scripta Mater 2007, 56, 473–8.

45. Li, H.; Qian, M.; Li, D. The effect of intermetallic compounds on laser weldability of dissimilar metal joint between magnesium alloy AZ31B and aluminium alloy 6061. Laser J 2007, 28(5), 61–3.

46. Zhang, H. T.; Feng, J. C.; He, P.; Zhang, B. B.; Chen, J. M.; Wang, L. The arc characteristics and metal transfer behaviour of cold metal transfer and its use in joining aluminium to zinc-coated steel. Mater Sci Eng A. 2009, 499(1–2), 111–3.

47. Hermans, M. J. M. Process behavior and stability in short circuit gas metal arc welding. Weld J 1999, 78(4), 141–73.

48. KAH P.; SUORANTA R.', MARTIKAINEN J.; Advanced gas metal arc welding processes [J]. The International Journal of Advanced Manufacturing Technology, 2013, 67(1−4): 655−674.

49. RAJEEV G. P.; KAMARAJ M.; BAKSHI S. R. Al-Si-Mn alloy coating on aluminum substrate using cold metal transfer (CMT) welding technique [J]. The Journal of the Minerals, Metals & Materials Society, 2014, 66(6): 1061−1067.

50. FENG Ji-cai.; ZHANG Hong-tao, HE Peng. The CMT short-circuiting metal transfer process and its use in thin aluminium sheets welding [J]. Materials & Design, 2009, 30(5): 1850−1852.

51. Zhang C.; Li G.; Gao M.; Yan J.; Zeng X. Y. Microstructure and process characterization of laser-cold metal transfer hybrid welding of AA6061 aluminum alloy [J]. The International Journal of Advanced Manufacturing Technology, 2013, 68(5−8): 1253−1260.

52. Schierl, A. The CMT – process – a revolution in welding technology. Weld World 2005, 49(9), 38.

53. Groover MP. Fundamental of modern manufacturing, materials, processes and systems. 3rd Edition. John Wiley and Sons; 2007.

54. Huang CH, Hou CH, Hsieh TS, et al. Investigation of distinct welding parameters on mechanical and corrosion properties of dissimilar welded joints between stainless steel and low carbon steel. Science Progress 2022; Vol. 105(4) 1–18. DOI: 10.1177/00368504221126795.

55. Campbell SW, Galloway AM, McPherson NA, et al. Evaluation of gas metal arc welding with alternating shielding gases for use on AA6082T6. J Engineering Manufacture 2012; 226(6) 992–1000. DOI: 10.1177/0954405412439672.

56. Verma RP, Pandey KN, and Sharma Y. Effect of ER4043 and ER5356 filler wire on mechanical properties and microstructure of dissimilar aluminium alloys, 5083-O and 6061-T6 joint, welded by the metal inert gas welding. J Engineering Manufacture 2014; 1–8. DOI: 10.1177/0954405414535771.

57. Alshaer AW, Li L, and Mistry A. Effect of filler wire properties on porosity formation in laser welding of AC-170PX aluminium alloy for lightweight automotive component manufacture. J Engineering Manufacture 2015; 1–13. DOI: 10.1177/0954405415578584.

58. Jahn M T, and Luo J, 1988 J. Mater. Sci. 23 4115.

59. Rajan R, Kah P, Martikainen MBJ. Trends in aluminium alloy development and their joining methods Rev.Adv. Mater. Sci. (2016) 44383–97.

60. Tiryakioglu M, and Staley J T. Physical metallurgy and the effects of alloying additions in Aluminium alloys (New York: Marcel Dekker, 2003).

61. Thomas W, Nicholas E, Needham J, Church M P, Smith T, and. Dawes C. Friction stir welding, England PCT/ GB92102203, 1991.

62. Hynes NRJ, Prabhu MV, Velu PS, et al. An experimental insight of friction stir welding of dissimilar AA 6061/Mg AZ 31 B joints. J Engineering Manufacture 2022; Vol. 236(6-7) 787–797. DOI: 10.1177/09544054211043474.

63. Qiao F, Cheng K, Wang L, et al. An experimental investigation on the dissimilar joining of AA6061 and 1Cr18Ni9Ti by refill friction stir spot welding and its mechanical properties. J Engineering Manufacture 2015; 1–7. DOI: 10.1177/0954405415603599.

64. Rajendran CK, Srinivasan V, Balasubramanian H, et al. "Evaluation of load-carrying capabilities of friction stir welded, TIG welded and riveted joints of AA2014- T6 aluminium alloy," Aircraft Engineering & Aerospace Technology, vol. 19, no. 9, 2019.

65. Gungor B, Kaluc E, Sik AS, et al. "Mechanical and microstructural properties of robotic cold metal transfer (CMT) welded 5083-H111 and 6082-T651 aluminum alloys," Materials & Design, vol. 54, pp. 207–211, 2014.

66. Rajeev G. P.; M. Kamaraj M.; and Srinivasa R. Bakshi Effect of correction parameters on deposition characteristics in cold metal transfer welding, journal of materials and manufacturing processes Taylor & Francis 2019, https://doi.org/10.1080/10426914.2019.1628260.

67. Zhang, H. T.; Feng, J. C.; He, P.; Hackl, H. Interfacial microstructure and mechanical properties of aluminium–zinc-coated steel joints made by a modified metal inert gas welding–brazing process. Mater Charact 2007, 58, 588–592.

68. Shu F Y, Tian Z, Lü Y H, He W X, Lüjian-Jun Lin F Y, Zhao H Y, Xu B S 2015 Trans. Nonferrous Met.

69. Kadoi K, Murakami A, Shinozaki K, Yamamoto M, Matsumura H 2016 Materials Science and   Engineering: A 666 11–18.

70. Gungor B, Kaluc E, Taban E, Sik A 2014 Materials & Design (1980-2015) 54 207–211.

71. Pickin C G, Williams S W, Lunt M 2011 Journal of Materials Processing Technology 211 (3) 496–502.

72. Barrett T., the future of metal is in matrix composites, Materials (Mach. Des.) (2017).

73. Poovazhagan L., K. Kalaichelvan, T. Sornakumar, Processing and performance characteristics of aluminum-nano boron carbide metal matrix nanocomposites, Mater. Manuf. Process. 31 (10) (2016) 1275–1285.

74. Agarwal B.D., L. Broutman, C.K., Analysis and performance of fiber composites. 2017: John Willey & Sons Ltd. References.

75. Mohal S., H. Kumar, Study on the Multiwalled Carbon Nano tube Mixed EDM of Al-SiC p Metal Matrix Composite, Mater. Today: Proc. 4 (2) (2017) 3987–3993.

76. Balguri P.K., D.G.H. Samuel, U. Thumu, A review on mechanical properties of epoxy nanocomposites, Mater. Today: Proc. 44 (2021) 346–355.

77. Thiagarajan R., K. Palanikumar, S. Arumugam, Synthesis and characterization of sintered hybrid aluminium matrix composites reinforced with nanocopper oxide particles and microsilicon carbide particles, Compos. B Eng. 59 (2014) 43–49.

78. Schiøtz J., F.D. Di Tolla, K.W. Jacobsen, Softening of nanocrystalline metals at very small grain sizes, Nature 391 (6667) (1998) 561–563.

79. Khorshid M.T., S.A.J. Jahromi, M.M. Moshksar, Mechanical properties of tri-modal Al matrix composites reinforced by nano- and submicron-sized Al_2O_3 particulates developed by wet attrition milling and hot extrusion, Mater. Des. 31 (8) (2010) 3880–3884.

80. Haghighi R.D., S.A.J. Jahromi, A. Moresedgh, M.T. Khorshid, A Comparison Between ECAP and Conventional Extrusion for Consolidation of Aluminum Metal Matrix Composite, J. Mater. Eng. Perform. 21 (9) (2012) 1885–1892.

81. Varol T., A. Canakci, Synthesis and characterization of nanocrystalline Al 2024–B_4C composite powders by mechanical alloying, Philos. Mag. Lett. 93 (6) (2013) 339–345.

82. Reddy R., Processing of nanoscale materials, Rev. Adv. Mater. Sci 5 (2003) 121–133. 193.

83. Kang Y.-C., S.-L.-I. Chan, Tensile properties of nanometric Al2O3 particulate-reinforced aluminum matrix composites, Mater. Chem. Phys. 85 (2) (2004) 438–443.

84. Wang G., Z. Lu, C. Wang, Q. Ren, K. Zhang, Fabrication and mechanical properties of Al2O3–Si3N4/ZrO2–Al2O3 laminated composites, Powder Technol. 214 (2) (2011) 188–202.

85. Mussert K.M. et al, A nano-indentation study on the mechanical behaviour of the matrix material in an AA6061 Al2O3 MMC, J. Mater. Sci. 37 (4) (2002) 789–794.

86. Deng K.K., K. Wu, Y.W. Wu, K.B. Nie, M.Y. Zheng, Effect of submicron size SiC particulates on microstructure and mechanical properties of AZ91 magnesium matrix composites, J. Alloy. Compd. 504 (2) (2010) 542–547.

87. Seyed Reihani S.M., Processing of squeeze cast Al6061–30vol % SiC composites and their characterization, Mater. Des. 27 (3) (2006) 216–222.

88. Su B., H.G. Yan, G. Chen, J.L. Shi, J.H. Chen, P.L. Zeng, [13] D. Nestler, S. Siebeck, H. Podlesak, S. Wagner, M. Hockauf, B. Wielage, 2011, in: M. Fathi, A. Holland, F. Ansari, C. Weber (Eds.), Integrated Systems, Design and Technology 2010, Springer Berlin Heidelberg, Berlin, Heidelberg, 2011, pp. 93–107.

89. Yang Y., X. Li, Ultrasonic Cavitation Based Nanomanufacturing of Bulk Aluminum Matrix Nanocomposites, Journal of Manufacturing Science and Engineering-transactions of The Asme - J MANUF SCI ENG 129 (2007) 497–501.

90. Rohatgi P., B. Schultz, Light weight metal matrix composites Stretching the boundaries of metals, Material Matters 2 (2007) 16–19.

91. Hermans, M. J. M. Process behavior and stability in short circuit gas metal arc welding. Weld J 1999, 78(4), 141–73.

92. Schierl, A. The CMT – process – a revolution in welding technology. Weld World 2005, 49(9), 38.

93. Fang, X.;, Zhang, L.; Chaolong, Li. H.;, Huang, H. K.; Bingheng, Lu. Microstructure Evolution and Mechanical Behavior of 2219 Aluminum Alloys Additively Fabricated by the Cold Metal Transfer Process Materials (Basel). 2018 May, 11(5), 812.

94. Baoqiang, C.; Ruijie, O.; Bojin, Q.; Jialuo, D. Influence of Cold Metal Transfer Process and Its Heat Input on Weld Bead Geometry and Porosity of Aluminum-Copper Alloy Welds Rare Metal Materials and Engineering, 2016, 45(3), 0606-0611.

95. Pickin, C. G.; Williams, S. W.; Lunt, M. Characterization of the cold metal transfer (CMT) process and its application for low dilution cladding, Journal of Materials Processing Technology 2011, 211, 496–502.

96. Junde, X. Special Casting and Nonferrous Alloys[J], 1993, 14(1), 30.

97. Shu, Da.; Sun, B. Foundry Engineering[J], 1998, 22(1), 49.

98. Lianghong, Xu.; Zhiling, T.; Xiaomu, Z. Transaction of the China Welding Institution[J], 2006, 27(12), 69.

99. Zhengyang, Li.; Mingfang, Z.; Dai, T. D. Acta Metallurgica Sinica [J], 2013, 49(9), 1032.

100. Zapico, E.P.; Lutey, A. H. A.; Ascari, A.; Gómez, P. C. R, Liverani E, Fortunato A. An improved model for cold metal transfer welding of aluminium alloys. J Therm Anal Calorim. 2018, 131(3), 3003–3009.

101. Lee, P, D.; Hunt, J. D. Acta Materialia [J], 2001, 49, 1383.

102. Pickin, C. G.; Young, K. Evaluation of cold metal transfer (CMT) process for welding aluminium alloy. Sci Technol Weld Join 2006, 11(5), 583–5.

103. Cornacchia, G.; Cecchel, S.; Panvini, A. A comparative study of mechanical properties of metal inert gas (MIG)-cold metal transfer (CMT) and fiber laser-MIG hybrid welds for 6005A T6 extruded sheet. Int J Adv Manuf Technol. 2018, 94(5–8), 2017–2030.

104. Ahmad, R.; Bakar, M.A. Effect of a post-weld heat treatment on the mechanical and microstructure properties of AA6061 joints welded by the gas metal arc welding cold metal transfer method. *Materials & Design* 2011, 32 (10), 5120 – 5126.

105. Demir, H.; Gunduz, S. The effects of aging on machinability of 6061 aluminium alloy. J Mater Des 2009, 30, 1480–3.

106. Elangovan, K.; Balasubramanian, V. Influences of post weld heat treatment on tensile properties of friction stir-welded AA6061 aluminium alloy joints. J Mater Char 2008, 59, 1168–77.

107. Mrowka, G.; Sreniawski, J. Influence of heat treatment on the microstructure and mechanical properties of 6005 and 6082 aluminium alloys. J Mater Process Technol 2005, 162, 367–72.

108. Ozturk, F.; Sisman, A.; Toros, S.; Kilic, S.; Picu, R.C. Influence of aging treatment on mechanical properties of 6061 aluminium alloy. J Mater Des 2010, 31, 972–5.

109. Pascoal, A.; Izeda, AE.; Cecilio, V.; Mineiro, N.; Gonçalves, J.; Ribeiro, J, E. Ribeiro Robotic Welding Tests MIG Standard and CMT+P in Aluminum Alloy 6082-T6 for Optimization of Penetration, Cord Width and Reinforcement Proceedings 2018, 2, 425, doi:10.3390/ICEM18-05295.

110. Pang, J.; Hu, S.; Shen, J.; Wang, P.; Liang, Y. Arc characteristics and metal transfer behavior of CMT + P welding process. J Mater Process Technol. 2016, 238, 212–217. Available from: http://dx.doi.org/10.1016/j.jmatprotec.2016.07. 033.

111. Caruso, S.; Sgambitterra, E.; Rinaldi, S.; Gallone, A.; Viscido, L.; Filice, L. Experimental comparison of the MIG, friction stir welding, cold metal transfer and hybrid laser-MIG processes for AA 6005-T6 aluminium alloy. AIP Conf Proc. 2016, 1769, 100004; doi: 10.1063/1.4963498.

112. Lei, H. Y.; Li, Y. B.; Carlson, B. E. Cold metal transfer spot welding of 1 mm thick AA6061-T6. J Manuf Process 2017, 28, 209–219. Available from: http://dx.doi.org/10.1016/j.jmapro.2017.06.004.

113. Guojin, L.; Peilei, Z.; Xi, W.; Yunpeng, N.; Zhishui, Y.; Hua, Y. Gap bridging of 6061 aluminum alloy joints welded by variable-polarity cold metal transfer. J Mater Process Technol. 2018, 255, 927–935.

114. Koli, Y.; Yuvaraj, N.; Vipin, Aravindan, S. Investigations on weld bead geometry and microstructure in CMT, MIG pulse synergic and MIG welding of AA6061-T6 Mater. Res. Express 6 (2019) 1265e5.

115. Elrefaey, A. Effectiveness of cold metal transfer process for welding 7075 aluminum alloys. Sci Technol Weld Join. 2015, 20(4), 280–5.

116. Ashton, R. F.; Wesley, R. P.; Dixon, and C. R, 'The effect of porosity on 5086-H116 aluminum alloy welds', Weld. J., N.D., 95s–98s.

117. Senthilnathan, T.; Balachandar, K. Evaluation of microstructure and mechanical properties of AA7475 hybrid composites, International Journal of Pure and Applied Mathematics 2017, Volume 117 No. 16, 251-256.

118. Kadlec, M.; Ruzek, R.; Novakova, L. Mechanical behavior of AA 7475 friction stir welds with the kissing bond defect, International Journal of Fatigue 2015, 74, 7–1.

119. Selvamani, S. T.; Govindarajan, P.; Ajaymohan, M.; Hariharan, S. J.; Vigneshwar, M. Correlation between Microhardness and Microstructure of CMT Welded AA 7075 Al Alloy Materials Science and Engineering 2018, 390, 012058 doi:10.1088/1757-899X/390/1/012058.

120. Fengyuan, Shu.; Yaohui, Lv.; Yuxin, Liu.; Fujia, Xu.; Zhe, S.; Peng, He.; Bianchi, Xu. Residual stress modeling of narrow gap welded joint of aluminum alloy by cold metal transferring procedure Construction and Building Materials 2014, 54, 224–35.

121. Carlos, D. J.; Silva, R. H. G.; Savi, B. M.; Marques, C.; Alarcon, O. E. Metallurgical characterization of the 5083H116 aluminum alloy welded with the cold metal transfer process and two different wire-electrodes (5183 and 5087) Weld world 2015, 59, 797-807.

122. Zhang, H. T.; Feng, J. C.; He, P.; Zhang, B. B.; Chen, J. M.; Wang, L. W. The arc characteristics and metal transfer behavior of cold metal transfer and its use in joining aluminum to zinc-coated steel Materials Science and Engineering 2009, A 499, 111–113.

123. Shang, J.; Wang, K.; Zhou, Q.; Zhang, D.; Huang, J.; Li, G. Microstructure characteristics and mechanical properties of cold metal transfer welding Mg/Al dissimilar metals, Journal of Materials and Design 2012, 34, 559–565.

124. Gungor, B.; Kaluc, E.; Taban, E.; SIK, Ş. Ş. A. Mechanical and microstructural properties of robotic Cold Metal Transfer (CMT) welded 5083-H111 and 6082-T651 aluminum alloys, Materials and Design 2014, 54, 207–211. Available from:http://dx.doi.org/10.1016 / j. matdes.

125. Rajeshkumar R;, Niranjani V.L.;, Devakumaran K.;, and Banerjee K. "Fusion Boundary Microstructure Evolution and Mechanical Properties of Cold Metal Transfer Welded Dissimilar A5754 and A5083 Joint," Materials Letters 284, part 1(February 2021): 128877, https://doi.org/10.1016/j.matlet.2020.128877.

126. Koli Y.;, Yuvaraj N.;, Aravindan S.;, and Vipin. "Enhancement of Mechanical Properties of 6061/6082 Dissimilar Aluminium Alloys through Ultrasonic-Assisted Cold Metal Transfer Welding," Arabian Journal for Science and Engineering, 2021, https://doi.org/10.1007/s13369-021-05844-9.

127. Çömez N.; and Durmuş H. "Corrosion Behavior and Mechanical Properties of Cold Metal Transfer Welded Dissimilar AA7075-AA5754 Alloys," Journal of Central South University 27 (January 2020): 18–26, https://doi.org/10.1007/s 11771-020-4274-5.

128. Çömez N.; and Durmuş H. "Mechanical Properties and Corrosion Behavior of AA5754-AA6061 Dissimilar Aluminum Alloys Welded by Cold Metal Transfer," Journal of Materials Engineering and Performance 28, no. 6 (June 2019): 3777–3784, https://doi.org/10.1007/s11665-019-04131-x.

129. Cao, R.; Chang, J. H.; Zhu, H. X.; Mao, G. J.; Xu, Q. W.; Shi, Y. Investigation of wire selection for CMT plug joining Mg AZ31-to-galvanized stee, Journal of Manufacturing Processes, April 2018, Volume 32, Pages 65-76.

130. Li, L. Q.; Tan, C. W.; Chen, Y. B.; Guo, W.; Hu, XB. Influence of Zn coating on interfacial reactions and mechanical properties during laser welding-brazing of Mg to steel. Metal Mater Trans A 2012, 43A, 4740–54.

131. Miao, Y. G.; Han, D. F.; Yao, J. Z.; Li, F. Effect of laser offsets on joint performance of laser penetration brazing for magnesium alloy and steel. Mater Des 2010, 31, 3121–6.

132. Cao, R.; Yu, J. Y.; Chen, J. H.; Wang, P. C. Feasibility of cold-metal-transfer welding magnesium AZ31 to galvanized mild steel. Weld J 2013, 92, 274S–82S.

133. Liu, L. M.; Zhao, X. Study on the weld joint of Mg alloy and steel by laser-GTA hybrid welding. Mater Charact 2008, 59, 1279–84.

134. Qj, X. D.; Song, G. Interfacial structure of the joints between magnesium alloy and mild steel with nickel as interlayer by hybrid laser-TIG welding. Mater Des 2010, 31, 605–9.

135. Liu, L. M.; Qi, X. D.; Wu, ZH. Microstructural characteristics of lap joint between magnesium alloy and mild steel with and without the addition of Sn element. Mater Lett 2010, 64, 89–92.

136. Wu, D. S.; Huang, J. L.; Kong, L.; Hua, X. M.; Wang, M. Coupled Mechanisms of Arc, Weld Pool and Weld Microstructures in High-Speed Tandem TIG Welding. *Int. J. Heat Mass Transf.* 2020, 154, 119641. OI: 10.1016/j.ijheatmas stransfer.2020.119641.

137. Qi, X. D.; Liu, L. M. Investigation on welding mechanism and interlayer selection of magnesium/steel lap joints. Weld J 2011, 90, 1S–7S.

138. Song, G.; An, G. Y.; Liu, L. M. Effect of gradient thermal distribution on butt joining of magnesium alloy to steel with Cu-Zn alloy interlayer by hybrid laser-tungsten inert gas welding. Mater Des 2012, 35, 323-9.

139. Koba, M.; Araki, T.; Nambu, S.; Inoue, J.; Koseki, T. Bonding interface formation between Mg alloy and steel by liquid-phase bonding using the Ag interlayer. Metal Mater Trans A 2012, 43, 592–7.

140. Liu, L. M.; Qi, X. D.; Zhang, ZD. The effect of alloying elements on the shear strength of the lap joint of AZ31B magnesium alloy to Q235 steel by hybrid laser-TIG welding technique. Metal Mater Trans A 2012, 43A, 1976–88.

141. Santella, M.; Brown, E.; Pozuelo, M.; Pan, T. Y.; Yang, J. M. Details of Mg-Zn reactions in AZ31 to galvanized mild steel ultrasonic spot welds. Sci Technol Weld Join 2012, 17, 219–24.

142. Patel, V. K.; Bhole, S. D.; Chen, D. L. Formation of zinc interlayer texture during dissimilar ultrasonic spot welding of magnesium and high strength low alloy steel. Mater Des 2013, 45, 236–40.

143. Liu, L.; Xiao, L.; Feng, J. C.; Tian, Y.H.; Zhou, S. Q.; Zhou, Y. The mechanisms of resistance spot welding of magnesium to steel. Metal Mater Trans A 2010, 41A, 2651–61.

144. Chen, Y. C.; Nakata, K. Effect of tool geometry on microstructure and mechanical properties of friction stir lap welded magnesium alloy and steel. Mater Des 2009, 30, 3913–9.

145. Schneider, C.; Weinberger, T.; Inoue, J.; Koseki, T.; Enzinger, N. Characterisation of interface of steel/magnesium FSW. Sci Technol Weld Join 2011, 16, 100–6.

146. Zhang, Z. K.; Wang, X. J.; Wang, P. C.; Zhao, G. Friction stir keyholeless spot welding of AZ31 Mg alloy-mild steel. Trans Nonferrous Met Soc China 2014, 24, 1709–16.

147. Lei, H. Y.; Li, Y. B.; Carlson, B. E.; Lin, Z. Q. Cold metal transfer spot joining of AA6061- T6 to galvanized DP590 under different modes. J Manuf Sci Eng Trans Asme 2015, 137, 10.

148. Kang, M.; Kim, C. Joining Al 5052 alloy to aluminized steel sheet using cold metal transfer process. Mater Des 2015, 81, 95–103. Available from: http://dx.doi.org/10.1016/j.matdes.2015.05.035.

149. Xie, C.; Yang, S.; Liu, H.; Zhang, Q.; Wang, Y. Microstructure and mechanical properties of robot cold metal transfer Al5.5Zn2.5Mg2.2Cu aluminium alloy joints. J Mater Process Technol. 2018, 255, 507–515. Available from: https://doi.org/10.1016/j.jmatprotec.12.045.

150. Lei, H.Y.; Li, Y. B.; Carlson, B. E. Corrosion Behaviors of CMT Spot-Joined AA6022-T4 to Galvanized DC03 welding journal 2019, VOL. 98.

151. Guang Yang, Kainan Guan, Li Zou, Yibo Sun, and Xinhua Yang, Weld Defect Detection of a CMT Arc-Welded Aluminum Alloy Sheet Based on Arc Sound Signal Processing, Appl. Sci. 2023, 13, 5152.https://doi.org/10.3390/app13085152h.

152. Yili Zhao, Furong Chen, Silong Cao, Chao Chen, and Ruijun Xie; Effect of CMT Welding Heat Input on Microstructure and Properties of 2A14 Aluminum Alloy Joint, Metals 2022, 12, 2100.https://doi.org/10.3390/met12122100h.

153. Rajendran Chinnasamy, Samson Jerold Samuel Chelladurai, and Tushar Sonar, "Investigation on Microstructure and Tensile Properties of High-Strength AA2014 Aluminium Alloy Welds Joined by Pulsed CMT Welding Process", Advances in Materials Science and Engineering, Volume 2021, Article ID 8163164, 8 pages, https://doi.org/10.1155/2021/8163164.

154. Zehua Zhang, Xiaoqiang Li, Dezhi Zhu, Shengguan Qu, Microstructural and Mechanical Characteristics of 7075-T6 Aluminum Alloy Joint by Double Wire Pulsed Cold Metal Transition Welding; Journal of Physics: Conference Series, IOP Publishing, 2383 (2022) 012103 doi:10.1088/1742-6596/2383/1/012103.

155. Rajesh kumar Gangaram Bhandare and Parshuram M. Sonawane (2014) Preparation of Aluminium Matrix Composite by using Stir Casting Method & it's Characterization, International Journal of Current Engineering and Technology ISSN 2277 – 4106.

156. Sijo M T, K R Jayadevan (2016) Analysis of stir cast aluminium silicon carbide metal matrix composite: A comprehensive review, Procedia Technology 24, 379 – 385.

157. James.S, Venkatesan.K, Kuppan.P, Ramanujam.R (2014) Hybrid Aluminium Metal Matrix Composite Reinforced with SiC and TiB2, Procedia Engineering 97, 1018 – 1026.

158. Saravanakumar et al. (2017) Assessment of microstructure and wear behavior of aluminum nitrate reinforced surface composite layers synthesized using friction stir processing on copper substrate, substrate, Surface & Coatings Technology (2017), PII: S0257-8972 (17) 30497-8.

159. Gangil N. et al. (2018) State of the art of Ex-Situ Aluminium matrix composite fabrication through friction stir processing, Arch. Metall. Mater. 63, 2, 719-738.

160. Taherzadeh R. Mousavian et al. (2016) Fabrication of aluminum matrix composites reinforced with nano- to micrometer-sized SiC particles, Journal of Materials and Design 89, 58–70.

161. Kishorekumar Nandyala, B. Santhosh Kumar, G.I.K. Durga Bhavani; "Developing of a hybrid composite of Al6068 and Al-7075 by reinforcing TiO$_2$/BN by the stir casting process and finding mechanical and wear behavior of the hybrid composition eur. chem. bull. 2023, 12 (6), 1036 – 1044, DOI: 10.31838/ecb/2023.12.6.95.

162. Ananth G., T. Muthu Krishnan, S. Thirugnanam, and Tewedaj Tariku Olkeba; Optimization on Stir Casting Process Parameters of Al7050/Nano-B$_4$C Metal Matrix Composites, Journal of Nanomaterials, Volume 2023, Article ID 3615093, 7 pages, https://doi.org/10.1155/2023/3615093.

163. Venkatesan S. and M. A. Xavior, "Tensile behavior of aluminum alloy (AA7050) metal matrix composite reinforced with graphene fabricated by stir and squeeze cast processes," Science and Technology of Materials, vol.30, no.2, pp.74–85, 2018.

164. Umanath K., K. Palanikumar, V. Sankaradass et al., Optimization of wear properties on AA7075/Sic/Mos2 hybrid metal matrix composite by response surface methodology, Materials Today: Proceedings, https://doi.org/10.1016/ j. matpr.2021.02.541.

165. Hawraa Kareem, Lalit Kumar Tyagi, Hemanth Raju, Annapoorna E, H Pal Thethi, Vandna Kumari, Advancements in Aluminum-Based Composite Manufacturing: Leveraging La2O3 Reinforcement through Friction Stir Process; E3S Web of Conferences, 01036 (2024) https://doi.org/10.1051/e3sconf/ 202450701036.

166. Xin Tan, Chang Zhou, Bin Zhang, Kai Liu, Xiaobo Yan, Jun Han, Xin Liu, Wenshu Yang, Zhenhe Yu, Puzhen Shao, Gaohui Wu, "Microstructure and mechanical property of the 2024Al matrix hybrid composite reinforced with recycled SiCp/2024Al composite particles, X. Tan et al. / Journal of Alloys and Compounds 815 (2020) 152330, https://doi.org/10.1016/j.jallcom.2019.152330.

167. Kaveripakkam Suban Ashraff Ali, Manickam Ravichandran, Vinayagam Mohanavel,, Subbiah Arungalai Vendan, Anshul Yadav, Marek Gucwa, and Jerzy Winczek, Mechanical and Microstructural Characterization of Friction Stir Welded SiC and B4C Reinforced Aluminium Alloy AA6061 Metal Matrix Composites; Materials 2021, 14, 3110.https://doi.org/10.3390/ma14113110.

168. Kumar   S., A. Yadav, V. Patel, et al., Mechanical behaviour of SiC particulate reinforced Cu alloy-based metal matrix composite, Materials Today: Proceedings, https://doi.org/10.1016/j.matpr.2020.08.580.

169. Jayashree P. K., Murthy B. R. N., Anupama Hiremath, Jayant Giri, Rajeh Alotaibi, Sathish T., and BhagyaLaxmi, an experimental analysis on sliding wear characteristics of TIG-welded Al6061 reinforced with SiC; AIP Advances 14, 065331 (2024); doi: 10.1063/5.0213976.

170. Ummal N., Salmaan, D. S. Robinson Smart & S. Antony Raja, Analysis on Aluminium Hybrid Metal Matrix Composite Reinforced with Hfc, Si3N4 and MoS2 Nanoparticles; International Journal of Mechanical and Production Engineering Research and Development (IJMPERD) ISSN (P): 2249–6890; ISSN (E): 2249–8001, Vol. 10, Issue 3, Jun 2020, 747–758.

171. Babu Erappa Rajj, Madeva Nagaral, Sanjay Chintakindi, Raman Kumar, Ali E. Anqi, Ali A. Rajhi, Alaauldeen A. Duhduh, Gedala Sridevi, Chander Prakash, Raman Kumar, and Choon Kit Chan Nano-Sized Al2O3−Gr Reinforced Al7075 Hybrid Composite: Impact of Cooling Agents on Mechanical, Wear, and Fracture Behavior; ACS Omega 2024, 9, 17878−17890, https://doi.org/10.1021/acsomega.3c08822.

172. Lindroos V. K.,and M. J. Talvitie Helsinki "Recent advances in metal matrix composites" University of Technology, Laboratory of Physical Metallurgy and Materials Science, FIN-02150 Espoo, Finland.

173. Talvitie M. J. "Recent advances in metal matrix composites" FIN-02150 Espoo, Finland Metal.

174. Alidokht S.A, A. Abdullah-Zadeh, S. Soleymani, H. Assadi, Microstructure and tribological performance of an aluminium alloy-based hybrid composite produced by friction stir processing, Mater. Des. 32 (2011) 2727–2733.

175. Hashim, J.; Looney, L.; Hashmi, M.S.J. "Metal matrix composites: Production by the stir casting method" Journal of Materials Processing Technology 1999, 92 (93), 1–7.

176. Hashim J., L. Loonry, M.S.J.Hashami., "The enhancement of wettability of SiC particles in cast Al Matrix composites, Journal of materials processing technology,119 (2001), 329.

177. Shorowordi K. M., T. Laoui, A.S.M.A. Haseeb, J.P. Celis, L.Froyen "Microstructure and interface characteristics of B4C, SiC, and Al2O3 reonforced Al matrix composites: a Comparative study" 5 june 2003.

178. Yu P., Z. Mei, S. Tjong, (2005) Structure, thermal and mechanical properties of in situ Al-based metal matrix composite reinforced with Al2O3 and TiC submicron particles, Materials Chemistry and Physics 93, 109–116.

179. Zhanh Q., G. Wu, L. Jiang, (2008) Tensile deformation behavior of a sub-micrometer Al2O3/6061Al composite, Materials Science and Engineering A 483 281–284.

180. Ahmad S. N., J. Hashim, And M. I. Ghazali "The Effect of Porosity on mechanical properties of cast Discontinuous reinforced Metal Matrix Composites" Batu Pahat, Johore, Malaysia.

181. Gurusamy P., S. Balasivanandha Prabu, and R. Paskaramoorthy "Interfacial Thermal Resistance and the Solidification behaviour of the Al/SiCp composites", LLC ISSN: 1042-6914.

182. Muzakkir, A. K.: An Overview on Effect of Reinforcement and Process Parameters on Properties of Aluminium Based Metal Matrix, International Journal of Research in Engineering and Science (IJRES), Volume 2 Issue 10, 2014.

183. Naher, S.; Brabazon, D.; Looney, L. "Simulation of the stir casting process" Journal of Materials Processing Technology 2004, 143 (144), 567–571.

184. Gowri Shankar, M.C, Jayashree,et.al: Individual and Combined Effect of Reinforcements on Stir Cast Aluminium Metal Matrix Composites. A Review, International Journal of Current Engineering and Technology, Vol.3, No.3, 2013.

185. Rajesh Kumar, Gangaram Bhandare, Parshuram M. Sonawane: Preparation of Aluminium Matrix Composite by Using Stir Casting Method, International Journal of Engineering and Advanced Technology, Vol, 3, Issue 2, 2013.

186. Pradeep Sharma, Gulshan Chauhan, Neeraj Sharma (2008), Production of AMC by stir casting- an overview International Journal of Contemporary Practises Vol.2 Issue1.

187. Pradeep, R., Praveen Kumar, B.S and Prashanth: Evaluation of mechanical properties of aluminium alloy 7075 reinforced with silicon carbide and red mud composite, International Journal of Engineering Research and General Science, Vol. 2, Issue 6, (1081-88), 2014.

188. Ravichandran, M. and Dineshkumar, S.: Synthesis of Al-TiO2 Composites through Liquid Powder Metallurgy Route, International Journal of Mechanical Engineering, Vol. 1 Issue 1, 2014.

189. Lloyd D J 1999," Particle reinforced aluminium and magnesium matrix composites". Int. Mater. Rev.39: 1–23.

190. Soleymani S., A. Abdullah-Zadeh∗, S.A. Alidokht, Microstructural and tribological properties of Al5083 based surface hybrid composite produced by friction stir processing (2012) Wear 278– 279 (2012) 41– 47, doi: 10.1016/j.wear.2012.01.009.

191. Chaojie X, Shanglei Y B, Haobo L, et al. Microstructure and mechanical properties of robot cold metal transfer Al5.5Zn2.5Mg2.2Cu aluminium alloy joints, Journal of Materials Processing Tech. 255 (2018) 507–515.

192. Ohya Y, Ito S, Ban T, and Takahashi Y 2000 Key Engineering Materials 181 113-116.

193. Satyanaryana, V.V.; Madhusudhan Reddy, G.; Mohandas, T. Dissimilar metal friction welding of austenitic-ferritic stainless, steels. Journal of Materials Processing Technology 2005, 160, 128–137.

194. Alhamed M and Abdullah W 2013 Journal of Electron Devices 18 1563-1567.

195. Feng J, Zhang H, He P 2009 Materials & Design 30 1850–1852.

196. Roată I C, Pascu A, Stanciu E M, Pop M A 2014 Advanced Materials Research 1029 pp. 140- 45.

197. Chen M, Zhang D, Wu C 2017 Journal of Materials Processing Technology 243 395–404.

198. Yang WH, Tarng YS, Design optimization of cutting parameters for turning operations based on the Taguchi method, Journal of Material Processing Technology, 84, 1998, 122–129.

199. Taguchi G, Introduction to quality engineering, (Asian Productivity Organization, Tokyo, 1990).

200. Switzner et al. 2020 N. Switzner, H. Queiroz, and J. Duerst, Mater Sci Eng A 709 (2018) 55.

201. Ramachandran et al. 2020 S. Ramachandran, and A. K. Lakshminarayanan, Trans Nonferr Met Soc China 30 (2020) 727.

202. Abioye et al. 2019 T. E. Abioye, I. S. Omotehinse, Effects of post-weld heat treatments on the microstructure, mechanical and corrosion properties of gas metal arc welded 304 stainless steel, World Journal of Engineering 17/1 (2020) 87–96 © Emerald Publishing Limited [ISSN 1708-5284] [DOI 10.1108/WJE-11-2019-0323].

203. Phadke, S. M., Introduction to Quality Engineering, Asian Productivity Organization, 1989, Dearborn.

204. Krishnaiah K., Shahabudeen P., Applied Design of Experiments and Taguchi Methods, PHI Learning Private Limited, 2012.

205. Staley et al., 1993   J. Staley, and D. Lege, J. de Phys. 3 (1993) C7-179.

206. Vazquez et al., 2012 J. Vazquez, C. Navarro, J. Dominguez, Experimental results in fretting fatigue with shot and laser peened Al 7075-T651 specimens. Int. J. Fatigue, 40 (2012) pp. 143–53.

207. Thomas et al., 1991 W. Thomas, E. Nicholas, J. Needham, M. Church, P. Templesmith, and C. Dawes. Friction stir welding. England Patent (1991), PCT/GB92102203.

208. Pickin et al., 2011 C.G. Pickin, S.W. Williams, M. Lunt, Characterisation of the cold metal transfer (cmt) process and its application for low dilution cladding. J. Mat. Pro. Tech. 211 (2011), pp. 496–502.

209. Hu et al., 2007 B. Hu, I.M. Richardson, Microstructure and mechanical properties of aa7075(t6) hybrid laser/gma welds. Mater. Sci. Eng. A 459 (2007), pp. 94–100.

210. Elrefaey et al. 2015   A. Elrefaey, Effectiveness of cold metal transfer process for welding 7075 aluminium alloys. Sci. and Tech. of Weld. and Joi. 20 pp. 280-85. doi.org/10.1179/1362171815Y.0000000017.

211. Verma et al. 2019 A. Verma, B. Kotteswaran, A. C. Abhyankar, T. Shanmugasundaram, Microstructure and Mechanical Properties of AA7005 Alloy Joint by Fusion and Solid-State Welding Processes, Trans Indian Inst Met, https://doi.org/10.1007/s12666-020-01917-9.

212. Akhter et al., 2007 R. Akhter, L. Ivanchev, H. P. Burger, Effect of pre/post t6 heat treatment on the mechanical properties of laser welded ssm cast a356 aluminium alloy. Mat. Sci. Eng. A 447 (2007), pp. 192–6.

213. Ambriz et al. 2011 R. R. Ambriz, D. Chicot, and N. Benseddiq, "Local mechanical properties of the 6061-T6 aluminium weld using micro traction and instrumented indentation," European Journal of Mechanics–A/Solids, vol. 30, pp. 307–315, 2011.

214. Bertini et al., 1998 L. Bertini, V. Fontanari, G. Straffellini, Influence of post-weld treatments on the fatigue behaviour of al-alloy welded joints. Int. J. Fatigue 20 (1998), pp. 749–55.

215. Necsulescu et al., 2011 D. Necsulescu, UPB Science Bulletin 73 (2011) p. 223.

216. Bobbili et al. 2016 R. Bobbili, V. Madhu, and A, K. Gogia, "Tensile behaviour of aluminium 7017 alloys at various temperatures and strain rates", Journal of Materials Research and Technology, Vol. 5 No. 2, pp. 190-197.

217. Ahmad et al., 2011   R. Ahmad, M.A. Bakar, Effect of post-weld heat treatment on the mechanical and microstructure properties of AA6061 joints welded by the gas metal arc welding cold metal transfer method. Mat. and Design 32 (2011), pp. 5120–5126. doi: 10.1016/j.matdes.2011.06.007.

218. V. Balasubramanian, V. Ravisankar, G.M. Reddy, Influences of pulsed current welding and post-weld aging treatment on fatigue crack growth behaviour of aa 7075 aluminium alloy joints. Int. J. Fatigue, 30 (2008), pp. 405–16.

LIST OF PUBLICATIONS

SCI / SCIE

1. Hari Shanker and Reeta Wattal, A comprehensive survey on the cold metal transfer process in welding similar and dissimilar materials and for cladding, Proc IMechE Part C: J Mechanical Engineering Science, 2023, Vol. 237(10) 2360–2391, https://doi.org/10.1177/09544062221139947 (**SCIE Indexed, Impact Factor: 2.0**).

2. Hari Shanker and Reeta Wattal, Mechanical and microstructure characteristics of 7475-T7351 aluminium alloy joints welded by robot cold metal transfer. Proc IMechE Part B: J Engineering Manufacture (2023) 1–13, https://doi.org/10.1177/09544054231178956 (**SCIE Indexed, Impact Factor: 2.6).**

3. Hari Shanker and Reeta Wattal, Comparative Study of Microstructural and Mechanical Properties of Robotic CMT and GMAW Welded 7475-T7351 Aluminium Alloy Joints. Journal of Materials Today Communication 37 (2023) 106994, Available online 30 August 2023, 106994, https://doi.org/10.10 16/j.mtcomm.2023.106994 (**SCIE Indexed, Impact Factor: 3.8).**

SCOPUS Indexed Conferences

4. Hari Shanker and Reeta Wattal, A comprehensive survey on the cold metal transfer process in additive manufacturing, Advancements & Key Challenges in Green Energy and Computing (AKGEC 2023) Journal of Physics: Conference Series 2570 (2023) 012001, IOP Publishing, doi:10.1088/1742-6596/2570/1/012001.

5. Hari Shanker and Reeta Wattal, 'Experimental Analysis of GMAW Welded AA7475 T7351 Alloy Joints, International Conference on Smart and Innovative Development in Science, Engineering, and Technology, (SIDSET 2023), AIP Conf. Proc. 3111, 060008 (2024) https://doi.org/10.1063/5.0221497.

CURRICULAM VITAE

HARI SHANKER

❖

E-170, Sector-9, New Vijay Nagar, Ghaziabad

(U.P.) Pin.Code-201009, Mob. No. 09717020898

E-mail: chaursiyahs@akgec.ac.in
hari_chaursiya@rediffmail.com

CAREER OBJECTIVE

Wish to attain a responsible position in a prestigious organization, which offers opportunities to make the best use of knowledge and technical skills and to further enhance personal knowledge in the Profession and offer high growth prospects.

ACADEMIC QUALIFICATION

- Pursuing PhD in welding Technology from Delhi Technological University Delhi.

- M. Tech: Mechanical Engineering (Machine Design) from (2004- 2006.) Aligarh Muslim University, Aligarh (INDIA).

- B.E.: Mechanical Engineering from (1999- 2003), C.C.S university Meerut (UP).

- School Education:

Class	Board	Year of passing
10th	U.P Board, Allahabad	1996
12th	U.P Board, Allahabad	1998

JOB PROFILE: **Teaching experience**: Total teaching experience 19$^+$ years.

1-Worked as a lecturer in S.I.T.M. Lucknow from 15/08/2003 to 20/08/2004.

2-Worked as a lecturer in S.S.I.T.M. Aligarh from 07/07/2006 to 24/07/2007.

3-Presently working as an assistant professor in Ajay Kumar Garg Engineering College Ghaziabad, from 25/07/2007 to till date.

ORCID-https://orcid.org/0000-0002-9170-6142.